Contribution to the Study of Topological Defects and their Applications in Optics

Frankbelson dos Santos Azevedo

Université de Lorraine - ED C2MP

Thèse

pour obtenir le grade de

Docteur

de l'Université de Lorraine

par

Frankbelson dos Santos Azevedo

Contribution to the Study of Topological Defects and their Applications in Optics

---

Contribution à l'étude des Défauts Topologiques et leurs Applications en Optique

Fernando Moraes	Professeur, UFRPE-Brésil	Président du jury
Erms Pereira	Professeur associé, UFRPE-Brésil	Rapporteur
Ernesto Medina	Professeur, Yachay Tech-Équateur	Rapporteur
Alexander Lopez	Professeur, ESPOL-Équateur	Rapporteur
Claire Michel	Maître de conférences, UNS-France	Examinateur
Bertrand Berche	Professeur, UL-France	Directeur de thèse
Sébastien Fumeron	Maître de conférences, UL-France	Co-Directeur de thèse

Nancy

2018

"*Spacetime tells matter how to move; matter tells spacetime how to curve*"

John Wheeler

Abstract

***

In this thesis, we study topological defects in cosmology and condensed matter physics. We propose to investigate the analogy between defects that appear in these two realms with respect to aspects of formation and gravity. For instance, we discuss the analogy between cosmic strings and disclinations existing in liquid crystals. In particular, we concentrate our efforts on the study of gravity/geometric aspects of two linear defects: wiggly cosmic string and hyperbolic disclination. The gravitational field of wiggly strings is analogous to the one of regular strings, but with a non-vanishing Newtonian potential. For that reason, besides the spacetime has conical geometry, the string also produces gravitational pullings on objects located in its vicinity. This new fact leads to new effects in addition to the already expected gravitational lensing. In fact, we find that both massive and massless fields are confined to the string when we examine non-perpendicular propagation to the string axis. This statement is based on the analysis of trajectories and by applying the wave formalism. Finally, we propose the design of an optical waveguide having the specific refractive index likely to simulate the effects of wiggly strings in the laboratory. Even though the hyperbolic disclination is very similar to the ordinary one, the resulting medium is an anisotropic metamaterial, in which the ratio between ordinary and extraordinary permittivities is negative. In fact, as our analysis concerning the hyperbolic medium is very close to the previous one for the wiggly string, we also apply the wave formalism together with geometrical optics treatment to understand how light propagates. Interestingly, we find that for one specific director field arrangement of the hyperbolic liquid crystal metamaterial, light is confined and directed to the metamaterial axis. More specifically, we come into possession of an optical device that concentrates light rays, no matter how they are injected in it.

Résumé

***

Dans cette thèse, notre étude porte sur les défauts topologiques en cosmologie et en physique de la matière condensée. Nous proposons d'étudier l'analogie entre les défauts qui apparaissent dans ces domaines. Par exemple, nous discutons l'analogie entre les cordes cosmiques et les disinclinaisons présentes dans les cristaux liquides. Cependant, nous concentrons nos efforts sur l'étude de la gravité et des aspects géométriques des défauts linéaires; cordes cosmiques «ondulées» et les disinclinaisons hyperboliques. Le champ gravitationnel des cordes ondulées est analogue à celui des cordes régulières mais avec un potentiel newtonien non nul. Pour cette raison, outre le fait que l'espace-temps a une géométrie conique, les cordes produisent également une traction gravitationnelle sur les objets situés dans leur voisinage. Ceci a pour conséquence: l'apparition de nouveaux effets en plus de la lentille gravitationnelle. En réalité, nous constatons que les champs massiques et non-massiques sont confinés au voisinage de la corde quand nous examinons la propagation non perpendiculaire à son axe. Cette affirmation est basée sur l'analyse des trajectoires et l'application du formalisme ondulatoire. Enfin, nous proposons la conception d'un guide d'onde optique ayant l'indice de réfraction spécifique permettant de simuler l'effet des cordes ondulées en laboratoire. Bien que la disinclinaison hyperbolique soit très similaire à la disinclinaison ordinaire, le milieu résultant est un métamatériau anisotrope dans lequel le rapport entre les permittivités ordinaire et extraordinaire est négatif. En fait, notre analyse concernant la disinclinaison hyperbolique étant très proche de la précédente pour la corde ondulée, nous appliquons alors le formalisme ondulatoire avec des traitements d'optique géométrique pour comprendre la propagation de la lumière. Nous trouvons que pour un agencement spécifique du champ directeur du cristal liquide hyperbolique, la lumière est confinée et dirigée vers l'axe du métamatériau. Plus précisément, on obtient un dispositif optique qui concentre les rayons de lumière, quelles que soient les conditions d'injection.

Acknowledgements

***

I would like to start thanking to both of my supervisors Bertrand Berche and Sébastien Fumeron, for offered me the opportunity to participate in this project. Their guidance and support were fundamental for achieving the results to be presented here.

I offer my sincere thanks to Fernando Moraes for having me in his Department of Physics at UFRPE, and also for the great collaboration.

I am thankful to Francisco Mireles for the collaboration and hospitality at CNyN-UNAM.

I want to thank my collaborators David Figueiredo and Antonio de Padua.

Furthermore, I am thankful to all the members of the thesis committee for accepting our invitation.

I also thank my former supervisors Cleverson Figueiras and Diego Cogollo.

I am grateful to the professors and staff members of the LPCT and UL for their help and advice.

I am grateful to my fellow students Sascha Wald, Yannis Brun, Rúbia Araújo, Stefano Scopa, Adam Hammoumi, Walter Dalmaz, Hugo Tschirhart, Luiz Silva, Dimitrios Voliotis and all those I shared my office with.

Also I would like to thank my closest friends from Nancy and those I have met in Mexico and Recife-Brazil. I am also thankful to my former roommates with whom I shared good times during my stay in Nancy. Naturally, I thank as well to all my old friends.

Finally, I would like to thank my whole family and my girlfriend for their support throughout these three years.

Contents

***

List of Figures

***

List of Tables

***

List of Abbreviations

***

CMB	**C**osmic **M**icrowave **B**ackground
CMP	**C**ondensed **M**atter **P**hysics
LCs	**L**iquid **C**rystals
SSB	**S**pontaneous **S**ymmetry **B**reaking
GUT	**G**rand **U**nified **T**heory
NLCs	**N**ematic **L**iquid **C**rystals
SM	**S**tandard **M**odel
SUSY	**SU**per**SY**mmetry
LHC	**L**arge **H**adron **C**ollider
STR	**S**pecial **T**heory of **R**elativity
GTR	**G**eneral **T**heory of **R**elativity
FDM	**F**inite **D**ifference **M**ethod

Dedicated to Preta, Mariquinha
and Maria.

Chapter 1

Introduction

***

The ambition to explain the origin of the Universe is as old as the humanity itself, and such intent was not always led by a scientific method. Mysticism, religion and philosophy also had such topic in debate in many civilizations at different times of our history. However, the scientific questioning about the origin of the Universe inaugurates cosmology, which has been developed by many great scientific minds through the history [Wei89; Ste06]. Nevertheless, "the most sophisticated cosmology" only started in the beginning of twentieth century with pioneering work on expanding Universe by Lemaître [Lem27], based on the theory of relativity, and corroborated a little later by Hubble [Hub29] in his work on galaxy redshifts. At present, cosmology is mostly related to the ideas of the Big Bang, a well accepted theory also known as *standard cosmology*, which states the Universe is homogeneous and isotropic with origin around 14 billion years ago. According to the Big Bang model, at the beginning, the Universe was hot and dense and from then it is expanding and cooling down continuously. Nonetheless, this course would have been interrupted by an early period of large and fast expansion named as *inflation era*. Namely, following the inflationary epoch, an extremely hot and dense quark-gluon plasma, where quarks and gluons are no longer confined takes place [Che14]. The early times of evolution are characterized by many symmetry breaking phase transitions which may be responsible for creating *topological defects*. Thus, the study of topological defects is of great importance because the more we understand about them, the more we will know about the early stages of the Big Bang and how it has evolved [Kib97; VS94]. Even though the standard cosmology is in agreement with the most fundamental observational measurements (for example the anisotropies from the Cosmic Microwave Background (CMB) radiation and the redshifts of the galaxies), it is still nowadays subject of criticism and alternative theories (such as bouncing cosmology [IS18], for instance) have been proposed to replace it, by reason of supposedly presenting cosmological discordances with some of the observational data [LC17].

Topological defects can be described as topologically stable ground state configurations in field theories with finite energy. In this context, string-like solutions (known as cosmic strings) have been discussed for the first time by Nielsen and Olesen [NO73]. Other possible cosmic topological solutions are the domain walls, monopoles and textures [VS94]. However, cosmic strings are without a shadow of a doubt the most interesting cosmic defects, mostly

because they are the only ones[1] to have favorable cosmological conditions for their existence after the inflation period. Here, we intend to understand their role in the early Universe and to recall the possible manners of observing them in the present day. We also discuss aspects of formation and evolution, and some of their many cosmological implications. Topological defects can also be found in the Condensed Matter Physics (CMP) realm under many forms. As in cosmology, they are expected to appear during Spontaneous Symmetry Breaking (SSB) processes at phase transitions. Indeed, this assumption has been confirmed by the Kibble mechanism [Kib76], a mechanism first created to explain formation and evolution of cosmic defects, but which also holds to explain the arising of defects in CMP systems. A first example is provided by appearance of vortex lines during quench-induced phase transition in superfluid helium [Zur85] as well as disclination lines in the isotropic-nematic phase transition in Liquid Crystals (LCs) [Chu+91; Bow+94]. Hence, defects in cosmology have topological analogues in the CMP context as they share common topological properties. As the Grand Unified Theory (GUT) proposed in particle physics is mostly based on the notion of symmetry breaking, we realize that such objects are an interesting link between particle physics, field theory, cosmology, and CMP. In addition, the study of such structures is not just important for the understanding of the GUT and early history of the Universe, but also for their unusual physical properties. Interestingly, defects in both context (cosmological and CMP) mentioned here also exhibit analogy with respect to the way light propagates around them. For example, cosmic strings create unusual geometries in the surrounding spacetime, so that light propagating in their vicinity behaves in a characteristic way that can be used for observing evidences of their existence.

This thesis mainly seeks to study the geometric (gravity) aspects of some topological defects. More specifically, we are interested in line-like defects, cosmic strings in cosmology and line disclinations in CMP. We are going to examine how these objects influence light and particle propagation. We have organized this thesis as follows: in Chapter 2 we introduce the topological defects, where we briefly summarize the essential ideas concerning its formation. In Chapter 3, we introduce the linearized gravity of regular cosmic strings. Still here, we describe a geometric method for disclinations based on Fermat's principle and cosmic string gravity. Our main work is introduced in Chapters 4 and 5 of the manuscript. In Chapter 4 we examine the effects of the wiggly cosmic string on both massless and massive fields and we propose an analogy with an optical waveguide [Aze+17]. In Chapter 5 we investigate light propagation in a liquid crystal metamaterial endowed with a hyperbolic disclination [Aze+18]. Finally, Chapter 6 is intended to conclusions and perspectives.

Below we find a list with articles that have been published or submitted during the preparation of this thesis:

- Frankbelson dos S Azevedo et al. "Wiggly cosmic string as a waveguide for massless and massive fields". In: Physical Review D, 96 8 (2017), p.

[1] *Textures* are also supposed to exist at present. However, they are not considered topological defects at all. We will discuss that in the next Chapter.

084047;

- Frankbelson dos S Azevedo et al. "Optical concentrator from a hyperbolic liquid crystal metamaterial". In: eprint arXiv:1806.11514 (2018).[2].

In the course of this manuscript, we will adopt the metric signature convention $(+,-,-,-)$ and will use Einstein's summation convention on repeated indices. Greek letters[3] are used to describe indices in relativity that take the values $0,1,2,3$. Besides, we will consider the units as $\hbar = c = 1$[4].

[2]Accepted and published in EPL (Europhysics Letters), 124 3 (2018), p. 34006 after this thesis manuscript has been submitted.

[3]We were forced to use in some instances same Greek letters to represent physical variables and indices.

[4]For convenience, in Sections 5.3 and A.3 we do not consider $c = 1$.

Chapter 2

Topological Defects

***

Topological defects are exotic objects that appear in both, condensed matter systems and in the Universe, during the phase transitions in nature. Interestingly, they share the same mechanism of formation, known as Kibble mechanism [Kib76], and for that reason ideas of cosmology may be tested in the laboratory. Among the defects that can be found in CMP, we can cite the magnetic flux lines in superconductors [Abr57], vortex lines in superfluids [Zur85] and domain structures in ferromagnetic materials [Kit49]. The appearance of disclination lines in Nematic Liquid Crystals (NLCs) together with a large variety of other defects in other phases of liquid crystals [Klé89] show up as a nice matter of study still nowadays. The possible cosmic defects are the domain walls, monopoles, textures and cosmic strings [VS94].

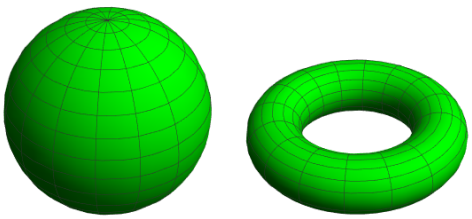

FIGURE 2.1: Sphere and torus are examples of objects with different topology.

In the next sections of this chapter we are going to give more details about topological defects and their formation.

2.1 Topological Defects Formation

According to the *Hot Big Bang Model*, which describes the history of the Universe from the initial instant ("explosion") to the present days, the Universe started about 14 billion years ago and since then it has expanded and cooled

down. During the earliest times of evolution the existing expansion rate scenario had been interrupted by an *inflation era*, that is a period of very rapid (exponential) expansion where the Universe was dominated by a vacuum energy density. To understand how the Universe has expanded one may study the thermodynamics of the CMB. In the past, the CMB radiation was much hotter and then dominated the gravity of the Universe. This period is known as *radiation era*. However, as time went on, the CMB cooled down and decreased energy. At some point, the radiated energy became equal to the energy of the ordinary matter (*matter-radiation equality*). At present, we live in the *matter era*, where the gravity of all matter in the Universe is much greater than the radiation gravity. Therefore, by measuring the content of the energy of the matter and radiation of a large region of space, we are able to understand how this region expands with the Universe [HH05]. Incidentally, observations of the anisotropy spectrum of the CMB have been mentioned as evidence for supporting the idea of an accelerating Universe [Spe+03]. With the expansion of the early Universe it has undergone a succession of phase transitions involving spontaneous symmetry breaking mechanisms which may have led to formation of cosmic topological defects [KT90]. To better understand the general idea of a SSB phase transition let us to have a look at a very common example, the freezing of water to ice[5]. *When the water is still a liquid at some temperature it is constituted of translational and rotational symmetry (high symmetry). However, once the water temperature cools down it gets frozen and such symmetries are broken. That is, the symmetry of the system is reduced to the discrete symmetry (low symmetry) of the ice crystal. During such process, the crystalline orientations of the ice are led to be different in different parts, so that some "defects" are then formed.* At this point, we recognize a strong connection between particle physics and cosmology, since the Standard Model (SM) of particle physics is mostly based on the concept of symmetry breaking. Indeed, the early universe has been often studied as a manner of testing the ideas of the SM at non-accessible energy scales to terrestrial accelerators. By the way, the SM has been tested to a very high precision and shows up that below an energy scale $M_{\mathrm{GUT}} \sim 10^{16}$ GeV [Wei08], the electroweak interactions (weak and electromagnetic forces), represented by the symmetry group $SU(2) \times U(1)$ and the strong interactions associated with the gauge group $SU(3)$ can be unified, forming what is called *Grand Unified Theory*. The idea here is that in the early times (close to the singularity) of the Hot Big Bang model, when the universe was at the highest temperature, all interactions were merged into a single one. Actually, gravity is the only force that does not make part of the GUT; besides being a geometric theory, at the nuclear scale, such interaction is insignificantly weak as compared to the others fundamental forces. However, at the *Planck energy* scale ($M_{\mathrm{Pl}} \sim 10^{19}$ GeV), the gravitational interaction becomes as strong as the others forces [Kib97]. Above M_{GUT}, strong and electroweak interactions unify within a larger gauge symmetry group G, where grand unified theories involving Supersymmetry (SUSY) have been considered as suitable description for such energy scales [Baj+04; Fuk+05; Rab11]. For such reason, SUSY GUT

[5]This example have also been mentioned by Chuang et al [Chu+91] and Gangui [Gan01] with the same intent of exemplify a symmetry breaking phase transition.

arises as a possible way to unify all the four fundamental forces of nature in a single one (this unification is often called as *Theory of Everything*) [Kib97].

As we have mentioned before, the ideas of the GUT are generally speaking based on the notion of SSB phase transitions: a system represented by a high symmetric group G is spontaneously broken to a subgroup H with less symmetry,

$$G \to H \to \cdots SU(3) \times SU(2) \times U(1) \to SU(3) \times U(1)_{em}.$$

That happens always the system cools down to a critical temperature $T = T_c$ defined by symmetry breaking scales [Vil85]. Thus, the symmetries of the system are no longer determined by the group G, but by the smaller group H (the unbroken subgroup) instead. The choice of the minimum of the system corresponding to some point at the ground states (or vacuum manifold), is randomly determined and can differ for different regions of the space if the regions are separated by a distance greater than some finite correlation length ξ. Such mechanism can lead to formation of defects, and it is known as Kibble mechanism [Kib76], being generic for all type of phase transitions, including those in CMP systems. As it happens in CMP systems where the symmetries spontaneously broken are restored as the system increases temperature until it reaches some critical temperature T_c, spontaneously broken symmetries in field theories (e.g. symmetries of elementary particles) are also expected to be restored above a critical temperature. In the cosmological context the breaking pattern showed above implies in successive phase transitions in the very early Universe, in which defects are formed [KT90; VS94].

In what follows, we briefly discuss about the topology of the defects: domains walls, monopoles, textures and cosmic strings.

2.2 Topological Classification of Defects

In order to determine what kind of topological defect emerges for a given SSB transition $G \to H$, one may study the content of homotopy groups $\pi_k(G/H)$ of the vacuum manifold $\mathcal{M} = G/H$, since the defect to arise is strictly determined by the topology of $\mathcal{M}$. When the vacuum manifold $\mathcal{M}$ has a non-trivial topology, is multiply connected, $\pi_k(G/H) \neq 1$ (1 corresponds to the trivial topology), stable topological defects of dimension[6] $2-k$ will appear with a characteristic length scale of the size of the correlation length ξ [VS94; JRS03; Ken06].

Below, we present further details about domain walls, monopoles and textures, where the type of non-trivial mapping of the vacuum manifold $\mathcal{M}$ in each defect is specified. Cosmic strings being the main topic of this manuscript will be left for a more extensive presentation in Section 2.3 and Chapter 3.

[6]This rule does not hold for the formation of textures where $k = 3$ as evidenced in the table 2.1.

2.2.1 Domain Walls

Domain walls appear when the vacuum manifold $\mathcal{M}$ of the SSB phase transition is disconnected, consisting of several components. In this case we have a breaking of a discrete symmetry associated, as $\pi_0(\mathcal{M})$ is non-trivial, where π_0 is the homotopy group representing disconnected components. For instance, the symmetry breaking $G \to H$, where $G = \mathcal{Z}_2$ and H is the trivial group, leads the vacuum manifold to be given by $\mathcal{M} = G/H = \mathcal{Z}_2$. Therefore, the homotopy content of the vacuum manifold is $\pi_0(\mathcal{M}) = \mathcal{Z}_2$, where the $\mathcal{Z}_2$ symmetry $\Phi \to -\Phi$ is spontaneously broken when the field chooses on $\langle\Phi\rangle = \pm\eta$. Hence, domain walls are formed at the boundaries whenever the field changes between regions of the different vacuum expectation values $+\eta$ and $-\eta$, see Fig. 2.2. The formation of analogous defects in CMP is known as grain boundaries [KT90; VS94].

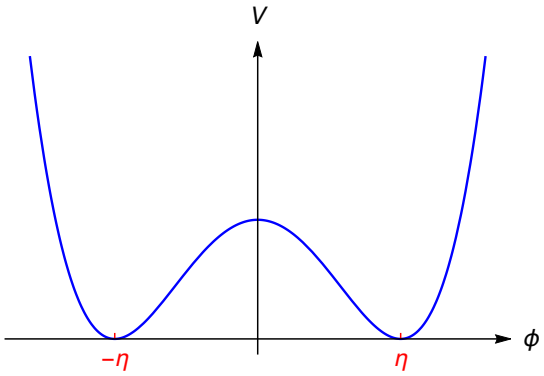

FIGURE 2.2: Symmetry breaking potential $V(\Phi) = \frac{\lambda}{4}(\Phi^2 - \eta^2)^2$.

Topological defects are source of gravitational fields which are important to be considered due to their cosmological implications. The gravitational effects by domain walls are exotic. Indeed the gravity of walls (2D defects) is very different from ordinary massive planes, the gravitational field of such objects is repulsive rather than attractive. Then, test particles are repelled when in presence of the walls, besides walls repel one another. However, contrary of cosmic strings, light is not deflected by domain walls [Vil81; KT90].

2.2.2 Monopoles

The monopoles (and hedgehogs in CMP) are point-like defects formed when the vacuum manifold $\mathcal{M}$ possess non-contractible two-spheres S^2, that is $\pi_2(\mathcal{M}) \neq 1$. For example, monopoles arise when the $SO(3)$ group is spontaneously broken to $U(1)$ group. In this case the vacuum manifold has homotopy group $\pi_2(G/H) = \pi_1(H)/\pi_1(G) = \mathcal{Z}/\mathcal{Z}_2$ [KT90]. Since $\pi_2(G/H) \cong \pi_1(H)$, if G is simply connected[7] $\pi_1(G) = \pi_2(G) \cong 1$, then once a symmetry group G is broken down to a subgroup $H = U(1)$ monopoles are formed with homotopy group $\pi_1(U(1)) = \mathcal{Z}$. The first field theory solution of monopoles were found independently by 't Hooft [Hoo74] and Polyakov [Pol96], and for that reason it is

[7] This is not the case of the $SO(3)$ group since it is multiply connected.

known as 't Hooft-Polyakov monopoles. 't Hooft showed their existence through the Georgi-Glashow model [GG72] which possesses the symmetry of the $SO(3)$ group, but it is represented by symmetry breaking pattern $G \to H$ in which the group of symmetry $SU(2)$ is broken to $U(1)$ group. Thus, as the $SU(2)$ group is simply connected, we have $\pi_2(SU(2)/U(1)) \cong \pi_1(U(1)) \cong \mathcal{Z}$. A very interesting fact is that since the GUT passes by several stages of breaking of symmetries down to $U(1)$ group: $H = SU(3) \times U(1)$, the existence of monopoles was unavoidable in the very early Universe, as they are predicted into the GUT. Even though we do realize that monopoles (as others defects) are expected to exist in virtue of topological reasons, still in the year of 1931, Paul Dirac [Dir31] already predicted the magnetic monopoles from quantum electrodynamics theory without using any topological arguments.

Barriola and Vilenkin [BV89] have provided an approximate solution of the Einstein field equations for a static global monopole, where the spacetime is revealed to be spherically symmetric. On the surface $\theta = \pi/2$ (or $z = const.$), the gravitational effect is that of a conical geometry due to a deficit angle (as in the cosmic string metric (3.13) in Section 3.2) plus the gravitational contribution of a tiny mass at the core. Exact solutions of the Einstein equations [HL90; SL91] showed that the gravitational field of the core of monopoles is repulsive. However, except the tiny repulsive effect of the core, monopoles do not exert gravitational pulling on surrounding massive objects. Moreover, the geometry around a monopole generates gravitational lensing in a similar fashion to any spherically symmetric object. Besides, monopoles have been believed to cause some other interesting cosmological implications: anisotropies in the cosmic microwave background, density fluctuations that can evolve into clusters and galaxies and a moving monopole can produce wakes which lead to accretion of matter surrounding it [VS94].

We should mention here that domain walls and monopoles are apparently discarded to exist after the inflation era; if there exist such defects somewhere in the Universe, because of their huge amount of energy they would have dominated the energy density of the Universe and then close it. In fact that was the main reason motivating the idea of inflation, because if the Universe has inflated by a huge factor, the existence of defects as domain walls and monopoles should be highly constrained or totally diluted at present [Kib97; JRS03].

2.2.3 Textures

Textures are very generic defects that occur always when a non-abelian group of symmetries is continuously broken. The vacuum manifold possesses the non-trivial homotopy group $\pi_3(\mathcal{M}) \neq 1$ with non-contractible three-spheres S^3 [Tur91]. As an example of symmetry breaking that gives rise to such objects we have the $SO(4)$ group spontaneously broken to $SO(3)$, so that we obtain $\pi_3(SO(4)/SO(3)) = \mathcal{Z}$ [VS94; Gan01]. Contrary to other defects, formation of textures does not require the scalar field to vanish anywhere. As the scalar field is present everywhere in the ground state, the energy is then uniformly distributed. For that reason, textures have no core unlike cosmic strings, for example [Gan01]. Actually, they may not be considered absolutely as defects

also because the scalar field is not topologically constrained to the vacuum manifold [VS94; Kib97]. Texture-like objects also appear in superfluid ^{3}He, some LCs phases and quantum chromodynamics. They could be three, two and one dimensional objects, and also point-like defects (the Skyrmions in three dimensions [Sky61]) [Chu+91; VS94].

Although textures can exist as stable objects, they may also be unstable and they can collapse. The collapse of textures can lead to strong gravitational fields which are very different from those with collapse of ordinary matter [VS94]. The solution for the Einstein equations from a spherically symmetric collapse shows that the spacetime geometry depends on a deficit angle which is time and space dependent, see Nötzold [Nöt91] for example. Besides, if massive objects have no angular momentum with respect to the texture origin, there are no gravitational force acting on them.

Interestingly, textures could survive to the inflation period because of their massless forming feature. Then, they are expected to be observed at present. Indeed, Cruz et al [Cru+07] have detected features from the CMB consistent with existence of cosmic textures. However, five years later a work by Feeney et al [Fee+12] which considers a more extensive data showed no evidence of textures.

In the Table 2.1, we have summarized the different types of possible cosmic topological defects.

Table 2.1: Summary of defects according topology and dimension.

Topological defect	Dimension	Classification	Non trivial mappings in $\mathcal{M}$
Domain walls	2	$\pi_0(\mathcal{M})$	Disconnected
Cosmic strings	1	$\pi_1(\mathcal{M})$	Non-contractible loops
Monopoles	0	$\pi_2(\mathcal{M})$	Non-contractible S^2 spheres
Textures	-	$\pi_3(\mathcal{M})$	Non-contractible S^3 spheres

In the next section we show how cosmic strings can be formed in the Abelian field theory based on the $U(1)$ group, which contains string-like solutions.

2.3 Cosmic Strings

The theoretical justifications are more favorable for the existence of cosmic strings "nowadays", since there exist some models where they have been formed during late stages of the inflation period. Because of that and their incredible cosmological consequences, cosmic strings have dominated the subject (cosmic topological defects) in the literature during the past years [Kib97]. To realize the importance of cosmic strings, it is enough to remind that they have been considered as seeds for formation of galaxies [Zel80; Vil85], for quite some time

until this idea was ruled out by cosmic microwave background measurements. Besides cosmic strings being well predicted into the GUT, the supersymmetric extension (SUSY GUT) to this model provides a route to the formation of such objects as well. For instance, Jeannerot et al [JRS03] examined all possible SSB patterns from the large possible SUSY GUT gauge groups down to the standard model $SU(3) \times SU(2) \times U(1)$ and concluded that cosmic string formation was unavoidable. However, the SUSY still has to pass experimental verification, since the first run of the LHC found no evidence for supersymmetry. Another possibility for generation of cosmic strings is during the brane inflationary epoch [DT99]. More specifically, they may have been abundantly produced by brane collision towards the end of this period [ST02]. In this case, cosmic strings are seen as lower-dimensional D-branes which are one-dimensional in the non-compact directions. On the contrary of GUT strings, strings in braneworld appear with a spectrum in tension.

Cosmic strings and disclinations/dislocations (line-like defects) in CMP appear as the topology of the vacuum manifold is non-trivial due to the existence of non-contractible loops (can not be contracted to a point) in the vacuum manifold [VS94; Kib76]. The simplest model that gives rise to cosmic strings consists in the Abelian theory of a local (or global) symmetry breaking of the $U(1)$ gauge group. The field solutions for this theory was first found by Nilsen-Olesen [NO73]. In formation of strings the non-trivial homotopy group is $\pi_1(\mathcal{M}) = \mathcal{Z}$, where the fundamental group $\mathcal{Z}$ is the group of integers that transform with a phase multiple of 2π, with ground state given by $\mathcal{M} = S^1$, which defines a circle [HK95; CK10]. In this theory the field Φ is a complex scalar that self interacts according to a "Mexican hat" potential $V(\Phi) = (\lambda/4)(\Phi^*\Phi - \eta^2/2)^2$. Below a critical temperature T_c, the scalar field first null at high temperatures, acquires a vacuum expectation value $\langle\Phi\rangle = (\eta/\sqrt{2})e^{i\vartheta(\theta)}$, where $\vartheta(\theta)$ is an arbitrary phase factor varying on the scale of a correlation length ξ. That is, the choice of the phase factor is given independently in different regions of the space separated by length ξ. Besides, the periodicity of the function $\vartheta(\theta)$ defines a circle where any winding must be defined as: $n = (\vartheta(2\pi) - \vartheta(0))/2\pi$, which is integer number known as winding number ("topological invariant") [Pre86]. Local cosmic strings have an interior magnetic flux which is quantized by the winding number as $\Phi_B = 2\pi n/e$, in the same way as the magnetic flux lines in superconductors [Abr57]. The asymptotic form of the field solutions far from the core assumes that the energy decays exponentially to zero at infinity as the energy per unit of length of string is finite. For a $U(1)$ cosmic string, the mass per unit of length is given by $\mu_0 = T_0 \approx \eta^2$, where T_0 is the string tension. In the GUT scale, $\eta \approx 10^{16}$ GeV, which means a cosmic string with enormous energy [VS94]. In the case of a global symmetry breaking, the same topological conditions for formation of local cosmic strings are considered but now the vector potential in the $U(1)$ Lagrangian is set to zero. In other words, this means absence of magnetic flux associated to global strings. For a global cosmic string the mass energy density is of the form $\mu_0 \approx 2\pi\eta^2 \ln R/\delta$, where R is a cut-off radius and δ is the string core thickness [Vil84; VS94].

2.3.1 Observational Evidences of Cosmic Strings

There are many theoretical justifications for the existence of cosmic strings, but the observational evidences are still feeble and mostly indirect. Nevertheless, if cosmic strings do exist, important cosmological effects should be observed as consequence. Among the possible ways of observing their presence in the Universe are: the gravitational lensing signatures (see Section 3.2.1) and gravitational waves left behind by such objects. The presence of a cosmic string somewhere in the Universe affects light trajectories, forming double images of objects behind the string. Such effect is known as planar gravitational lensing and has not been detected yet. Curiously, the observation of a pair of giant elliptical galaxies was erroneously reported by Sazhin et al. [Saz+03], as detection of lensing signatures induced by a cosmic string. However, high quality data from the Hubble space telescope showed that was not a lensing effect (two images of the same galaxy), but a pair of similar galaxies [AHP06; Saz+06]. Another possibility for detecting cosmic strings is through observation of gravitational waves, since the oscillating string loops created as a mechanism for loss of energy by strings emit gravitational radiation. Infinite cosmic strings also emit gravitational radiation as the small-scale structures (wiggles) on the string are source of gravitational waves as well [VV85; VS94; HK95; BPOS18]. Cosmic strings can also be observed by formation of a wake of matter behind moving strings. Actually, this is an important fact that may corroborate the density inhomogeneity in the Universe. However, maybe the most suitable manner to observe strings is through the measurements of the induced anisotropies in the cosmic microwave background radiation [Kib97; CPV11]. For example, the conical geometry of a cosmic string may cause discontinuity in the temperature of the cosmic microwave background as a string moves through the space. Such phenomenon is known as Kaiser-Stebbins effect [KS84].

Data on the CMB collected from *Planck Satellite* have not confirmed the existence of these objects yet, but they have set upper boundaries on their mass-energy density $G\mu_0 < 10^{-7}$ $(c = 1)$ [Ade+14]. As warned by Copeland and Kibble [CK10], "*Both cosmic strings and superstrings are still purely hypothetical objects. There is no direct empirical evidence for their existence, though there have been some intriguing observations that were initially thought to provide such evidence, but are now generally believed to have been false alarms. Nevertheless, there are good theoretical reasons for believing that these exotic objects do exist, and reasonable prospects of detecting their existence within the next few years.*" Indeed, the search for cosmic strings is currently still very active and it happens in all the fronts mentioned above: CMB radiation measurements [Her+17] and gravitational wave bursts [SES17].

It is worth mentioning here that topological defects found in CMP systems have been explored as a laboratory for better understanding of the ideas of cosmology. For example, string-like defects as line disclinations in liquid crystals, vortex-line in superfluid helium and magnetic flux lines in type II superconductors have been used for creating analogies with cosmic strings. On the other hand, such analogies have helped out the CMP defects be better comprehended by themselves.

In the next section, we explain the formation of linear defects in LCs, so that it becomes clear how incredible is the analogy behind these two "different universes".

2.4 Topological Defects in Liquid Crystals

In 1888, the botanist Friedrich Reinitzer reported the physicist Otto Lehmann about the existence of certain organic substance (cholesteryl benzoate) that curiously exhibited properties of both liquid and solid. Besides having been assigned to Lehmann the invention of the term *liquid crystal* to describe such substance, he was the first to detect the birefringence (anisotropy) and main structural properties of nematic[8] substances. But it was just in 1922 that Georges Friedel in collaboration with Grandjean rigorously described the mesophases (nematic, smectic and cholesteric) according a molecular order criterion [Fri22]. Surprisingly, even after these interesting findings, the study of LCs gradually lost interest. The interest for physics of liquid crystal was intentionally revived by Frank [Fra58], who introduces the word "disinclination" later renamed *disclination* for line singularities in LCs. However, maybe the most important fact about the study of LCs was the contribution of Pierre-Gilles de Gennes, rewarded by the Nobel Prize in 1991 for his studies on Soft Matter.

The structure of a liquid crystal can be understood as a fluid made of rod-like (cigar-shaped) molecules being symmetric by rotation about its own axis. At high temperatures no order is established, as thermal agitation effects domain dipole ordering effects all molecules are equally oriented, and the phase is isotropic (an ordinary liquid). However, when the temperature cools down interactions (dipole-dipole interactions) between the molecules lead them to be nearly aligned (approximately parallel to each other on average). Such ordered configuration is known as nematic phase, which is symmetric under rotations around a parallel axis to the molecules (average order). The orientation of the molecules in the LCs is measured by introduction of an order parameter, which is zero in the isotropic phase and non-zero in the nematic phase. Such order parameter is related to a unit three vector $\vec{n}$ named *director field*, which describes the average direction of alignment relative to the axes $\vec{a}$ (unit vector) of the individual molecules, see Fig. 2.4. If we chose $\vec{n}$ along the axis z, we find that the degree of orientational order is given by $s = (1/2)\langle 3\cos^2\theta - 1\rangle$ [Tsv42]. For the most ordered phase, we would have $\theta = 0$ or $\theta = \pi$, with the molecules $\vec{a}$ parallel to the optical axis $\vec{n}$. On the other hand, when the sample is entirely random we should get $s = 0$. Because the molecules are rod-like the director vector has no preferred polarity, that is $\vec{n}$ and $-\vec{n}$ are equivalent. The orientation of the director field leads to formation of defects, and it is given by an angle that changes as $2\pi m$, where the topological factor m gives the strength (winding number) of the defect. For example, when the director field $\vec{n}$ goes around π along a closed loop as we circle around the defect, $m = \pm 1/2$ disclinations arise. On the other hand, when the director points outwards or inwards everywhere,

[8] The nomenclature *nematic* was introduced later by Friedel to describe Lehmann's thread-like liquids.

defects with strength $m = \pm 1$ appear. More precisely, for disclination in the z-const plane ($\vec{n}$ confined to planes perpendicular to the defect axis), the director field components are $\vec{n} = \cos(m\phi + \phi_0)\hat{x} + \sin(m\phi + \phi_0)\hat{y}$, where m measures the director field rotation as one goes around the defect, ϕ is the angular coordinate and ϕ_0 is a constant parameter. The two-dimensional cross-section for $m = 1$ disclinations is well represented in Fig. 2.3 [KL07; GPP95].

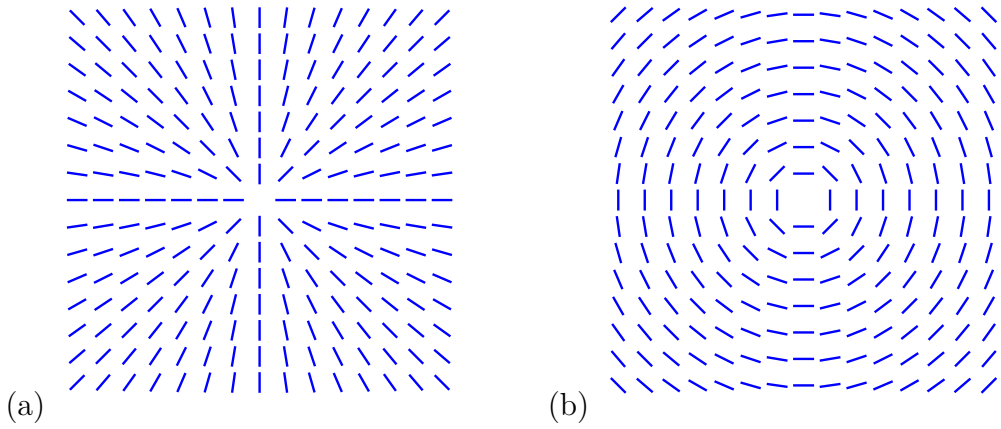

FIGURE 2.3: Director field configurations for disclinations in NLCs with $m = 1$. (a) For $\phi_0 = 0$ (radial director field). (b) For $\phi_0 = \pi/2$ (circular director field) .

Although defects in LCs are unwanted in most technological applications (as in displays, for example), once they are well controlled they could become a nice aspect for many other devices (microlenses, vortex beam generators...) [GBY17]. In Chapter 5, we will discuss the optical properties of a medium made of NLCs that works as an optical concentrator device. Moreover, topological defects in NLCs are on their own of great interest for the study of physics because their stupendous physical properties, and of course, due to the possibility of using them as a way of "testing" ideas of cosmology in the laboratory, taking advantage of the similarity with aspects of formation and light propagation.

Below, we discuss more about the interface between liquid crystals and cosmology by showing how defects are formed in the nematic phase and how this process obeys the Kibble mechanism. The isotropic-nematic phase transition will provide a better insight into the formation of defects during a SSB process, regarding to concepts in cosmology which are not easly tractable.

2.4.1 Isotropic-Nematic Phase Transition

Spontaneous phase transitions in LCs are strictly related to the production of defects in cosmology, as the Kibble mechanism used to describe the formation and evolution of defects in the cosmological context revealed to be relevant in the formation of defects in nematic liquid crystals [Chu+91; Bow+94]. Indeed, the different phases in LCs can be obtained through SSB transitions, which lead to the appearance of topological defects exactly as it happens in cosmology; the sample in the most symmetric phase (at high temperatures) cools down into a less symmetric phase (at low temperatures), and during this

process "defects" can appear. This is exactly what we have in the isotropic-nematic phase transition; suitably we can identify the isotropic phase where the molecules are randomly oriented as having the symmetry (invariant under spatial rotations and translations) of the $SO(3)$ group, and as the phase transition occurred the symmetry is reduced to the $O(2)$ group that characterize the order parameter in the nematic phase, where the molecules are locally aligned. Therefore, the transition from the isotropic to the nematic phase can be understood as a spontaneous breaking of symmetry (global because the absence of gauge fields in NLCs) with pattern given by $SO(3) \to O(2)$, in which $\mathcal{M} = SO(3)/O(2) = S^2/\mathcal{Z}_2$ represents the ground states of the nematic phase. Here, the unbroken group is invariant under rotations about the molecular axis and rotations of π about axes which are perpendicular to the molecular axis. Analogously to what happens in cosmology, during such transition we also have formation of defects. The string-like defects (disclination lines) are formed due to the non-trivial topology $\pi_1(\mathcal{M}) = \mathcal{Z}_2$ of the ground state manifold. The $\mathcal{Z}_2$ string corresponds to the non-trivial path (non-trivial loop in $\mathcal{M}$) to identify two diametrically opposite points on the S^2 sphere, since the director field rotates π as one goes around the defect [Chu+91; Pre86; Rao02]. In figure 2.4 we attempt to schematize the isotropic-nematic phase transition.

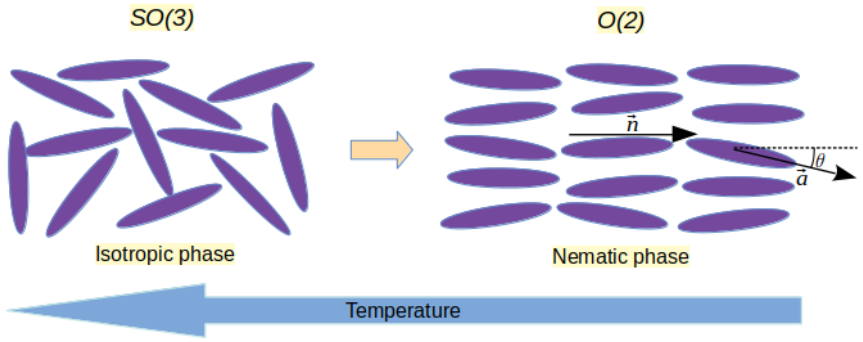

FIGURE 2.4: The isotropic-nematic phase transition being represented (with director field $\vec{n}$ and molecular axes $\vec{a}$).

Interestingly, there is a model in relativistic field theory (cosmology) that treats of the same spontaneous breaking pattern discussed here, named Alice string electrodynamics (also called Alice string theory) [Sch82], which is perfectly analogue to the formation of $\mathcal{Z}_2$ strings in NLCs [Pre86; VS94; HK95].

2.4.2 Nematic Liquid Crystals as a Laboratory for Cosmology

In this section, we briefly discuss how strings arise in the isotropic-nematic phase transition in a liquid crystal sample by means of the Kibble mechanism, which by the way was first suggested to account for formation of defects in cosmology. Zurek [Zur85] was the first to suggest an experiment in a CMP system (superfluid helium) for observing formation of defects according to predictions of cosmological theories. A bit later in two very cited works by Chuang et al [Chu+91] and Bowick et al [Bow+94], the same proposal with using NLCs

came up; the probability of formation of a network of disclination lines observed during the isotropic-nematic phase transition is in total agreement with the expected theoretical value via Kibble mechanism for the ground state of the nematic liquid phase, see Fig. (2.5). As the sample of NLCs cools down,

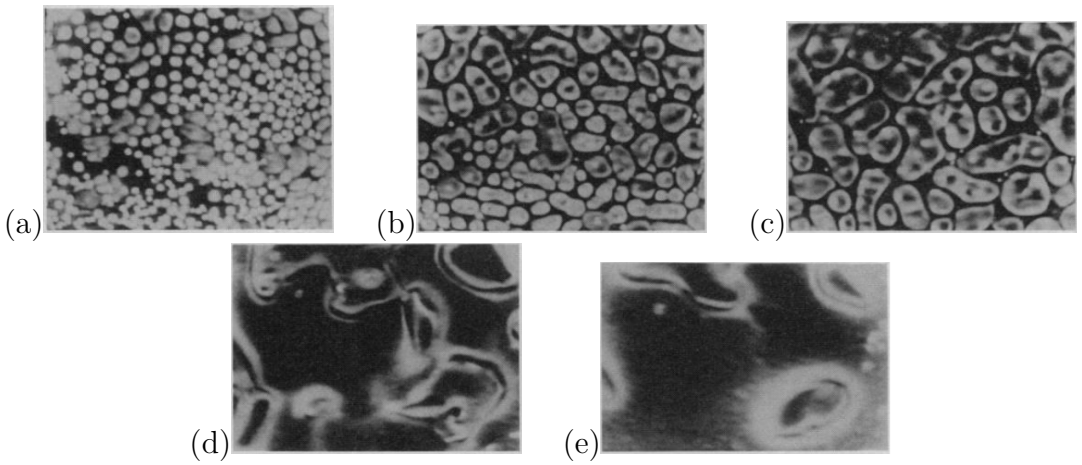

FIGURE 2.5: A sequence of five images of defects formation at the isotropic-nematic phase transitions in liquid crystal. (a) Bubble nucleation (2s), (b) growth (3s), (c) bubble coalescence (5s), (d) string formation (11s) and (e) string coarsening (23s) [Bow+94].

the bubbles of the ground state (nematic phase) nucleate. During the bubble nucleation the director field takes random directions, and for energetic reasons they will be roughly oriented inside each bubble. Here, the correlation length will depend on aspects such as the rate of collisions between bubbles and the bubble sizes. The small bubbles have too much energy, then they reduce the total energy of the system by growing, which consequently leads them to merge again. As a set of bubbles collide there is a considerable probability of disclination (string) and loops are formed at the bubble boundaries. Besides the Kibble mechanism successfully predicted the density of strings per bubble, it also provides the scaling dynamics of the string network and aspects of the defect-antidefect correlation [Bow+94; Chu+91].

We have here a perfect analogy of what happens in the laboratory during the cooling of a NLCs sample with phase transitions in the very early Universe. In fact, disclinations are perfectly analoguous to *global cosmic strings*; because the absence of gauge fields in NLCs, the global strings become most similar to NLCs dynamics than local cosmic strings do [HK95].

In the next chapter, we discuss further details about the geometric aspects of linear topological defects. There exists a way to propose an effective geometry to study of light ray trajectories in LCs and it is showed to be analogue to the geometry of the cosmic string spacetime.

Chapter 3

Geometric Aspects of Linear Defects

***

Cosmic strings are very intriguing linear objects having sizes much greater than their width (the same of an atomic nucleus, or smaller) and possessing an enormous energy. For instance, an ordinary GUT string with length at the order of the diameter of the Sun would have approximately the same solar mass [HK95]. Cosmic strings are analogs of linear defects in condensed matter physics, following the same mechanism of formation and evolution. Among them, the line disclinations are present in nematic liquid cristals [Chu+91; Bow+94]. The analogy also holds from the stand point of gravitation [Mor00], as effects on light propagation due to both objects are equivalent [SM05]. Hence, we emphasize that CMP systems are an incredible laboratory for testing cosmological ideas.

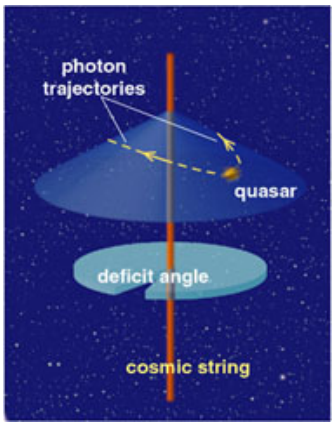

FIGURE 3.1: The geometry surrounding a cosmic string affecting light trajectories [Gan01].

In the following we present the gravitational effects of regular[9] cosmic strings.

[9] In the remainder of this thesis, besides the term *regular*, we also make mention to regular string as *idealized*, *straight* and *unperturbed* string.

Besides, we discuss more about the analogy between cosmic strings and disclinations, showing a geometric method for propagation of light of particular interest in our work.

3.1 Geometric Theory of Gravitation

The Special Theory of Relativity (STR) replaces the Newtonian mechanics in the study of moving bodies with speed at the order of the speed of light. The STR states that each event is represented for the four coordinates (x, y, z, t) in the Minkowskian spacetime

$$ds^2 = dt^2 - dx^2 - dy^2 - dz^2 = \eta_{\mu\nu} dx^\mu dx^\nu, \tag{3.1}$$

where $\eta_{\mu\nu} = \text{diag}\,(1, -1, -1, -1)$. However, the generalization of this theory taking into account gravity gave rise to a most general theory, named General Theory of Relativity (GTR). An important statement in this theory is that a non-inertial frame is equivalent to a given gravitational field, that is, we can not distinguish between the motion of a particle under the influence of a gravitational field or in a reference frame with the same acceleration than by the gravitational field, this is the so called *Principle of Equivalence*. Therefore, the GTR differs from the STR with respect to the geometry of the space representing each one; whereas the later is described in a flat spacetime, the former is associated with a curved spacetime (pseudo-Riemannian manifold) as a direct consequence of the principle of equivalence. Therefore, the line element in a curved geometry is given by

$$ds^2 = g_{\mu\nu} dx^\mu dx^\nu, \tag{3.2}$$

where $g_{\mu\nu}$ are the components of the metric tensor which depends on the space and time coordinates. In general relativity, gravity is essentially comprehended as an effect of the geometry of the spacetime. This fact is well represented in the Einstein field equations:

$$R_{\mu\nu} - \frac{1}{2} g_{\mu\nu} R = \kappa T_{\mu\nu}, \tag{3.3}$$

with κ being a constant called *Einstein's gravitational constant*. $R_{\mu\nu}$ is the Ricci tensor components,

$$R_{\mu\nu} = \frac{\partial \Gamma^\gamma_{\mu\nu}}{\partial x^\gamma} - \frac{\partial \Gamma^\gamma_{\mu\gamma}}{\partial x^\nu} + \Gamma^\sigma_{\mu\nu}\Gamma^\gamma_{\gamma\sigma} - \Gamma^\sigma_{\mu\gamma}\Gamma^\gamma_{\nu\sigma}, \tag{3.4}$$

where

$$\Gamma^\mu_{\gamma\sigma} = \frac{1}{2} g^{\mu\lambda} \left(\frac{\partial g_{\lambda\gamma}}{\partial x^\sigma} + \frac{\partial g_{\lambda\sigma}}{\partial x^\gamma} - \frac{\partial g_{\gamma\sigma}}{\partial x^\lambda} \right) \tag{3.5}$$

is the usual Levi-Civita connection of Riemann spaces (Christoffel symbols). The Ricci scalar curvature R is obtained by taking a contraction of the Ricci tensor $R = g^{\mu\nu} R_{\mu\nu}$. The left-hand side of this equation provides the geometry of

the spacetime whereas the right-hand side, $T_{\mu\nu}$, gives the mass (energy) content of the gravitational source. Then, we have an equivalence between energy and geometry, where the presence of a given object in the Universe deforms the geometry of the surrounding spacetime as a reaction to its amount of energy. Thus, the general relativity is indeed a geometric theory, with gravity not being an ordinary force but a property of spacetime geometry. The Newtonian gravity is retrieved in the ordinary Euclidean space for the weak energy limit of the Einstein equations. In addition, the value of the constant κ in the equation (3.3) is derived as the Newtonian limit is reached [Car01; Car04].

3.1.1 Geodesic Equation

Another important feature of general relativity is the way a given object located in a curved spacetime moves. Actually, the object moves in accordance with the geometry in its vicinity, namely, the gravitational field tells how the particle has to move, defining the geodesics [WF00]. The motion of a particle in a Riemannian manifold can be derived from the variational principle

$$\delta \int \Big(g_{\mu\nu} \frac{dx^\mu}{ds} \frac{dx^\nu}{ds} \Big)^{1/2} ds = 0, \tag{3.6}$$

where s is a parameter along the geodesic line with $ds = (g_{\mu\nu} dx^\mu dx^\nu)^{1/2}$ and from which geodesic equations follow,

$$\frac{d^2 x^\gamma}{ds^2} + \Gamma^\gamma{}_{\alpha\beta} \frac{dx^\alpha}{ds} \frac{dx^\beta}{ds} = 0. \tag{3.7}$$

Here, $\Gamma^\gamma{}_{\alpha\beta}$ is the usual Levi-Civita connection (see Eq. (3.5)). Regarding the equation above, we assumed $ds^2 \neq 0$, such that

$$g_{\mu\nu} \frac{dx^\mu}{ds} \frac{dx^\nu}{ds} = 1 \tag{3.8}$$

along the geodesic line. This is valid for timelike geodesics, which describe the motion of massive particles in the gravitational field. Here, the affine parameter s in Eq. (3.8) can be identified as the proper time. On the other hand, for null geodesics, where we have $ds^2 = 0$, the parameter s cannot be used as the affine parameter along the geodesic line. However, we should still find another affine parameter λ for which the null geodesic equation are given in the form (3.7)

$$\frac{d^2 x^\gamma}{d\lambda^2} + \Gamma^\gamma{}_{\alpha\beta} \frac{dx^\alpha}{d\lambda} \frac{dx^\beta}{d\lambda} = 0, \tag{3.9}$$

where now

$$g_{\mu\nu} \frac{dx^\mu}{d\lambda} \frac{dx^\nu}{d\lambda} = 0 \tag{3.10}$$

along the geodesic line. The null geodesics describe the light propagation in the gravitational field [Car01; Car04].

3.2 Weak Field Approximation for Regular Cosmic String

The Einstein field equations are commonly difficult to solve. In order to get exact solutions[10], restrictions are imposed on the metric and energy-momentum tensor, such that the problem is endowed with a significant degree of symmetry. Moreover, when the gravitational field is weak enough, a method called linearized gravity (or weak field approximation) can be used as a great approximation for solving several problems. The idea of such method consists in expanding the components of the metric tensor as $g_{\mu\nu} = \eta_{\mu\nu} + h_{\mu\nu}$, where $\eta_{\mu\nu}$ is the ordinary component of the Minkowskian space and $|h_{\mu\nu}| \ll 1$ is a perturbative term responsible for the curved spacetime.

In order to study the influence of a regular cosmic string on the geometry of the spacetime, one inserts the components of the energy-momentum tensor associated to these objects in Einstein field equations. Generally, equations in this context are solved only numerically [Gar85; LCM87]. But, some simplifications can be done in order to get qualitative information on the geometry. For instance, by considering the energy of the string confined to its core, the string energy-momentum tensor components can be approximated as δ-function source. That is, the string thickness is considered to be much smaller than any other dimensions. With this assumption, and considering that the gravity of the string is sufficiently weak to allow the use of the linearized Einstein field equations, Vilenkin [Vil81] was able to supply the spacetime geometry of a cosmic string for the first time. Note that the weak field approximation cannot be used in the case of supermassive strings, but only when $\eta << m_P$, with η being the energy scale of the symmetry breaking and m_P the Planck mass [VS94].

By considering the zero thickness limit, a static straight cosmic string located along the z-axis has the energy-momentum tensor components given by [Vil81; Vil85; VS94]:

$$T^{\mu}_{\nu} = \mu_0 \delta(x)\delta(y)\,\mathrm{diag}\,(1,0,0,1), \tag{3.11}$$

where μ_0 is the energy density per unit length of the string. For an unperturbed string (with no wiggle/kink), the energy density μ_0 exactly matches the line tension T_0, such that the equation of state of the string is written as $\mu_0 = T_0$ [Car90]. On the z-axis (string core), the spacetime curvature is infinite, whereas outside the string we may assume the gravitational field as being sufficiently weak such that the spacetime is nearly Minkwoskian $g_{\mu\nu} = \eta_{\mu\nu} + h_{\mu\nu}$, with $|h_{\mu\nu}| \ll 1$ being a perturbative term. Therefore, we can use the linearized Einstein equations, to obtain

$$h_{\mu\nu} = 8G\mu_0 \ln(r/r_0)\,\mathrm{diag}\,(0,1,1,0), \tag{3.12}$$

with $r = \left(x^2 + y^2\right)^{1/2}$ and r_0 is a cutoff length (set as the effective string radius) [Vil81; Pet94]. This solution is valid only within the region $r_0 < r \ll r_0 e^{1/4G\mu_0}$,

[10] The term "exact solutions" does not mean that the properties of the metric are fully known, but that solutions are given in term of the well-known analytic functions [Ste+09].

since the logarithm diverges at small and large distances from the defect. Introducing a new radial coordinate ρ as $(1-8G\mu_0\ln(r/r_0))r^2 = (1-8G\mu)\rho^2$, we obtain the line element in the new coordinates to order $G\mu_0$ as

$$ds^2 = dt^2 - dz^2 - d\rho^2 - (1-8G\mu_0)\,\rho^2 d\theta^2. \tag{3.13}$$

Finally, defining a new angular coordinate by $\phi = (1-4G\mu_0)\theta$, the line element (3.13) gets the Minkowskian form

$$ds^2 = dt^2 - dz^2 - d\rho^2 - \rho^2 d\phi^2. \tag{3.14}$$

This metric describes the spacetime where the geometry is flat everywhere (locally flat), except on the string core ($\rho = 0$). The geometry is not globally Euclidean, since the angular coordinate ϕ ranges from 0 to $2\pi(1-4G\mu_0)$. That is, the string introduces a small deficit angle in the spacetime, which is given by $\Delta = 8\pi G\mu_0$, with $G\mu_0 \ll 1$. Therefore, straight strings are linear defects for which the geometry is globally that of a cone [Vil81; VS94; HK95]. For a better understanding of the conical geometry of Eq. (3.14), see representation in Fig. 3.2; a slice is removed from a flat space and with identification of the edges, we get a cone. This process of "cut and glue" is known in theory of defects in solids as Volterra process [KV92]. Perhaps knowing the geodesics is the best

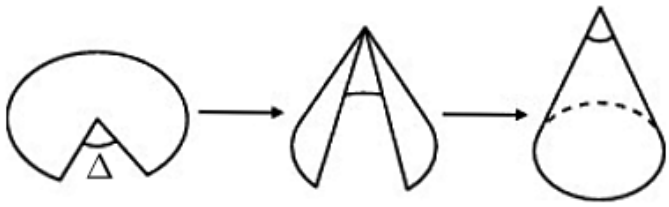

FIGURE 3.2: Cone of an angular deficit Δ (adapted from [FM08]).

way to understand the conical geometry of the cosmic string spacetime. In the conical space in the xy-plane, see figure (3.3), the frame in the left represents the geodesics in the coordinates of the metric (3.13), which are curved lines deflected by an angle Δ. In the right frame, the geodesics for the metric (3.14) are straight lines that intersect at one point on the space.

Although we have considered here the zero thickness limit model of cosmic strings, models in which they are considered as extended gravitational sources (with finite radius), with uniform/non-uniform energy density in its interior, show that the interior spacetime matches the exterior spacetime, being Minkowskian minus a wedge exactly as in Eq. (3.14) [His85; GI85; Lin85].

3.2.1 Gravitational Lensing

Regular cosmic strings do not exert gravitational pulling on non-relativistic particles at rest in its vicinity. That is, particles will keep their state of motion due to non-existence of any gravitational force acting on them. To understand

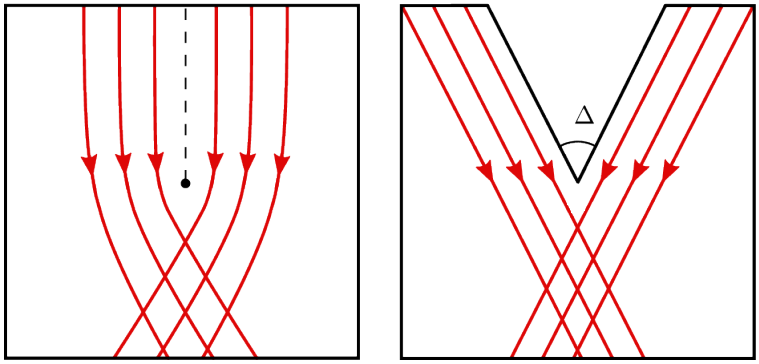

FIGURE 3.3: Geodesics in the conical space (left) and geodesics in the flat space with deficit angle Δ (right) (adapated from [FNB16b]).

it, first note that for a static gravitational source the components of the energy-momentum tensor can be written as

$$T^{\mu}_{\nu} = \text{diag}\,(\sigma, -p_1, -p_2, -p_3), \tag{3.15}$$

and then the Newtonian limit of the Einstein field equations is

$$\nabla^2\Phi = 4\pi G(\sigma + p_1 + p_2 + p_3), \tag{3.16}$$

with Φ being the Newtonian potential. For a non-relativistic gravitational source, $p_i << \sigma$, then $\nabla^2\Phi \cong 4\pi G\sigma$. However, for a straight string along z-axis, $p_1 = p_2 = 0$ and $p_3 = -\sigma$ (equivalence between energy density and tension), which leads the right-hand side of the Eq. (3.16) to vanish. Hence, this is a suggestion that straight strings do not interact with surrounding objects [VS94]. Otherwise, we can note that the Newtonian limit of the Einstein equations lead to the identification:

$$\Phi = \frac{h_{00}}{2}, \tag{3.17}$$

which means $\Phi = 0$ since $h_{00} = 0$ for regular strings [Car04]. In fact, the absence of a non-vanishing Newtonian potential is a consequence of the equality between the mass density and tension on the string: effects due to the energy density are canceled by effects of the tension, which acts as a gravitational source of opposite sign (negative pressure) [Kib97].

Even though regular strings do not produce any gravitational pulling, the globally conical geometry of their spacetime gives rise to interesting phenomena [VS94]. For example, the geometry around straight strings affects propagation of light giving rise to a phenomenon known as planar gravitational lensing; a light source behind the string will appear to the observer as two images, see Fig. (3.4). According to geometry of the Fig. (3.4), the angular separation $\varphi = 2\gamma$ between the two images is given by [Sch09]

$$\varphi = \Delta\left(1 + \frac{l}{d}\right)^{-1}. \tag{3.18}$$

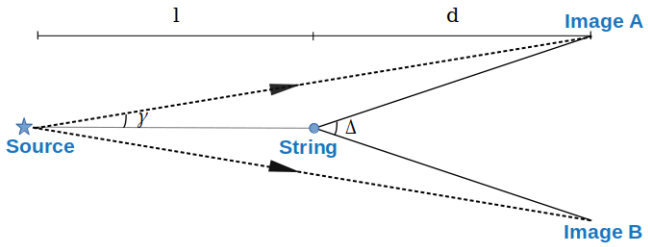

FIGURE 3.4: Planar gravitational lensing by a straight cosmic string (adapted from [Sch09]).

If the angular separation between the string and the source is greater than φ only a single image is formed [Vil84]. Unlike to what happens with stars (Eintein's rings), lensing effects by cosmic strings are purely planar. For a GUT string the angular separation is typically of the order of ≈ 2 arcsec [Saz+03; Saz+07].

3.3 Geometric Method for Disclination

The first geometric model for description of topological defects was built by Katanaev and Volovich [KV92], where they showed that defects in elastic solids (disclinations, dislocations...) can be described in the framework of Riemann-Cartan geometry. Following this standpoint, in this section, we describe an effective metric spacetime from which we can study the propagation of light in NLCs endowed with disclination into the gravity background.

In uniaxial anisotropic media as nematic liquid crystals, light propagation is described in terms of two indices, $n_\perp$ the ordinary refractive index where the medium behaves as an isotropic medium and $n_{||}$, the extraordinary refractive index that depends on the direction of propagation. In what concerns light propagation, one has to distinguish between an *ordinary ray* and an *extraordinary ray*. The ordinary ray propagates in such a way that the electric field of the electromagnetic wave remains perpendicular to the director $\vec{n}$. For instance, if we assume that the xz-plane contains the parallel vectors $\vec{N}$ ("refractive index vector") and wavevector $\vec{k}$ (that is $N_y = k_y = 0$), by solving Fresnel equation for uniaxial media, we find that the ordinary wave is polarized along the y-axis, and therefore orthogonal to the plane formed by the optic axis $\vec{n}$ and wave vector $\vec{k}$ [KL07]. On the other hand, the extraordinary wave propagates in such a way that the $\vec{E}$ has a non-vanishing component along $\vec{n}$, and the Poynting vector $\vec{S}$ differs in direction from that of the wave vector $\vec{k}$. In this case, energy velocity (energy propagation) is thus governed by a *ray index*

$$N_r^2 = n_\perp^2 \cos^2\beta + n_{||}^2 \sin^2\beta \tag{3.19}$$

with β being the angle between the director field and the Poynting vector, and differs from phase velocity, governed by another index, the *phase index*

$$N_p^2 = \frac{n_\perp^2 n_{||}^2}{n_{||}^2 \cos^2\gamma + n_\perp^2 \sin^2\gamma} \tag{3.20}$$

with γ being the angle between the director field and the wave vector [BW99; KL07]. Since the ray path is parametrized by the arc length l, the tangent unit vector along the path is thus $\vec{t} = d\vec{r}/dl$ and the angle β which measures the tangent orientation with reference to the director is given by $\cos\beta = \vec{t}\cdot\vec{n}$, see Fig. 3.5. In polar coordinates, $\vec{r}(l) = r\hat{r}$, thus $\vec{t} = \dot{r}\hat{r} + r\dot{\phi}\hat{\phi}$ where the "dot" stands for d/dl. For the radial director field configuration 2.3(a) with $\hat{n} = \hat{r}$,

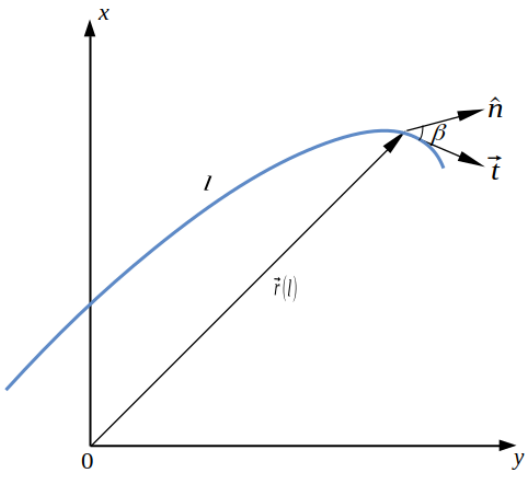

FIGURE 3.5: The parameter l and the position vector $\vec{r}(l)$ along the ray path, the tangent vector $\vec{t}$ and the director field $\hat{n}$ (optical axis) (adapted from [SM06]).

we thus have $\cos\beta = \dot{r}$. Besides, the two-dimensional Euclidean line element in polar coordinates $dl^2 = dr^2 + r^2 d\phi^2$ leads to $\dot{r}^2 + r^2\dot{\phi}^2 = 1$. In fact, this also follows from the normalization constraint $|\vec{t}|^2 = 1$. Therefore, we get $\sin\beta = r\dot{\phi}$. Rescaling the coordinates according to $\rho = n_\perp r$, the ray index in configuration (a) is then

$$N_r^2 = \dot{\rho}^2 + \alpha^2\rho^2\dot{\phi}^2, \tag{3.21}$$

where $\alpha = n_{||}/n_\perp$. It is clear that due to the anisotropy, N_r depends on the position on the curve followed by light, $N_r = N_r(\vec{r})$. Note that the isotropic limit holds for $n_\perp = n_{||}$. Extraordinary rays propagation obey the eikonal equation,

$$\vec{\nabla}N_r = \frac{d}{dl}\left(N_r\frac{d\vec{r}}{dl}\right) \tag{3.22}$$

which follows from the fact that the energy propagation for extraordinary rays obeys a variational prescription (Fermat's principle)

$$\delta\int_A^B N_r dl = 0, \tag{3.23}$$

where dl is the arc length element along the path, and A and B are two generic points on the path. Both Fermat's principle and geodesics in a Riemannian manifold obey a variational principle, then we realize that the equation (3.23) is a nice example of analogue gravity. Fermat's principle can be viewed as equivalent to Eq. (3.6), from which the geodesic equation Eq. (3.7) in an analogue Riemann space follows. That is, light rays obeying Fermat's principle

can be identified as geodesics in some Riemannian geometry [BW99]. Hence, the metric tensor is essentially determined by the refraction index [SM06; BDL16]:

$$\int_A^B ds = \int_A^B N_r dl, \tag{3.24}$$

where ds is the spatial part of the metric spacetime. That is, known the effective refractive index of a given medium it is possible to determine an effective geometry for light propagation. Therefore, light trajectories can be identified as geodesics in the curved spacetime:

$$ds_{4D}^2 = dt^2 - \sum_{i,j} g_{ij} dx^i dx^j, \tag{3.25}$$

where the sum term is purely the spatial part of the metric. The given trajectories by Fermat's principle in a three-dimensional spatial metric are the same from null geodesics in a four-dimensional metric, that considers the time coordinate part [PM11a]. From Eq. (3.24), we identifying $ds^2 = N_r^2 dl^2$, and by using Eq. (3.21), we obtain the line element

$$ds^2 = d\rho^2 + \alpha^2 \rho^2 d\phi^2, \tag{3.26}$$

which is exactly the cross-section with $t = \text{const.}$ and $z = \text{const.}$ of the cosmic string given by metric Eq. (3.13),

$$ds_{4D}^2 = dt^2 - d\rho^2 - \alpha^2 \rho^2 d\phi^2 - dz^2, \tag{3.27}$$

where $\alpha^2 = 1 - 8G\mu_0$ for the straight string. In a similar manner, the line element of the circular director field configuration 2.3(b), where $\hat{n} = \hat{\phi}$, is given by Eq. (3.27) but now with $\alpha = n_\perp / n_{||}$. Hence, light in a nematic liquid crystal with a disclination defect feels the effective conical geometry of a regular cosmic string. However, there is an important fact to be mentioned here: since for NLCs composed of elongated molecules, typically $n_\perp < n_{||}$ (optically positive nematic) [KL07], this leads the disclination of configuration 2.3(a) to be analogue of the more exotic cosmic string with excess of deficit angle ($\mu_0 < 0$), while the disclination configuration 2.3(b) mimics the ordinary cosmic string of positive mass density ($\mu_0 > 0$) [Mor00; SM05].

Light trajectories around a disclination are the geodesics of the effective geometry Eq. (3.27) as have been found in Refs. [PPFM98; SM06] they exhibit lensing effects as predicted by the conical geometry. Besides simulating the spacetime of cosmic strings, liquid crystals also have been used to mimic the Schwarzschild spacetime [PM11b].

Although we did not use it here, there is an alternative geometric model to study light propagating in a anisotropic medium. This method is based on the geometry of Finsler [JR94], and leads to the same result when used to describe disclination defects as the Riemannian geometry [SM05]. For more details about the more general Finslerian method, see Appendix A.1.

In Chapter 5 of this manuscript, we return to use the geometric method

(Riemannian geometry) discussed in this section when the study of light propagation in a hyperbolic metamaterial based on nematic liquid crystal.

Chapter 4

Wiggly String as a Waveguide

***

More realistic and refined models for cosmic strings show that long strings may not be perfectly straight but involve small-scale perturbations such as kinks and wiggles on them [AS90; BB90]. These cosmic strings are known as wiggly strings, which are basically a generalization of the regular cosmic string models [VV91; VS94]. However, the presence of wiggles generates a far away gravitational field contribution that may be responsible for an elliptical distortion of the shape of background galaxies [DB07; Fen12] or for the accretion of dark energy around the defect [GDJM06]. Besides, wiggles are a mitigating factor for increasing formation of wakes of matter behind a moving string [Kib97; CPV11].

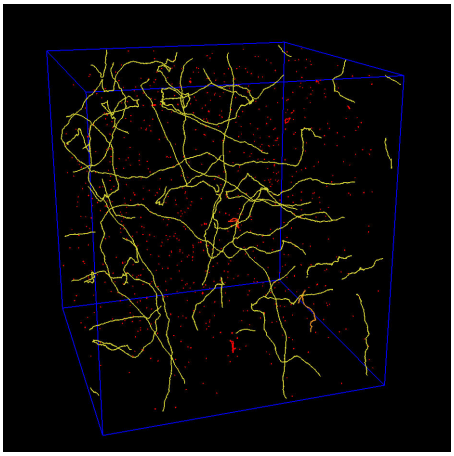

FIGURE 4.1: The "wiggliness" of long strings (in yellow) and small string loops (in red) in the matter era [AS90].

In this chapter we present the wiggly string gravity and its effect on propagation of massless and massive fields along the string axis. Besides that, we propose an analogy with an optical waveguide likely to mimic the wiggly string in laboratory [Aze+17].

4.1 The Wiggly Cosmic String

Because the similarity between regular and wiggly string, the gravity of those objects might be analogue. Roughly speaking, these objects differ from each other as the quantity of energy per unit length of string is larger on the wiggly string ought to the wiggles [HW90]. Thus, the averaging of the effect of these perturbations (wiggles) along the string increases the linear mass density $\tilde{\mu}$ and decreases the string tension $\tilde{T}$, respecting the equation of state $\tilde{\mu}\tilde{T} = \mu_0^2$. In fact, this is reached when we consider that the propagation of longitudinal speed $c_L = (-d\tilde{T}/d\tilde{\mu})^{1/2}$ for sound-type perturbations and transverse speed $c_T = (\tilde{T}/\tilde{\mu})^{1/2}$ for extrinsic perturbations are equivalent [Car90; Vil90; Gan01].

Similarly to the straight string case, an infinite wiggly string at rest lying along z-axis has the components of the energy-momentum tensor given by [VV91; VS94]

$$T^{\mu}_{\nu} = \delta(x)\delta(y)\,\mathrm{diag}\,(\tilde{\mu}, 0, 0, \tilde{T}). \tag{4.1}$$

Using the weak field approximation method to solve the Einstein's equations,

$$\begin{aligned} h_{00} &= h_{33} = 4G(\tilde{\mu} - \tilde{T})\ln(r/r_0), \\ h_{11} &= h_{22} = 4G(\tilde{\mu} + \tilde{T})\ln(r/r_0), \end{aligned} \tag{4.2}$$

are obtained as solution for the perturbative terms at $g_{\mu\nu} = \eta_{\mu\nu} + h_{\mu\nu}$, where $\eta_{\mu\nu}$ stands for the ordinary flat spacetime metric. Here, $r = \left(x^2 + y^2\right)^{1/2}$ and r_0 is a constant of integration that can be considered as the effective radius of the string [Vil81; Pet94]. Introducing a new radial coordinate r' as $(1 - h_{11})r^2 = (1 - 4G(\tilde{\mu} + \tilde{T}))r'^2$, the linearized line element representing the spacetime of a wiggly string can be found as[11] [VV91; VS94]:

$$ds^2 = (1 + 8\varepsilon\ln(r/r_0))\,dt^2 - dr^2 - \alpha^2 r^2 d\theta^2 - (1 - 8\varepsilon\ln(r/r_0))\,dz^2, \tag{4.3}$$

where $\alpha^2 = 1 - 4G(\tilde{\mu} + \tilde{T})$, with $4G(\tilde{\mu} + \tilde{T}) \ll 1$ meaning that the conical deficit angle $\tilde{\Delta} = 4G\pi(\tilde{\mu} + \tilde{T})$ associated to the string is very small. The straight string metric (3.13) is recovered by setting $\tilde{\mu} = \tilde{T} = \mu_0$ (absence of wiggles). The parameter ε is defined as the excess of mass-energy density, $2\varepsilon = G(\tilde{\mu} - \tilde{T})$. It must be emphasized that $G(\tilde{\mu} + \tilde{T})$ and ε are two independent parameters; the former accounts for the discrepancy between flat and conical geometries, whereas the latter accounts for the discrepancy between straight and wiggly strings. The solution Eq. (4.3) is only valid within the region $r_0 < r \ll r_0 e^{1/8\varepsilon}$, in order to avoid the logarithmic divergence at small and large distances from the defect. This metric is very similar to that from unperturbed string at least in the sense of representing a globally conical space, but now the deficit angle is larger than in the straight string case. The excess of mass-energy density represented by the parameter ε, leads the wiggly string to exert a gravitational pull on neighboring objects. Indeed, the term $h_{00} \neq 1$ provides a non-vanishing Newtonian potential $\Phi = h_{00}/2 = 2G(\tilde{\mu} - \tilde{T})\ln r/r_0$ [HK95; VS94]. Hence, a very important

[11] For mere convenience the primes from r in Eq. (4.3) have been dropped.

distinction from the regular strings comes out: because of the presence of wiggles non-relativistic massive particles will experience an attractive force when in the vicinity of a wiggly string.

In the next sections of this chapter, we are going to investigate effects caused by presence of the wiggles on propagation of light and massive particles around the wiggly string.

4.2 Propagation of Massless Fields

If we consider the direction of propagation as being perpendicular to the wiggly string (in the $z = const.$ plane), then it can be shown that the effective wiggly string metric can be reduced to [VS94]:

$$ds^2 = (1 + h_{00})[dt^2 - dr^2 - (1 - 8G\tilde{\mu})r^2 d\theta^2]. \tag{4.4}$$

Taking into account that equation (3.10) gives the light trajectories (null geodesics), it is simple to notice that any conformal factor (that appears multiplying all terms) in the metric tensor will not produce any effect on null geodesics. Hence, the factor $(1 + h_{00})$ in the metric tensor (4.4) does not affect light trajectories and can be dropped. Therefore, in a plane perpendicular to the string light trajectories in the spacetime given by metric (4.3) reduces to trajectories in the spacetime of metric (3.13). Thus, light behaves in the same way as in the vicinity of a regular straight string, that is, without experiencing any gravitational pulling. However, light is still affected by the conical geometry, in such a way that gravitational lensing effect is observed, but now the deficit angle to be considered in Eq. (3.18) is given by $\tilde{\Delta} = 8\pi G\tilde{\mu}$. The angular separation is larger for the wiggly string spacetime, since it has a larger effective mass per unit length. Because the small-scale structure on the wiggly strings a large number of small images are formed in addition to the double images [DLKV97].

On the other hand, when the direction of propagation is not chosen to be perpendicular to the string, the wiggly string exerts gravitational pulling on light passing by, as the background spacetime is not locally Euclidean. Hence, new effects on propagation of light can be expected as we consider light propagating along the string. The wave equation governing propagation of a scalar field (light as a scalar wave) in a curved background geometry needs to account for its curvature. This is done by using the 4-dimensional Laplace-Beltrami operator in the wave equation [Ful89; PM11a]

$$\frac{1}{\sqrt{-g}}\partial_\mu(\sqrt{-g}g^{\mu\nu}\partial_\nu)\Phi = 0, \tag{4.5}$$

where $\Phi = \Phi(r, \theta, z, t)$ is the scalar wave amplitude and $g = \det(g_{\mu\nu})$ with $g_{\mu\nu}$ being the metric tensor components. By writing equation (4.5) for the background spacetime of a wiggly string, we obtain in terms of the metric (4.3) the following equation:

$$-(1 - h_{00})\partial_t^2\Phi + \frac{1}{r}\partial_r\left(r\partial_r\right)\Phi + \frac{1}{\alpha^2 r^2}\partial_\theta^2\Phi + (1 + h_{00})\partial_z^2\Phi = 0. \tag{4.6}$$

As the field is single-valued, Φ has to be periodic in θ, $\Phi(\theta) = \Phi(\theta + 2\pi)$. Then, to solve equation (4.6) we make the ansatz

$$\Phi(r,\theta,z,t) = e^{il\theta}e^{i(\omega t - kz)}R(r), \tag{4.7}$$

where the wave vector $k \in \mathbb{R}$, $l = 0, \pm 1, \pm 2...$ specifies the angular momentum and ω is an angular frequency. Substituting the general solution (4.7) into equation (4.6), we get

$$-\frac{1}{r}\frac{d}{dr}\left(r\frac{dR}{dr}\right) + \frac{l^2}{\alpha^2 r^2}R + h_{00}\left(\omega^2 + k^2\right)R = \left(\omega^2 - k^2\right)R. \tag{4.8}$$

Defining the dimensionless variables $\rho = r/\gamma$, $\rho_0 = r_0/\gamma$, where $\gamma = \left[8\varepsilon\left(\omega^2 + k^2\right)\right]^{-1/2}$, then multiplying Eq. (4.8) by $\gamma^2 \sim O(\varepsilon^{-1})$ and rearranging terms gives the eigenvalue equation:

$$-\frac{1}{\rho}\frac{d}{d\rho}\left(\rho\frac{dR}{d\rho}\right) + \left(\frac{l^2}{\alpha^2\rho^2} + \ln\frac{\rho}{\rho_0}\right)R = \bar{\zeta}R \tag{4.9}$$

with

$$\bar{\zeta} = \frac{1}{8\varepsilon}\frac{\omega^2 - k^2}{\omega^2 + k^2}. \tag{4.10}$$

We note that the second term in the left-hand side plays the role of an effective potential. As this potential behaves logarithmically, the energy scale cannot be fixed at infinity so we work in the following with $\omega-$dependent length units such that $\rho_0 = 1$. Eq. (4.9) is formally equivalent to the Schrödinger equation that describes the 2D hydrogen atom; a system formed by a proton of charge q and an electron of charge $-q$ that interact in a two dimensional space via a logarithmic potential $V(\rho) = q^2 \ln\frac{\rho}{\rho_0}$, where ρ is the distance separating the two particles and ρ_0 a length scale [AA85]. Such logarithmic behavior is indeed the correct form for the 2D Coulomb potential since it is the one that satisfies the Gauss' theorem in two dimensions. As in the Schrödinger equation for the 2D hydrogen model where the potential term is attractive and infinite for infinite radius and near the origin ($V \to \infty$ as $\rho \to \infty$ and $\rho \to 0$), the potential term $V_{\text{eff}} = \frac{l^2}{\alpha^2\rho^2} + \ln\frac{\rho}{\rho_0}$ in Eq. (4.9) (see figure 4.2) only accommodates for bound states with no scattering states for the system [AA85; Eve+90; GMM13]. As a consequence, in the geometrical optics limit, trajectories are radially bounded helices around the string, as appears in Fig. 4.3, explicitly showing the gravitational pulling by the string. This is in agreement with Ref. [AS00], where geodesics near a Brans-Dicke wiggly cosmic string were also found to be bounded. The minimum and maximum radii are solutions of the transcendental equation $\bar{\zeta} = V_{\text{eff}}$ whereas the pitch is given by the ratio between the angular and effective linear momenta $\frac{l}{k}$. In the case of $l = 0$ the trajectory is rectilinear.

Concerning the solution of Eq. (4.9), Gesztesy and Pittner [GP78] and Garon et al [GMM13] used a semi-classical treatment, the Bohr–Sommerfeld

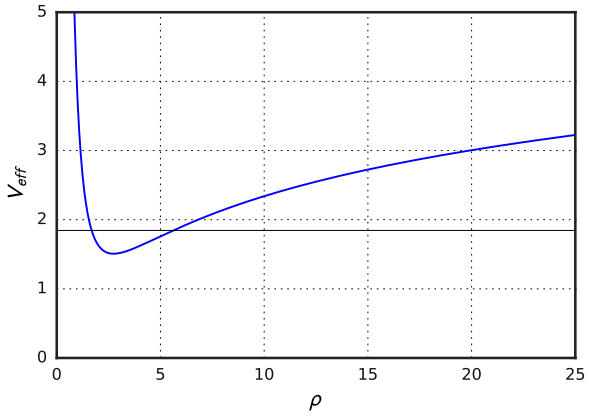

FIGURE 4.2: Effective potential, V_{eff} (in units where $\rho_0 = 1$), for $l = 2$. The horizontal solid line represents the ground state $\bar{\zeta}$ at that value of l.

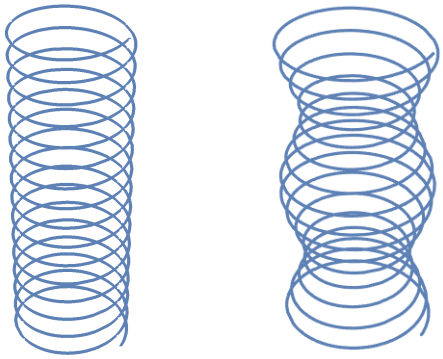

(a) (b)

FIGURE 4.3: Possible ray paths corresponding to the geometric optics limit of a scalar wave propagating along the wiggly string: (a) when the "total energy" $\bar{\zeta}$ is at the minimum of the effective potential and (b) at some point above it.

quantization, to find the spectrum of the two dimensional hydrogen atom. However, we should emphasize that such approach is an approximate solution. In order to find a more accurate solution, a complete treatment of quantum mechanics, numerical methods have to be applied. Indeed, we can find in the literature some methods used to do so through different techniques: linear variational method [AA85] and "shooting" method [Eve+90]. In addition to these, Garon et al [GMM13] have used a Finite Difference Method (FDM) in which the Hamiltonian (dimensionless form) is converted into a matrix, and then the eigenvalues of the matrix are numerically found, which consequently gives the energy spectrum of the hydrogen atom. They also show that such method is in agreement with the semi-classical model. For that reason, in order to solve equation (4.9) we used the FDM (for more details see Appendix A.2) and computed numerically the radial part of the waves traveling along the wiggly string

with their corresponding eigenvalues. The different states are labeled by quantum numbers n (radial quantum number) and l. In Fig. 4.4, we plot the lowest three eigenvalues $\bar{\zeta}_{nl}$ of the wave equation (4.9) and the corresponding radial wave amplitudes $R_{nl}(\rho)$ for $l = 0, \pm 1, \pm 2$. Although Eq. (4.9) is not exactly a Bessel equation, it is in fact nearly equivalent to it. This becomes clear when we observe the shape of the numerical solutions shown in Fig. 4.4, as they rapidly converge towards Bessel functions.

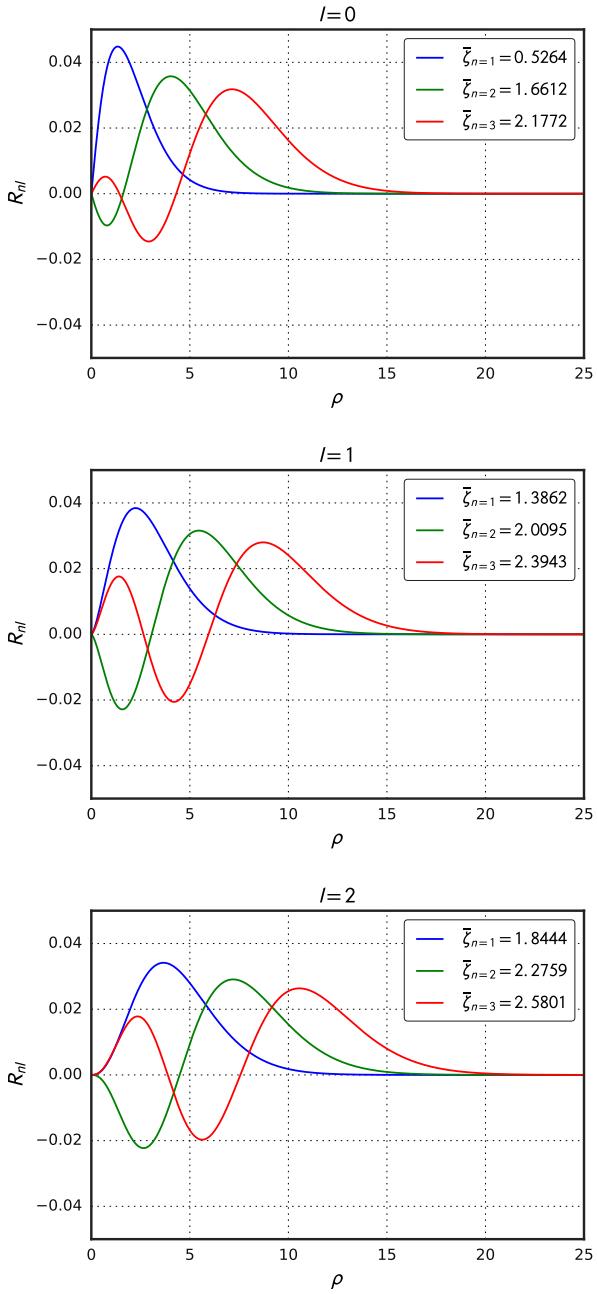

FIGURE 4.4: Wave modes for the first lowest eigenvalues $n = 1, 2, 3$ of Eq. (4.9) for each $l = 0, 1, 2$.

It has been suggested that cosmic structures with a non-vanishing Newtonian potential could generally behave as gravitational waveguide for light and massive

particles [DM89; Bim+98]. In the following, we examine this proposition for the wiggly string. From Eq. (4.10) we see that the wave modes that propagate along the wiggly string axis are quantized by n and l with dispersion relation given by:

$$\omega_{nl}^2 = \frac{1}{n_1^2} k^2 \tag{4.11}$$

where

$$n_1 = \left[\frac{1 - 8\varepsilon \bar{\zeta}_{nl}}{1 + 8\varepsilon \bar{\zeta}_{nl}} \right]^{1/2} \tag{4.12}$$

plays the role of an effective refractive index. From Eq. (4.11) we see that modes are propagative along the string provided that the following requirement is fulfilled:

$$0 < \bar{\zeta}_{nl} < \frac{1}{4G(\tilde{\mu} - \tilde{T})}. \tag{4.13}$$

This constraint establishes that the number of wave modes propagating along the wiggly string is large but finite as in an ordinary electromagnetic waveguide. As we would expect, we find that the allowed modes, besides being quantized by n and l, their frequency also depend on both the energy density and tension of the string.

4.3 Propagation of Massive Fields

Since light propagating along a wiggly string is radially confined, as seen in the previous section, it is interesting to investigate what happens to massive particles under the same circumstances. In order to study this possibility we write the Klein-Gordon equationin the wiggly string background geometry [Ful89]:

$$\left[\frac{1}{\sqrt{-g}} \partial_\mu (\sqrt{-g} g^{\mu\nu} \partial_\nu) - m^2 \right] \Phi(r, \theta, z, t) = 0, \tag{4.14}$$

where now Φ is a complex scalar field describing spinless relativistic particles. Using the ansatz given in Eq. (4.7) in Eq. (11), and following the same procedures used above in the case of massless particles propagation, we arrive to an identical eigenvalue equation as (4.9), but with eigenvalues given by

$$\bar{\mathcal{E}}_{nl} = \frac{1}{8\varepsilon} \frac{\omega^2 - k^2 - m^2}{\omega^2 + k^2}, \tag{4.15}$$

thus the wavefunctions $R_{nl}(\rho)$ and the eigenvalues $\bar{\mathcal{E}}_{nl}$ are numerically identical to the solution of the equation (4.9) (see figure (4.4)). In addition, the discussion on the geometric optics limit of the propagating massless field is still valid for massive particles. However, inclusion of the mass term in the dispersion relation

now introduces a cutoff:

$$\omega_{nl}^2 = \frac{1}{n_2^2}k^2 + \omega_c^2 \tag{4.16}$$

where n_2 is an effective refractive index defined by

$$n_2 = \left[\frac{1-8\varepsilon\bar{\mathcal{E}}_{nl}}{1+8\varepsilon\bar{\mathcal{E}}_{nl}}\right]^{1/2}, \tag{4.17}$$

which has an identical generic form than n_1, and

$$\omega_c^2 = \frac{m^2}{1-8\varepsilon\bar{\mathcal{E}}_{nl}} \tag{4.18}$$

is a *cutoff frequency*. The dispersion relation (4.16) presents a forbidden band

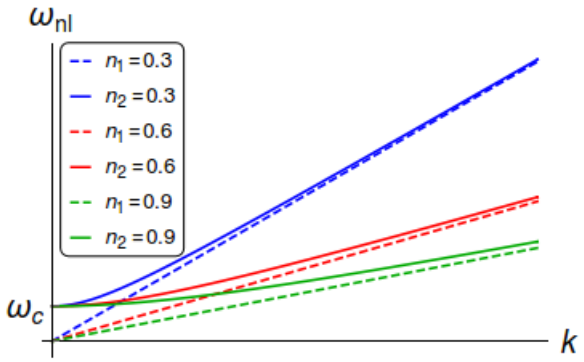

FIGURE 4.5: The angular frequency ω_{nl} in terms of the wavelength k for different values of n_1 and n_2. While the dashed lines corresponding to massless particles are obviously linear and the solid lines which correspond to the massive case have a quadratic start, both cases are fixed by mode-dependent parameters.

as it occurs for electromagnetic waves propagating in an unmagnetized plasma [Jac99]. The wave will propagate along the string when its frequency is larger than the cutoff frequency ω_c. On the other hand, for frequencies less than ω_c solutions are evanescent waves as the wave number k becomes imaginary. Thus, such waves named *cutoff modes* can not propagate. At high frequencies, $\omega \gg \omega_c$, we recover the massless dispersion relation (4.11). Moreover, the constraint

$$0 < \bar{\mathcal{E}}_{nl} < \frac{1}{4G(\tilde{\mu}-\tilde{T})}, \tag{4.19}$$

like in the massless case, sets a limit to a finite number of propagating modes. Besides the dependence on the density of energy and tension of the wiggly string, the allowed propagating modes also depend on the mass of the particle.

There is obviously a strong similarity between the propagation of both massless and massive scalar fields along a wiggly cosmic string and the propagation of electromagnetic waves in optical waveguides, as it could be observed through the trajectories obtained from the geometrical optics limit and solution of wave equations.

We further explore this analogy by proposing a way of designing an optical fiber that mimics the wiggly string in the context described above.

4.4 Optical Analogues of Spacetimes

The analogy between 3D gravity and optics is an old topic that started with the pioneering works of Gordon on Fresnel dragging effect in moving dielectrics [Gor23b]. To understand how to describe dielectric media as an effective metric (spacetime), let us present the Gordon's metric (or optical metric). First, we generalize a medium with refractive index n in three dimensional space to spacetime of gravity. Fermat's principle shows that electromagnetic waves perceive a 3D geometry given by

$$dl^2 = n^2(dx^2 + dy^2 + dz^2), \tag{4.20}$$

which is easily translated into a spacetime geometry as $dl^2 = dt^2 - dl^2$. After multiplying the spacetime metric by a conformal factor n^{-2}, we obtain the following metric tensor components

$$g_{\mu\nu} = \begin{pmatrix} n^{-2} & 0 & 0 & 0 \\ 0 & -1 & 0 & 0 \\ 0 & 0 & -1 & 0 \\ 0 & 0 & 0 & -1 \end{pmatrix}. \tag{4.21}$$

In this geometry, the medium influences only the measure of time through the element $g_{00} = n^{-2}$. We can rewrite the metric tensor (4.21) as

$$g_{\mu\nu} = \eta_{\mu\nu} + (n^{-2} - 1)u_\mu u_\nu, \tag{4.22}$$

where $\eta_{\mu\nu}$ is the ordinary Minkowski metric and $u^\mu = (1,0,0,0) = u_\mu$ in the co-moving frame. In fact, $u^\mu = \eta^{\mu\nu}u_\nu = dx^\mu/ds$ is regarded as the local four-velocity of the medium [LP10]. Equation (4.22) is known either as Gordon's metric or optical metric and establishes the spacetime of a such moving media [Gor23b].

On the other hand, it is well known (see [Car04], for example) that photons moving in a spacetime with a non-vanishing Newtonian potential, leads to deflection of light and gravitational time delay, that is equivalent to photons propagating in an anisotropic medium with refractive index given by

$$n = 1 - 2\Phi, \tag{4.23}$$

where Φ is the Newtonian potential. Fermat's principle applied for a medium with refractive index as the one in Eq. (4.23) leads to the same equation of motion obtained with theory of gravity for light propagating in a spacetime with g_{00} component of the metric tensor having a perturbed term ($g_{00} = \eta_{00} +$ *"perturbation"*) which is originated from the Newtonian potential (spacetime perturbed by a non-vanishing Newtonian potential).

It is worth noting that the ideas presented here follow the same key idea as what occurs when considering propagation of light in NLCs (see Section 3.3).

In the following section, we provide an optical analogue spacetime of the wiggly string, by design an optical fiber having such a refractive index likely to reproduce the effect of the wiggly string in the laboratory.

4.4.1 An Optical Waveguide Analogue of the Wiggly String

It has been proposed that, by spatially varying the doping concentration, the refractive index profile of optical fibers can be used to control optical transmission in a designer-specified way [LBM11]. Following this standpoint, we investigate the proposition of a graded-index optical fiber that reproduces some of the properties of the scalar field propagation along a wiggly string.

In general, the wave equations for electromagnetic waves propagating along a circular fiber are coupled [Jac99]. This implies that there is no separation into purely TE or TM modes but, in the specific case of a fiber with an azimuthally symmetric refractive index, if the fields have no dependence on the azimuthal angle, the equations uncouple into separate scalar wave equations of the form

$$\left[\frac{1}{r}\frac{\partial}{\partial r}\left(r\frac{\partial}{\partial r}\right)+\frac{\partial^2}{\partial z^2}+n^2(r)\omega^2\right]\Phi=0, \tag{4.24}$$

where ω is the angular frequency, $n(r)$ is the optical fiber refractive index and $\mathrm{Re}(\Phi)$ represents any real component of the field. For waves propagating along the optical fiber (z-direction), the ansatz $\Phi(r,z)=e^{-ikz}R(r)$, (where $k\in\mathbb{R}$) substituted into Eq. (4.24) gives

$$-\frac{1}{r}\frac{d}{dr}\left(r\frac{dR}{dr}\right)-n^2(r)\omega^2R+k^2R=0. \tag{4.25}$$

Here, we choose the refractive index to be given by (see Fig. 4.6):

$$n(r)=\left(1-\Omega\ln\frac{r}{r_0}\right)^{1/2}, \tag{4.26}$$

with the dimensionless parameter $\Omega\ll 1$ in order to be consistent with the wiggly string parameter ε. The quantity r_0 is considered to be much smaller than the radius r_f of the fiber and defines an opaque core radius. This way, by considering propagation in the region $r_0<r<r_f$, the logarithmic singularity at $r=0$ is avoided. Like in the previous sections, we change r to dimensionless units by doing the change of variables $\rho=r/\nu$, $\rho_0=r_0/\nu$ and setting $\nu=\Omega^{-1/2}\omega^{-1}$. Then, the dimensionless equation for the optical fiber can be written as:

$$-\frac{1}{\rho}\frac{d}{d\rho}\left(\rho\frac{dR}{d\rho}\right)+\left(\ln\frac{\rho}{\rho_0}\right)R=\bar{\beta}_nR, \tag{4.27}$$

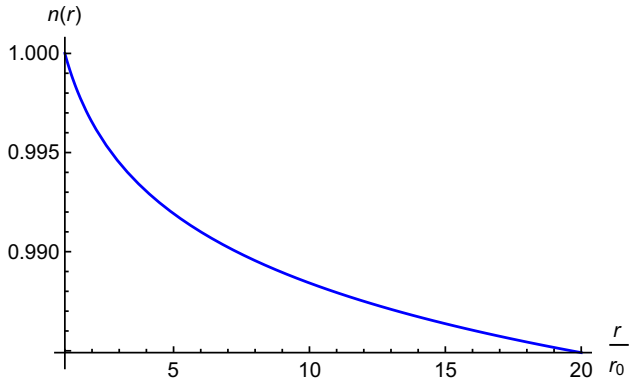

FIGURE 4.6: Refractive index in terms of the r coordinate (for $\Omega = 0.01$ and with r in units of the opaque radius r_0). The value of the refractive index decreases with the increasing of the distance from the center of the optical waveguide. The maximum value of $n(r)$ is found at $r = r_0$.

where

$$\bar{\beta}_n = \frac{1}{\Omega}\left(1 - \frac{k^2}{\omega^2}\right). \tag{4.28}$$

The radial amplitudes of the wave and their corresponding eigenvalues in the optical fiber with the refractive index given by Eq. (4.26) obey equations identical to the ones of massless and massive particles propagating with $l = 0$ in the spacetime of a wiggly string. For a given $z = const.$ plane, the intensity profiles for the propagating waves described by Eq. (4.9) are given by $2\pi\rho R_{nl}^2(\rho)$. In Fig. 4.7, we plot the intensity distribution for different wave modes, solutions of Eq. (4.9). The optical fiber modes described by Eq. (4.27) correspond to the cases where $l = 0$.

Here, we remark that the coupled equations for the electromagnetic field in the circular optical fiber, in the more general case where the field depends on the azimuthal angle but the refractive index remains azimuthally symmetric, give rise to hybrid HE modes (no longer TE or TM) [Jac99]. The case of a step-index fiber was studied in Ref. [Sni61] which found the field to be of the form $R_l(\rho)e^{il\theta}$, where R_l is a Bessel function. Even though Eq. (4.9) is not a Bessel equation, its symmetries and the shape of the numerical solutions shown in Fig. 4.4, suggest that a solution in terms of an expansion on Bessel functions might be rapidly convergent. The θ-dependence of the scalar fields solutions, for $l \neq 0$, is therefore reminiscent of what happens in the circular optical fiber. Also, it would be interesting to compare the coupled electromagnetic vector field equations for a wave propagating along a circular optical fiber with refractive index given by Eq. (4.26) with the electromagnetic field equations in the wiggly string background.

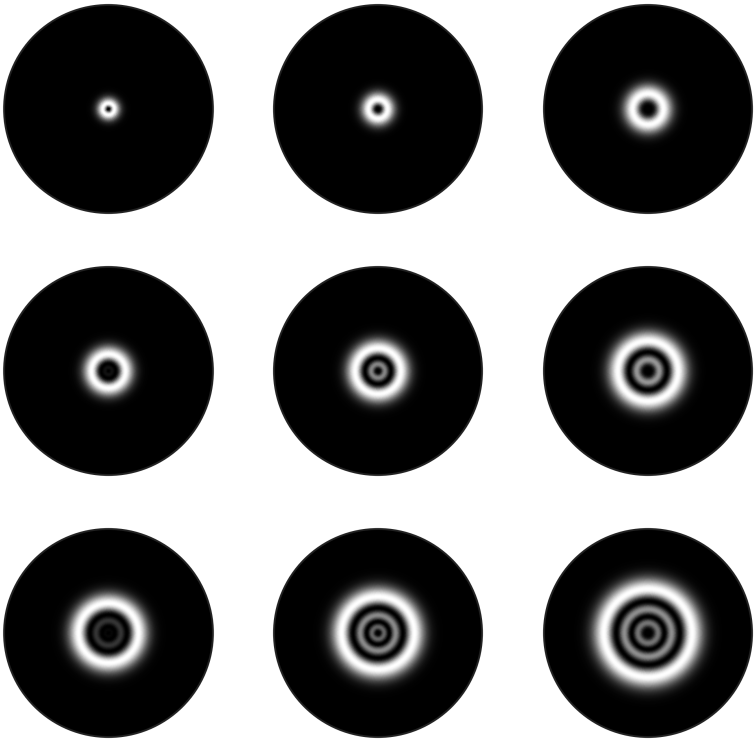

FIGURE 4.7: Intensity profiles for the first few solutions R^2_{nl} of Eq. (4.9), with $n = 1, 2, 3$ and $l = 0, 1, 2$. The profiles are disposed as in a matrix where n and l give the line and column number, respectively. The first column corresponds to the optical fiber modes described by Eq. (4.27).

4.5 Conclusions

In this chapter, we examined the effect of wiggly cosmic strings on propagation of massless and massive fields. We found that waves propagating along the string axis experience the small-scale perturbations which make the propagation qualitatively different from that of waves propagating in the background spacetime with a unperturbed cosmic string. The non-vanishing Newtonian potential acts as an inhomogeneous dielectric medium so that the massless particles are radially confined in a vicinity of the defect axis. Therefore, the wiggly string spacetime behaves as a gravitational waveguide in which wave modes are quantized. These latter depend on the string energy density and string tension. The number of allowed modes is finite as in a ordinary optical waveguide. On the other hand, the presence of wiggles cause gravitational pullings on massive objects, making the waveguide effect to be also valid for massive fields propagation. In this case, the frequencies of the waves also depend on the mass of the particle. Finally, we proposed the design of an optical fiber with a non homogeneous refractive index profile likely to mimic the effect of a perturbed cosmic string. The radial solutions with the corresponding eigenvalues were found by using a numerical method. Although we have considered here the propagation of massive and massless scalar fields along a wiggly string, the extension to vector fields like vector bosons or the electromagnetic field can be of

interest. However, we believe that what we have done here already provides a very interesting analogy between optics (optical fiber) and spacetime (wiggly string), to test expected behaviors of light propagating near wiggly string in the laboratory.

In the next Chapter of this thesis, we will study the hyperbolic metamaterial, a medium made of a liquid crystal endowed with a disclination [Fum+15]. That medium can be related to a particular effective geometry where its metric simulates a negative refractive index. Since a negative index environment is a strong criterion to enable the waveguide effect [SC11], the hyperbolic metamaterial seems to be a plausible medium for observing such effect.

Chapter 5

Optical Concentrator from a Hyperbolic Metamaterial

***

The metamaterials are optical materials that come up with possibility to have negative refractive indices [SPW04]. This characteristic besides provides many uses in technological applications and advances in the science of transformation optics [CCS10], also leads to get more analogies with cosmological systems. Recently, metamaterials have been proposed as a way to mimic aspects of curved spacetime in laboratory [GZZ09; ML15]. For instance, by manipulating the effective refractive index of the medium, Sheng et al. [She+13] were able to reproduce gravitational lensing and trapping of light. Anisotropic metamaterial has also been used to simulate black holes [Smo11; FNB16a] and spining cosmic string [ML10]. Incidentally, electronic metamaterials may also be used to emulate peculiar spacetime conditions, like a discontinuous Lorentzian to Kleinian metric signature change [Fig+16] which has also been modeled by optical metamaterials [SN10].

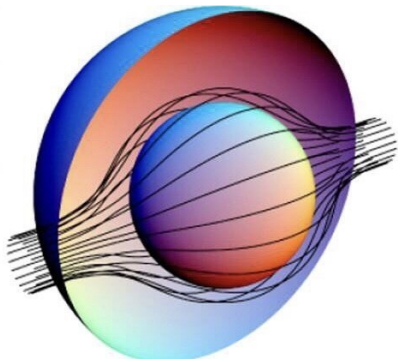

FIGURE 5.1: Light rays being guided around a cloaked region by a metamaterial medium [PSS06].

In this Chapter we present a new class of defects, the hyperbolic disclinations existing in a metamaterial made of nematic liquid crystal. We further apply

the geometric method previously introduced for finding the effective geometry of the medium. Then, we examine how light propagates in the metamaterial.

5.1 Hyperbolic Liquid Crystal Metamaterial

Hyperbolic metamaterial are subclass of metamaterials mostly artificial, but that can be also found in nature [NK15; KGP15]. Among the many forms to perform hyperbolic metamaterials, the most common realization is layered metal–dielectric structures [Pod+13]. The Hyperbolic Liquid Crystal Metamaterial (HLCM) is an example of artificial metamaterial that can be made from nematic liquid crystal layers alternate with metallic nanorods [Fig+17]. The HLCM have been used for design of hyperlens [JAN07; JAN06], and also for analogies in cosmology [Fig+16; Fig+17]. From the optical point of view, HLCM is a promising example of an unixial anisotropic medium that could exhibit permittivities of different signs, the ratio between ordinary and extraordinary permittivities is negative. The ordinary and extraordinary refractive indices in HLCM are appropriately given in terms of the permittivities, $n_{\perp}^2 = \epsilon_{\perp}$ and $n_{||}^2 = \epsilon_{||}$ [KL07]. The material shows a metallic behaviour along a common direction $\vec{n}$ (director field) of the nematic phase, resulting in a negative permittivity $\epsilon_{||} < 0$ along that direction. Strictly speaking, negative index material cannot circumvent dispersion phenomena and losses [WNW05]. However, losses due to metallic plasmonic components might be offset by using gain media [BS03; Nog+08] or highly doped oxides with lower dissipation levels [NB10; Wes+10]. As usual in transformation optics, in the design of hyperlenses or invisibility cloaks [Ves02; LP09; KS11], we will consider metamaterials in homogenization regime for which losses have been reduced so that one may focus on kinematic aspects of light propagation.

We examine the optical properties of two different configurations of HLCM with optical axis defined by circular and radial director field. First, we consider the director field as $\hat{n} = \hat{\phi}$ (circular director field), and then we consider as $\hat{n} = \hat{r}$ (radial director field), see Fig. 5.2. Actually, these are basically a generalization to three dimensions of the nematic liquid crystal configurations showed in Fig. 2.3. Hence, we are able to apply the same geometric method introduced in the Section 3.3. In three dimensional cylindrical space with ray path parametrized by arc length l (see Fig. 3.5), we have $\vec{r}(l) = r\hat{r} + z\hat{z}$, thus $\vec{t} = \dot{r}\hat{r} + r\dot{\phi}\hat{\phi} + \dot{z}\hat{z}$ where $\dot{x} = dx/dl$, and the normalization constraint follows, $|\vec{t}|^2 = \dot{r}^2 + r^2\dot{\phi}^2 + \dot{z}^2 = 1$. For configuration 5.2 (a), we thus have $\cos\beta = \vec{t}\cdot\vec{n} = r\dot{\phi}$ and $\sin^2\beta = \dot{r}^2 + \dot{z}^2$. The ray index in the form (3.19) is then

$$N_r^2 = \varepsilon_{\perp} r^2\dot{\phi}^2 - |\varepsilon_{||}|(\dot{r}^2 + \dot{z}^2). \tag{5.1}$$

Similarly, the ray index in configuration 5.2 (b) is given by

$$N_r^2 = \varepsilon_{\perp} \dot{r}^2 - |\varepsilon_{||}|(r^2\dot{\phi}^2 + \dot{z}^2). \tag{5.2}$$

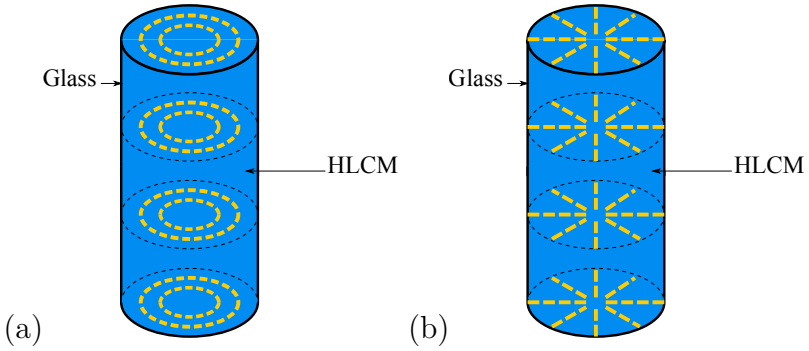

FIGURE 5.2: Two different cylindrical configuration of HLCM (according to director field arrangement) covered with a reflective material. (a) Director field configuration for HLCM with optical axis as $\hat{n} = \hat{\phi}$ (circular director field), obtained from planar anchoring of the molecules at the boundaries. (b) Director configurations for HLCM as $\hat{n} = \hat{r}$ (radial director field), obtained from homeotropic anchoring of the molecules at the boundaries.

Rescaling the coordinates according to $\rho = r\sqrt{|\epsilon_{\|}|}$, $\zeta = z\sqrt{|\epsilon_{\|}|}$, the elementary optical path $ds^2 = N_r^2 dl^2$ writes as:

$$ds^2 = N_r^2 dl^2 = -d\rho^2 + \alpha^2\rho^2 d\phi^2 - d\zeta^2, \tag{5.3}$$

for configuration 5.2 (a) and

$$ds^2 = N_r^2 dl^2 = \alpha^2 d\rho^2 - \rho^2 d\phi^2 - d\zeta^2, \tag{5.4}$$

for configuration 5.2 (b), where $\alpha^2 = \frac{\varepsilon_{\perp}}{|\varepsilon_{||}|}$. From Eqs. (5.3) and (5.4), we see that the spatial coordinate along which the refractive index is negative behaves as a "pseudotime coordinate". By the way, this is an important aspect motivating the study of such defects with respect to light propagation [Fum+15] and also for analogies in cosmology [Fig+17]. Once the line elements given in Eqs. (5.3) and (5.4) are formally equivalent of the line disclination metric in NLCs as in Fig. (2.3), we say that such metrics represent a so called *hyperbolic disclination*. The term "hyperbolic" comes from the fact that due to the exhibition of negative permittivity in metamaterials, the extraordinary rays obey a hyperbolic dispersion relation (the dependence of the refractive index on the frequency is hyperbolic) [JAN06]. For example, the HLCM dispersion relation for configuration Fig. 5.2 (a) is given by

$$-\frac{\left(k_r^2 + k_z^2\right)}{\left|\varepsilon_{\|}\right|} + \frac{k_\phi^2}{\varepsilon_{\perp} r^2} = \omega^2. \tag{5.5}$$

Next we discuss propagation of light into HLCM media, in both geometrical optics limit and in the framework of wave theory.

5.2 Light Trajectories in the HLCM Media

A large number of applications ranging from solar energy harvesting to optical sensing has been explored in order to focus (concentrate) light in the most efficient way. The first attempts were made by using lenses of dielectric material, but for a long time diffraction phenomena forbid beam sizes below half of a wavelength. Recently, plasmonic structures [MM11] and optical metamaterials [Pen00] are probably the best candidates to overcome the usual physical limits. These latter are artificial media that can be used in superlenses working beyond the diffraction limit.

In the remaining of this Chapter, we examine the possibility to focus light with a cylindrical device made from the HLCM configurations presented before, see Fig. 5.2. In both HLCM media, the optical path can be elegantly reinterpreted in terms of non-Euclidean geometry: following a pioneering idea by Gordon [Gor23a] discussed in Section 4.4, light propagation inside a refractive medium occurs in a similar fashion to light propagation on a Riemannian manifold. As will be illustrated next, differential geometry techniques is extremely powerful when dealing with calculations of light trajectories or with how to generalize the wave equation.

First, we consider the geometrical optics limit and start analyzing the path followed by light in the HLCM device with a purely circular director field (see Fig. 5.2 (a)). From the optical path Eq. (5.3), the metric tensor components representing such medium are given by:

$$g_{ij} = \begin{pmatrix} -1 & 0 & 0 \\ 0 & \alpha^2\rho^2 & 0 \\ 0 & 0 & -1 \end{pmatrix}. \tag{5.6}$$

The constants of motion are given by the Killing vectors, which correspond to the cyclic variables of the metric. A quick examination of Eq. (5.6) reveals two Killing vectors, $(\partial_\phi)^i = (0,1,0)^{\mathrm{T}}$ and $(\partial_\zeta)^i = (0,0,1)^{\mathrm{T}}$ (here $^{\mathrm{T}}$ denotes the transposition operation used to represent column vectors), associated with the covectors:

$$(\partial_\phi)_i = g_{ij}(\partial_\phi)^j = (0, \alpha^2\rho^2, 0), \tag{5.7}$$

$$(\partial_\zeta)_i = g_{ij}(\partial_\zeta)^j = (0,0,-1). \tag{5.8}$$

These vectors obey the Killing equations, which give the constants of motion:

$$(\partial_\phi)_i \frac{dx^i}{d\lambda} = \widetilde{C}, \tag{5.9}$$

$$(\partial_\zeta)_i \frac{dx^i}{d\lambda} = A. \tag{5.10}$$

Here λ is an affine parameter such that $ds^2 = Bd\lambda^2$ with $B > 0$ in order to preserve the causal regions in terms of the two variables. Denoting by $x' = \frac{dx}{d\lambda}$,

one gets

$$\zeta' = A, \tag{5.11}$$

$$\rho^2\phi' = \frac{\widetilde{C}}{\alpha^2} = C. \tag{5.12}$$

In the remainder, propagation along increasing values of z will be considered, therefore $A > 0$. A third constant of motion is obtained from energy conservation. From the line element Eq. (5.6) we get

$$-(\rho')^2 + \alpha^2\rho^2(\phi')^2 - (\zeta')^2 = B. \tag{5.13}$$

In fact, Eq. (5.13) can also be deduced for instance from the eikonal equation $k_\mu k^\mu = 0$ (see Appendix A.3). Now substituting Eqs. (5.11) and (5.12) into Eq. (5.13), we obtain

$$\frac{\rho'^2}{2} - \frac{\alpha^2 C^2}{2\rho^2} = \frac{-(A^2+B)}{2} = E. \tag{5.14}$$

Note that the particular form of the relation (5.14) requires that the energy parameter $E \leq 0$. With this assumption, we solve equation (5.14) to obtain:

$$\frac{\rho d\rho}{\sqrt{\rho_M^2 - \rho^2}} = \pm K d\zeta, \tag{5.15}$$

where ρ_M and K are constants given by

$$\rho_M = \frac{\alpha|C|}{\sqrt{2|E|}} \tag{5.16}$$

and

$$K = \frac{\sqrt{2|E|}}{A} \tag{5.17}$$

with K being positive, $K > 0$. Defining by ρ_0 the radius (position) at which the ray is injected at $\zeta = 0$, one finds the two families of solutions. The first family corresponds to the positive sign, then corresponding to rays of increasing radius:

$$\rho(\zeta) = \sqrt{\rho_M^2 - ((\rho_M^2 - \rho_0^2)^{1/2} - K\zeta)^2}. \tag{5.18}$$

We see that the orbits are confined with maximum radius ρ_M, with a given ray reaching the value ρ_M for

$$z_M = \frac{(\rho_M^2 - \rho_0^2)^{1/2}}{\sqrt{|\epsilon_\parallel|}K}. \tag{5.19}$$

For moderate injection angles, the light ray is not able to reach the outer metallic layer before falling down onto the defect core. In other words, rays undergo a total internal reflection for any frequency preserving the hyperbolic feature of the nematic phase. For large injection angles, light rays may reach the outer metallic layer but will be reflected back inside the HLCM to finally converge

on the core. The second family of solutions in Eq. (5.15) is obtained when considering the negative sign, which corresponds to rays of decreasing radius:

$$\rho(\zeta) = \sqrt{\rho_M^2 - ((\rho_M^2 - \rho_0^2)^{1/2} + K\zeta)^2}. \tag{5.20}$$

Here, the ray can decrease down to the defect core and hence be guided along the axis of the cylinder. When the light rays get closer to the defect core the angular momentum term in (5.14) gets very large and hence, the light rays make more turns, see (Fig. 5.3 and 5.4). By combining Eq. (5.18) with Eq. (5.12), we obtain for the first family of solutions,

$$\phi(\zeta) = \frac{1}{\alpha}\tanh^{-1}\left(\frac{K\zeta - (\rho_M^2 - \rho_0^2)^{1/2}}{\rho_M}\right) \tag{5.21}$$

and, by substituting Eq. (5.20) into Eq. (5.12), we get

$$\phi(\zeta) = \frac{1}{\alpha}\tanh^{-1}\left(\frac{K\zeta + (\rho_M^2 - \rho_0^2)^{1/2}}{\rho_M}\right) \tag{5.22}$$

for the second family of solutions. By manipulating Eq. (5.18) and Eq. (5.21), we find $\rho = \rho(\phi)$ as being the confined Poinsot spiral:

$$\rho(\phi) = \frac{\rho_M}{\cosh \alpha\phi}. \tag{5.23}$$

By combining Eq. (5.20) and Eq. (5.22) we obtain the same Eq. (5.23). With equation (5.23) we can get the confined trajectories for light traveling in a plane $z = const$. We see that the smaller the value of α, the stronger is the spiraling behavior as $1/\alpha$ can be understood as the "spiraling strength" (vorticity) of the defect [Fum+15; JAN07; Fig+17]. The same effect can be visualized in the three dimensional trajectories obtained from the parametric equations $\rho(\zeta)$ and $\phi(\zeta)$, see Fig. 5.4. For large values of α, for example $\alpha = 20$, the rays travel in nearly straight lines radially toward the defect core, see Fig. 5.3.

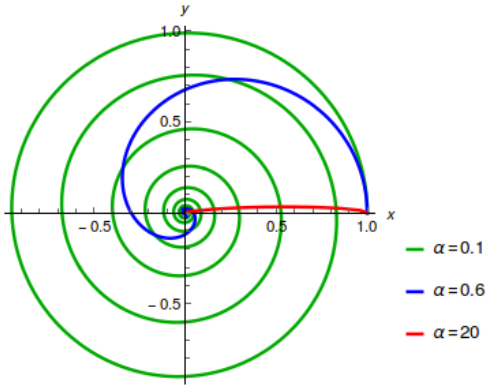

FIGURE 5.3: Projection of the trajectories onto the $x-y$ plane with ρ in units of ρ_M, for a few values of α.

We now examine the path followed by light in the HLCM device with a

purely radial director field (see Fig. 5.2 (b)). The metric tensor components in that case are given by:

$$g_{ij} = \begin{pmatrix} \alpha^2 & 0 & 0 \\ 0 & -\rho^2 & 0 \\ 0 & 0 & -1 \end{pmatrix}. \tag{5.24}$$

The two Killing vectors are the same as in the circular case, $(\partial_\phi)^i = (0,1,0)^{\mathrm{T}}$ and $(\partial_\zeta)^i = (0,0,1)^{\mathrm{T}}$, associated with the covectors:

$$(\partial_\phi)_i = g_{ij}(\partial_\phi)^j = (0,-\rho^2,0), \tag{5.25}$$
$$(\partial_\zeta)_i = g_{ij}(\partial_\zeta)^j = (0,0,-1). \tag{5.26}$$

Following the same procedure as before, the Killing equations are straightforwardly obtained as:

$$\zeta' = A, \tag{5.27}$$
$$\rho^2\phi' = C. \tag{5.28}$$

For this case the energy conservation gives

$$\frac{\rho'^2}{2} - \frac{C^2}{2\alpha^2\rho^2} = \frac{B+A^2}{2\alpha^2} = E. \tag{5.29}$$

The constant E in Eq. (5.29) is positive, then the solution is not exactly the same as Eq. (5.14) where E is negative. We can also see that, since the first term in the left-hand side of Eq. (5.29) cannot be zero, there is no turning point for the light trajectories (the trajectories are unbounded). Indeed, contrary to the first HLCM configuration Fig. 5.2 (a) light is not confined; if the ray starts with increasing ρ at ρ_0 it will never decrease to the defect core, unless it is reflected by an outer layer. These arguments hold when looking at the equation $\rho(\phi) \sim \frac{1}{\sinh\alpha\phi}$, which is another case of Poinsot's spiral, but not of a confined type now.

We then conclude that the circular field configuration should be favored to design a device to concentrate light. We also emphasize that, in practice, such configuration also avoids instabilities such as the escape in third dimension [MK72] that might break the director field arrangement and therefore the guiding effects.

5.3 Propagating Wave Modes

With the purpose of supporting the concentration effect, we are now examining the structure of the optical modes that propagate in the device (HLCM with circular director field, see Fig. 5.2(a)). In the scalar wave approximation, the complex amplitude Φ of the wave is governed by the generalized form of the d'Alembert equation

$$\nabla_i\nabla^i\Phi - \frac{1}{c^2}\frac{\partial^2\Phi}{\partial t^2} = 0, \tag{5.30}$$

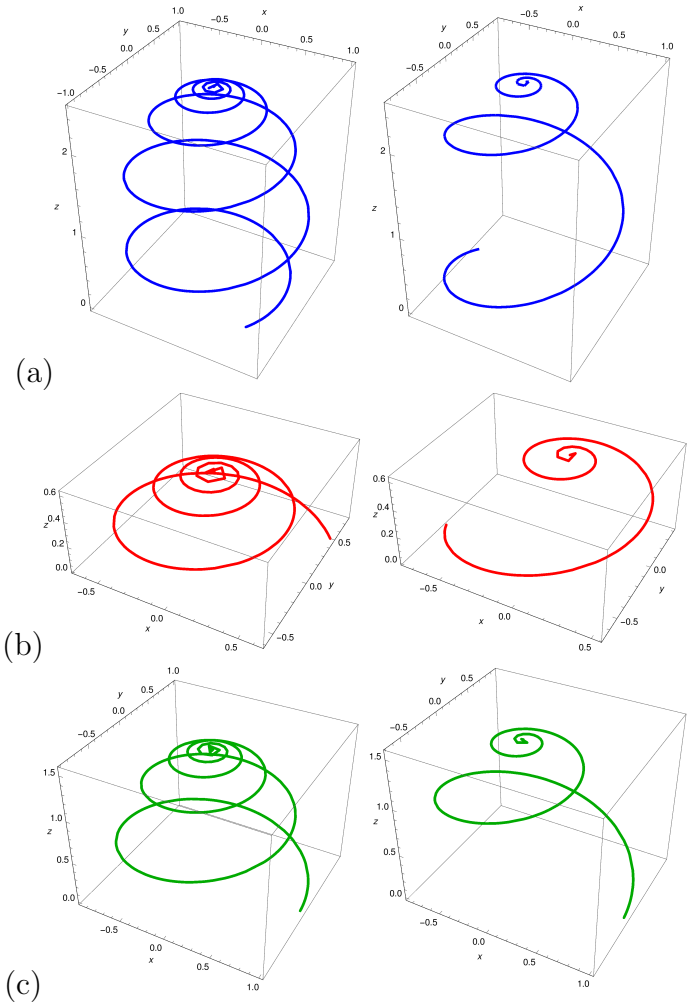

FIGURE 5.4: Light trajectories in three dimensions for $\rho_M = 1$, $\rho_0 = 0.8$, $K = 0.64$ and $\alpha = 0.1, 0.2$; the figures on the left (right) side refer to $\alpha = 0.1$ ($\alpha = 0.2$). (a) Light path for rays of increasing radius starting at $\rho_0 = 0.8$. (b) Light path for rays of decreasing radius starting at $\rho_0 = 0.8$. (c) Light path for rays starting at $\rho_0 = \rho_M$.

where $\nabla_i \nabla^i$ is the Laplace-Beltrami operator, whose action on the wave function Φ is given by (see equation (4.5))

$$\nabla_i \nabla^i \Phi = \frac{1}{\sqrt{|g|}} \partial_i \left(\sqrt{|g|} g^{ij} \partial_j \Phi \right). \tag{5.31}$$

In the case of harmonic time dependence of the form $\Phi(\rho, \phi, \zeta, t) = \psi(\rho, \phi, \zeta)\, e^{-i\omega t}$, Helmholtz equation is obtained from Eq. (5.31) as

$$-\frac{1}{\rho}\frac{\partial}{\partial \rho}\left(\rho \frac{\partial \psi}{\partial \rho}\right) + \frac{1}{\alpha^2 \rho^2}\frac{\partial^2 \psi}{\partial \phi^2} - \frac{\partial^2 \psi}{\partial \zeta^2} + \frac{\omega^2}{c^2}\psi = 0, \tag{5.32}$$

where ω is the angular frequency of the light rays. Using the ansatz as

$$\psi(\rho, \phi, \zeta) = F_{\ell, k_\zeta}(\rho) e^{\pm i \ell \phi} e^{\pm i k_\zeta \zeta} \tag{5.33}$$

we obtain the equation

$$\rho^2 \frac{d^2 F_{\ell,k_\zeta}}{d\rho^2} + \rho \frac{dF_{\ell,k_\zeta}}{d\rho} - \left[\left(\frac{\omega^2}{c^2} + k_\zeta^2 \right) \rho^2 - \frac{\ell^2}{\alpha^2} \right] F_{\ell,k_\zeta} = 0. \tag{5.34}$$

Equation (5.34) is the modified Bessel differential equation of imaginary order $i\ell/\alpha$, with solutions [Dun90; Olv+10]

$$F_{\ell,k_\zeta}(\rho) = e_\ell \tilde{I}_{\ell/\alpha}(\bar{\omega}\rho) + f_\ell \tilde{K}_{\ell/\alpha}(\bar{\omega}\rho), \tag{5.35}$$

where $\bar{\omega}$ is given by

$$\bar{\omega} = \sqrt{k_\zeta^2 + \omega^2/c^2} \tag{5.36}$$

with e_ℓ, f_ℓ being constants of integration. The functions $\tilde{I}_{\ell/\alpha} = \mathrm{Re} I_{i\ell/\alpha}$ and $\tilde{K}_{\ell/\alpha} = K_{i\ell/\alpha}$ are linearly independent solutions of Eq. (5.34), with $I_{i\ell/\alpha}, K_{i\ell/\alpha}$ being the modified Bessel functions of first and second kind, respectively [Olv+10]. Note that, in an ordinary defect-free Euclidean space, the radial solution of Helmholtz equation would be a linear combination of $J_\ell(\rho\sqrt{\omega^2/c^2 - k_\zeta^2})$ and $Y_\ell(\rho\sqrt{\omega^2/c^2 - k_\zeta^2})$ instead of $\Re(I_{i\ell/\alpha}(\rho\sqrt{\omega^2/c^2 + k_\zeta^2}))$ and $K_{i\ell/\alpha}(\rho\sqrt{\omega^2/c^2 + k_\zeta^2})$, which is the case here. We can see the effect in the solution of the metamaterial character of the metric via:

(i) the introduction of imaginary order Bessel functions;

(ii) the change of Bessel to modified Bessel functions and

(iii) the role of the defect amplitude through the appearance of α in the imaginary order of the modified Bessel functions.

The modified Bessel functions $\tilde{I}_{\ell/\alpha}, \tilde{K}_{\ell/\alpha}$ oscillate rapidly near the origin, as one can see from their behaviors as $\rho \to 0^+$ [Dun90; Olv+10],

$$\tilde{I}_{\ell/\alpha}(\bar{\omega}\rho) = \left(\frac{\sinh(\pi\ell/\alpha)}{\pi\ell/\alpha} \right)^{1/2} \cos\left[\frac{\ell}{\alpha} \ln\left(\frac{\bar{\omega}\rho}{2} \right) - \gamma_{\ell/\alpha} \right] + O(\bar{\omega}^2\rho^2), \tag{5.37}$$

$$\tilde{K}_{\ell/\alpha}(\bar{\omega}\rho) = -\left(\frac{\pi\alpha/\ell}{\sinh(\pi\ell/\alpha)} \right)^{1/2} \sin\left[\frac{\ell}{\alpha} \ln\left(\frac{\bar{\omega}\rho}{2} \right) - \gamma_{\ell/\alpha} \right] + O(\bar{\omega}^2\rho^2), \tag{5.38}$$

where $\gamma_{\ell/\alpha}$ is a constant defined as $\gamma_{\ell/\alpha} \equiv \arg\Gamma(1 + i\ell/\alpha)$, with Γ being the Gamma function. The rapid oscillations are due to the logarithmic argument of the trigonometric functions. Furthermore, for a fixed ℓ, the smaller the value of α, the stronger the oscillations become (reducing the value of α shrinks the period of the trigonometric functions). This behavior can be visualized in Figs. 5.5 (a) and (b). Despite the similarities between $\tilde{I}_{\ell/\alpha}$ and $\tilde{K}_{\ell/\alpha}$ near the origin,

their asymptotic behavior is exponential [Dun90; Olv+10],

$$\tilde{I}_{\ell/\alpha}(\bar{\omega}\rho) = \left(\frac{1}{2\pi\bar{\omega}\rho}\right)^{1/2} e^{\bar{\omega}\rho}\left[1+O\left(\frac{1}{\bar{\omega}\rho}\right)\right], \tag{5.39}$$

$$\tilde{K}_{\ell/\alpha}(\bar{\omega}\rho) = \left(\frac{\pi}{2\bar{\omega}\rho}\right)^{1/2} e^{-\bar{\omega}\rho}\left[1+O\left(\frac{1}{\bar{\omega}\rho}\right)\right]. \tag{5.40}$$

The first solution can be dismissed as it diverges at larges distances from the

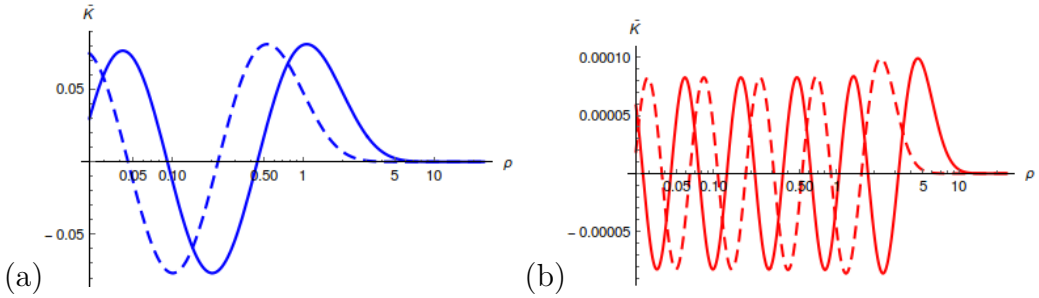

FIGURE 5.5: The corresponding radial wave amplitudes $\tilde{K}$ for fixed $\ell = 1$, $\alpha = 0.17, 0.5$ and $\bar{\omega} = 1, 2$. (a) for $\alpha = 0.5$ and (b) for $\alpha = 0.17$. The solid and dashed lines refers to $\bar{\omega} = 1$ and $\bar{\omega} = 2$, respectively. The smaller the value of α, the more the fields oscillate near the origin. At large distances (logarithmic scale on the $x-$axis here) the behavior is exponential and it does not depend on ℓ/α.

axis, which means that $e_\ell = 0$. Hence, as expected from the geometrical optics limits, the field concentrates along the axis of the device.

For a given $z = const.$ plane, the intensity distribution for the propagating fields may be represented in terms of $|\tilde{K}_{\ell/\alpha}(\bar{\omega}\rho)|^2$, see Fig. 5.6. We see that the bigger the value of α for a fixed ℓ, the brighter the rings are (fields of high amplitudes). Besides, the bigger the value of $\bar{\omega}$, the smaller the light rings are (the more concentrated fields are the ones near the origin).

5.4 Conclusions

In this Chapter, we studied two configuration of HLCM in order to investigate the possibility to focus light, more specifically the circular field configuration appears as a favorable candidate for designing optical concentrators. Both geometrical optics and wave optics treatments show that light is indeed concentrated while propagating in the HLCM medium. No matter how the rays are injected, they will fall onto the defect core with or without being reflected in the outer layer of the cylindrical concentrator. Because the losses, an optical device made from metamaterials will support evanescent waves. Thus, the length of the optical concentrator has to be short enough to avoid that the losses cancel the field propagation before it reaches the center of the device.

In practice, it has been shown that a given combination of materials forming metamaterials will keep hyperbolic properties only within a range of frequency defined in terms of the plasma frequency of the constituent materials [Smo11].

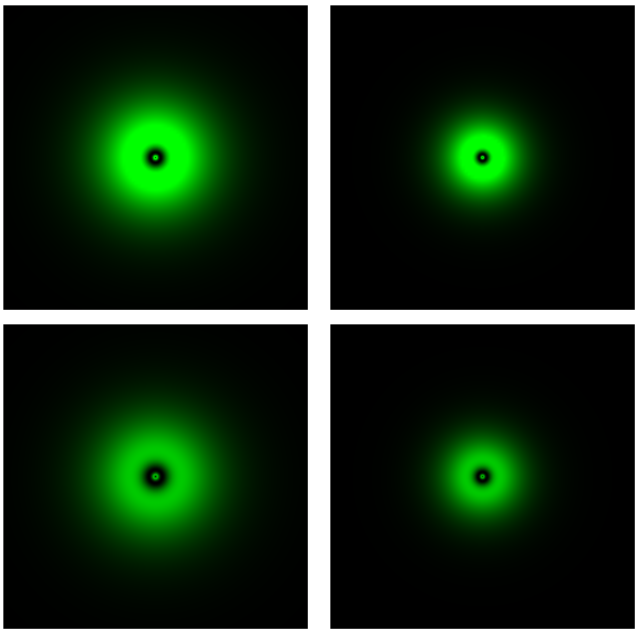

FIGURE 5.6: $|\tilde{K}|^2$ intensity profiles, representing the transverse field distributions. All plots are in the same scale and with $\ell = 1$. The ones on the left (right) correspond to $\bar{\omega} = 0.67$ ($\bar{\omega} = 1$). The top (bottom) ones correspond to $\alpha = 0.90$ ($\alpha = 0.83$).

However, hyperbolic metamaterials allow the propagation of waves with very large wavevectors, and consequently very small wavelengths [Fer+15] that are restricted to the metamaterial unit cell size (then introducing a natural cutoff) [Smo18].

Although we did not emphasize this before, our analysis showed a singularity at the origin that may be understood as an obstacle. Such singularity appears due to the model we use does not include a realistic description of the defect core, as the curvature associated to the core is concentrated on the axis. The singularity should not show up with model considering a distribution of curvature around the axis, i.e. to soften the singularity would be necessarily for a more realistic description of the core [AO90]. This would lead the defect core to have a finite size, leading to two different regions (interior and exterior to the core), with trajectories that match at the limit of the core. This also would prevent too strong oscillations near the center of the optical concentrator.

Chapter 6

Conclusions and Perspectives

***

In this thesis we have studied general aspects of topological defects from formation (Kibble mechanism) to their geometric effects on the dynamics of fields. The formation of topological defects is unavoidable according to the Grand Unified Theory. Cosmic defects may have been formed during the early times of the Universe as consequence of phase transitions occurring as the Universe expanded and cooled down. All possible defects, the domain walls, monopoles, textures and cosmic strings were discussed here. The latter was better explored since they are not ruled out by their mass energy content. Because their disastrous consequences for the viability of the present Universe, structures as domain walls and monopoles are not expected to exist after the inflation period. Although there are favorable evidences for the existence of cosmic strings, they are still not sufficient to ensure it. This work also dealt with interesting aspects about the analogy between condensed matter (liquid crystals is a great laboratory for cosmology) and cosmological objects. Besides it occurs with respect to their formation (since the Kibble mechanism is well established in both realms) the analogy also holds true in the geometric (gravitational) point of view, the way light propagates in the presence of such objects is analogous. For example, light trajectories in nematic liquid crystal endowed with disclination are exactly the same of the geodesics followed by light in the spacetime of cosmic strings.

However, our focus in this thesis was on the geometric (gravitational) aspects of the topological defects, wiggly string (in cosmology) and hyperbolic disclination (in nematic liquid crystal). Both defects proved to cause interesting effects on propagating fields as we examined trajectories and wave propagation in their background. For example, in Chapter 4, we saw that either massive and massless fields are confined to the wiggly string axis like it happens with electromagnetic waves in ordinary waveguides. Hence, we proposed the design of an optical waveguide likely to mimic the dynamics of fields on the spacetime of wiggly strings. In Chapter 5, we investigated the propagation of light in the HLCM, that is a medium in which the ratio between ordinary an extraordinary permittivities is negative. We conclude from geometrical optics treatment and wave formalism that light rays are concentrated along the defect axis no matter how they are initially injected. Thus, the HLCM behaves as a perfect optical concentrator device. Actually, we saw that such behaviour occurs for one specific director field configuration, the circular one. The same behavior is not found for the radial director field configuration.

In particular, as a perspective for future work we mention the study of propagating electromagnetic waves along the wiggly string and a possible correspondence with an optical fiber. This is more complex than the problem presented here since the vector field equations are coupled and cannot be reduced to scalar wave equations. Moreover, networks of cosmic topological defects have been proposed as models for solid dark matter [BS99]. This suggests that one might explore the optical signatures of a network of wiggly strings. For instance, for a periodic array of strings one might expect some of the properties of a photonic crystal, like the appearance of band gaps in the dispersion relation, which limit the propagation to the allowed regions of the spectrum. Finally, it is in our interest to use the Finsler geometry to investigate soft matter systems where the Riemannian geometry does not apply.

We have mentioned in Chapter 2 that the analogy between Alice strings and $m = \pm 1/2$ (half-integer) disclinations in NLCs. For that reason, we started investigating the gravity of Alice string (to our knowledge this is an absolute unknown aspect), since we have seen that light propagation in a medium endowed with $m = \pm 1$ disclinations is given by geodesics in the background spacetime of an ordinary cosmic string. At the present time, we have not finished with such investigation, but we do believe the Alice string spacetime is a perfect analogue of the effective geometry found for half-integer disclinations [SDMCM09]. This subject is presently under investigation and we hope to have results in the near future.

Appendix A

Appendix

***

A.1 Finslerian Method

An appropriate space for a geometrical description of light propagation is thus of a Finsler geometry [JR94; SM06], for which the line element is of the form

$$ds = N_r dl = F(x, \dot{x}) d\tau \tag{A.1}$$

where dl is the infinitesimal arc length along the curve followed by the propagating rays and $\dot{x}^\mu = dx^\mu/d\tau$ measuring local direction and $F(x, \dot{x})$ the Finsler function. Joets and Ribotta [JR94] have chosen $F(x, \dot{x}) = N_r$, where N_r is the *ray index* which governs the Energy velocity, see Section 3.3. Then, they have shown that the light rays which obey Fermat's principle for the energy propagation of the extraordinary ray

$$\delta \int N_r dl = 0 \tag{A.2}$$

are the geodesics in Finsler space

$$\frac{d^2x^\lambda}{d\tau^2} + \Gamma^\lambda{}_{\alpha\beta} \frac{dx^\alpha}{d\tau} \frac{dx^\beta}{d\tau} - \frac{d \ln N_r}{d\tau} \frac{dx^\lambda}{d\tau} = 0. \tag{A.3}$$

If the parameter τ is chosen to be the arc length l in Eq. (A.1), $F = 1$ and the Finsler geodesic equation simplifies into Riemannian geodesic equation (3.7).

By using the identity $ds^2 = N_r^2 dl^2 = g_{\alpha\beta}dx^\alpha dx^\beta = F(x,\dot{x})^2 d\tau^2$, we obtain the Finslerian metric tensor components as

$$g_{\alpha\beta} = \frac{1}{2}\frac{\partial^2 F^2}{\partial x^\alpha \partial x^\beta}. \tag{A.4}$$

Hence, it turns out that the use of Riemannian geometry to be exactly the same of the general Finslerian approach [SM06].

A.2 Numerical Analysis

In order to solve the wave radial equation (Eq. (4.9)) for propagating massless and massive fields on the background spacetime of the wiggly string we have used a finite difference method.

Following, we give more detail about such method and its application to our problem.

A.2.1 Finite Difference Method

FDM consists in to replace derivatives into differential equations with discrete differences approximations [MUGGMV96; Dat05; BF11; FG11]:

$$\frac{d\psi}{dx} = \frac{\psi_{j+1} - \psi_{j-1}}{2\Delta x} + O(\Delta x^2) \tag{A.5}$$

and

$$\frac{d^2\psi}{dx^2} = \frac{\psi_{j+1} - 2\psi_j + \psi_{j-1}}{\Delta x^2} + O(\Delta x^2), \tag{A.6}$$

on a regular grid $x_j = j\Delta x$, with $j = 0, 1, 2..., N, N+1$. Such approximations can be used to solve any differential equation leading to eigenvalue equations:

$$M\psi_j = \lambda\psi_j, \tag{A.7}$$

where M is a sparse matrix representing the discretized operator (the Hamiltonian in wave equations) and $\psi_j = \psi(x_j)$ is a vector. In theory, the matrix M can be infinitely large, but in practice we need to truncate it to a finite number of element, say N. For that, we have to set the boundary values ψ_0 and ψ_{N+1} equal to zero. In fact, such boundary condition is appropriate for the case where the "potential" is infinitely large at the point 0 and at the point $N+1$ (as it is the case of Eq. (4.9)), since wavefunctions are essentially zero at these points anyway. Therefore, after doing so, we get a finite matrix of dimension $N \times N$. Hence, solving equation (A.7) give us the N eigenvalues $(\lambda_1, \lambda_2, ...\lambda_N)$, and in turn, each one has an associated eigenvector.

A.2.2 Applying the Finite Difference Method

In the equation (4.9) the logarithmic term is infinitely large at the points 0 and ∞. In this case, we can use the boundary conditions $R(0) = 0$ and $R(\rho_\infty) = 0$, where ρ_∞ represents the value in which ρ is infinitely large. Hence, our discretization has a step size defined as:

$$\Delta\rho = \frac{\rho_\infty}{N}, \tag{A.8}$$

with N being the number of points on the grid. It is clear that decreasing the value of $\Delta\rho$ the method becomes more efficient.

By following the proceeding in Ref. [Gar11] we make a change of variables in the equation (4.9) of the type $u = \rho^{1/2}R$, then

$$-\frac{d^2u}{d\rho^2} + \left[\frac{(l/\alpha)^2 - 1/4}{\rho^2} + \ln\rho\right] u = \bar{\zeta}u. \tag{A.9}$$

For $l = 0$ we have to require that our wavefunction goes to zero faster, setting $u = \rho R$, we obtain

$$-\frac{d^2u}{d\rho^2} + \frac{1}{\rho}\frac{du}{d\rho} + \left[\frac{(l/\alpha)^2 - 1}{\rho^2} + \ln\rho\right] u = \bar{\zeta}u. \tag{A.10}$$

Obviously we will use equation (A.9) for $l \neq 0$ and equation (A.10) for $l = 0$. Both equations (A.9) and (A.9) obey the specified boundary conditions.

We have to set the two free parameters of our discretization, ρ_∞ and N. For N large means more eigenvalues to be obtained and consequently better efficiency, however, it can becomes a hard work for the computer. Then, we can increase N as large as the computer permit it. In fact, we need that the eigenvalues with small n and l have converged to some accuracy. In the case of ρ_∞, we need to find a value so that $u(\rho_\infty) = 0$. A prior we can looking at eigenvalues for large n and l and choose ρ_∞ so that wavefunction goes to zero within this bound [FG11; Gar11]. For our case, we have found values around $N = 10000$ and $\rho_\infty = 400$, that is $\Delta\rho = 4/100$. Here, we have used a trick, since we are looking at eigenvalues and eigenfunctions for small n and l, we can decrease ρ_∞ to improve our result. At the end of the day, our calculation was done by setting $\rho_\infty = 40$, then $\Delta\rho = 4/1000$.

A.2.3 Discretization Codes

We can implement the FDM using any language or numerical package that takes advantage of the sparsity feature of the matrix M. Following, we present the discretization code written in Mathematica and Python languages.

Listing A.1: Discretization code for equation (A.9) in Mathematica language

```
# ************************************************************
#  Wiggly waveguide
# ************************************************************
```

```
WigglyWaveguide[pinf_,NN_,L_,\[Alpha]_] :=

Module[{Mat, ret, d , l , sdata , dp, idex , p },
dp = pinf/NN;
l = L^2/\[Alpha];
d = 0.25;
sdata = {};

For[idex = 2, idex <= NN - 1 , idex = idex + 1,
p = idex  dp;
sdata =
Join[sdata, {{idex, idex} -> (Log[p] + (l - d)/p^2 + 2.0/dp^2),
{idex, idex + 1} -> -1.0/dp^2  , {idex , idex - 1} -> -1.0/
dp^2}];
];

idex = 1;
p = idex  dp;
sdata =
Join[sdata , {{idex , idex} -> (Log[p] + (l - d)/p^2 + 2.0/dp^2),
{idex , idex + 1} -> -1.0/dp^2}];

idex = NN;
p = idex  dp;
sdata =
Join[sdata, {{idex , idex} -> (Log[p] + (l - d)/p^2 + 2.0/dp^2),
{idex , idex - 1} -> -1.0/dp^2}];

Mat = SparseArray[sdata];
Return[Mat];
]
```

Listing A.2: Discretization code for equation (A.10) in Mathematica language

```
# ************************************************************
#  Wiggly waveguide
# ************************************************************

WigglyWaveguide[pinf_, NN_, L_,\[Alpha]_] :=

Module[{Mat, ret, d , l , sdata , dp, idex , p },
dp = pinf/NN;
l = L^2/\[Alpha]_;
d = 1;
sdata = {};

For[idex = 2, idex <= NN - 1 , idex = idex + 1,
p = idex  dp;
sdata =
Join[sdata, {{idex, idex} -> (Log[p] + (l - d)/p^2 + 2.0/dp^2),
{idex, idex + 1} -> -1.0/dp^2 + 1.0/(p 2.0 dp) , {idex ,
idex - 1} -> -1.0/dp^2 - 1.0/(p 2.0 dp)}];
];

idex = 1;
p = idex  dp;
```

```
sdata =
Join[sdata , {{idex , idex} -> (Log[p] + (l - d)/p^2 + 2.0/dp^2),
{idex , idex + 1} -> -1.0/dp^2 + 1.0/(p 2.0 dp)}];

idex = NN;
p = idex  dp;
sdata =
Join[sdata, {{idex , idex} -> (Log[p] + (l - d)/p^2 + 2.0/dp^2),
{idex , idex - 1} -> -1.0/dp^2 - 1.0/(p 2.0 dp )}];

Mat = SparseArray[sdata];
Return[Mat];
]
```

The discretization code in the first listing above can be found in Ref. [Gar11], where it was used in the context of the 2D hydrogen atom. Here, we have used it to solve our wave equation 4.9, which is indeed mathematically similar to the Schrödinger equation for the 2D hydrogen atom. The second listing code is not given in the Ref. [Gar11], but we also provide it here and it is showed to provide the same results found in such reference. Bellow, we present the listing code to be used for the users of Python from where they could get the same results.

LISTING A.3: Discretization code for equations (A.9) and (A.10) in Python language

```
# ************************************************************
# Wiggly waveguide
# ************************************************************

def DiscretizeWigglyWaveguide(length, size, L, l, d):
    dx = length / size
    x = np.linspace(dx, length, size)

    main = [ np.log(x) + (l - d) / x ** 2 + 2 / dx ** 2 ]

    if L != 0:
        other = (-1 / dx ** 2) * np.ones(size - 1)
        sData = np.diagflat(main, 0) + np.diagflat(other, -1)
        + np.diagflat(other, +1)
    else:
        upper = (-1 / dx ** 2 + 1 / (2 * x[:-1] * dx))
        lower = (-1 / dx ** 2 - 1 / (2 * x[1:] * dx))
        sData = np.diagflat(main, 0) + np.diagflat(lower, -1)
        + np.diagflat(upper, +1)

    return x, sparse.csc_matrix(sData)

# ************************************************************
#  Wiggly waveguide
# ************************************************************

def WigglyWaveguide(config):
```

```
    length = config['length']
    size   = config['size']
    L      = config['L']
    alpha  =  xu._get_kwarg('alpha', config, 1)

    l = L** 2 / alpha ** 2
    d = 0.25 if L != 0 else 1

    return DiscretizeWigglyWaveguide(length, size, L, l, d)
```

A.3 Eikonal Approximation

The eikonal approximation has been used to study optics in metamaterials [Ves02; JAN07; FNB16a] and supplies the same light trajectories as the Fermat's principle. Therefore, we show here that the eikonal approximation is also an alternative to study light propagation in hyperbolic metamaterial. By performing straightforward calculations we are able to obtain the same equations when using Fermat's principle (differential geometry tools) found in Chapter 5 of this manuscript.

The metric that defines the hyperbolic metamaterial of circular director field Fig. 5.2 (a) can be written in terms of the permittivities as (see Eq. (5.1)):

$$g_{\mu\nu} = \begin{pmatrix} -1 & 0 & 0 & 0 \\ 0 & -\left|\varepsilon_{\parallel}\right| & 0 & 0 \\ 0 & 0 & \varepsilon_{\perp} r^2 & 0 \\ 0 & 0 & 0 & -\left|\varepsilon_{\parallel}\right| \end{pmatrix}. \tag{A.11}$$

Therefore, proceeding in the same manner as in refs. [JAN07; FNB16a], and also [LL75], the eikonal equation $k_\mu k^\mu$=0 becomes

$$g^{\mu\nu} \frac{\partial \Psi}{\partial x^\mu} \frac{\partial \Psi}{\partial x^\nu} = 0 \tag{A.12}$$

$$-\frac{1}{c^2}\left(\frac{\partial \Psi}{\partial t}\right)^2 - \frac{1}{\left|\varepsilon_{\parallel}\right|}\left(\frac{\partial \Psi}{\partial r}\right)^2 + \frac{1}{\varepsilon_{\perp} r^2}\left(\frac{\partial \Psi}{\partial \phi}\right)^2 - \frac{1}{\left|\varepsilon_{\parallel}\right|}\left(\frac{\partial \Psi}{\partial z}\right)^2 = 0, \tag{A.13}$$

where Ψ is the eikonal. Substituting the usual relations $\omega = -\partial_t \Psi$ and $k_i = \partial_i \Psi$, one gets

$$-\frac{\left(k_r^2 + k_z^2\right)}{\left|\varepsilon_{\parallel}\right|} + \frac{k_\phi^2}{\varepsilon_{\perp} r^2} = \frac{\omega^2}{c^2}, \tag{A.14}$$

which is nothing more than the usual hyperbolic dispersion relation for metamaterials (see Eq. 5.5). Rescaling the coordinates according to $\rho = r\sqrt{\left|\varepsilon_{\parallel}\right|}$ and $\zeta = z\sqrt{\left|\varepsilon_{\parallel}\right|}$, the above equation becomes

$$-k_\rho^2 + \frac{k_\phi^2}{\alpha^2 \rho^2} - k_\zeta^2 = \frac{\omega^2}{c^2}, \tag{A.15}$$

with $\alpha^2 = \varepsilon_\perp / \left|\varepsilon_\parallel\right|$. According to ref. [LL71], the wave vector plays the same role in geometrical optics as the momentum of the particle in mechanics, while the frequency plays the role of the Hamiltonian. Therefore, we can use the Hamilton equations in the form

$$\dot{x}^i = \frac{\partial \omega}{\partial k_i}, \qquad \dot{k}_i = -\frac{\partial \omega}{\partial x^i}. \tag{A.16}$$

From Eq. (A.15), we recognize k_ϕ and k_ζ as constants of motion. As for the other equations:

$$\dot{\zeta} = -\frac{c^2}{\omega} k_\zeta \equiv A, \tag{A.17}$$

$$\dot{\phi} = \frac{c^2}{\omega} \frac{k_\phi}{\alpha^2 \rho^2} \Rightarrow \rho^2 \dot{\phi} = \frac{c^2}{\omega} \frac{k_\phi}{\alpha^2} \equiv \frac{\tilde{C}}{\alpha^2} \equiv C, \tag{A.18}$$

$$\dot{\rho} = -\frac{c^2}{\omega} k_\rho. \tag{A.19}$$

As one can see, Eqs. (A.17) and (A.18) are the same equations Eqs. (5.11) and (5.12). Since the Hamiltonian (frequency) does not depend explicitly on time, it is constant. Thus, substituting equations (A.17)–(A.19) in Eq. (A.15), one gets the following

$$-\dot{\rho}^2 + \alpha^2 \rho^2 \dot{\phi}^2 - \dot{\zeta}^2 = c^2 \equiv B, \tag{A.20}$$

which is exactly the same equation (5.13) obtained in Chapter 5 of this manuscript with help of Fermat's principle.

References

***

[Abr57] Alexei A Abrikosov. "On the magnetic properties of superconductors of the second group". In: *Sov. Phys. JETP* 5 (1957), p. 1174.

[Ade+14] Peter A R Ade et al. "Planck 2013 results. XXV. Searches for cosmic strings and other topological defects". In: *Astronomy & Astrophysics* 571 (2014), A25.

[AHP06] Eric Agol, Craig J Hogan, and Richard M Plotkin. "Hubble imaging excludes cosmic string lens". In: *Physical Review D* 73 (2006), p. 087302.

[AO90] Bruce Allen and Adrian C Ottewill. "Effects of curvature couplings for quantum fields on cosmic-string space-times". In: *Physical Review D* 42 (1990), p. 2669.

[AS90] Bruce Allen and Edward P S Shellard. "Cosmic-string evolution: a numerical simulation". In: *Physical review letters* 64 (1990), p. 119.

[AS00] Andés Arazi and Claudio Simeone. "Wiggly string in linearized Brans–Dicke Gravity". In: *Modern Physics Letters A* 15 (2000), p. 1369.

[AA85] Francisco J Asturias and Sergio R Aragon. "The hydrogenic atom and the periodic table of the elements in two spatial dimensions". In: *American Journal of Physics* 53 (1985), p. 893.

[Aze+17] Frankbelson dos S Azevedo et al. "Wiggly cosmic string as a waveguide for massless and massive fields". In: *Physical Review D* 96 (2017), p. 084047.

[Aze+18] Frankbelson dos S Azevedo et al. "Optical concentrator from a hyperbolic liquid crystal metamaterial". In: *arXiv preprint arXiv:1806.11514* (2018).

[Baj+04] Borut Bajc et al. "The Minimal supersymmetric grand unified theory. 1. Symmetry breaking and the particle spectrum". In: *Phys. Rev. D.* 70 (2004), p. 035007.

[BV89] Manuel Barriola and Alexander Vilenkin. "Gravitational field of a global monopole". In: *Physical Review Letters* 63 (1989), p. 341.

[BB90] David P Bennett and Francois R Bouchet. "High-resolution simulations of cosmic-string evolution. I. Network evolution". In: *Physical Review D* 41 (1990), p. 2408.

[BS03] David J Bergman and Mark I Stockman. "Surface plasmon amplification by stimulated emission of radiation: quantum generation of coherent surface plasmons in nanosystems". In: *Physical review letters* 90 (2003), p. 027402.

[BDL16] David Bermudez, Jonathan Drori, and Ulf Leonhardt. "Dialogues about geometry and light". In: *Frontiers in Modern Optics* 190 (2016), p. 1.

[Bim+98] G Bimonte et al. "Cosmological waveguides for gravitational waves". In: *Physical Review D* 58 (1998), p. 104009.

[BPOS18] Jose J Blanco-Pillado, Ken D Olum, and Xavier Siemens. "New limits on cosmic strings from gravitational wave observation". In: *Physics Letters B* 778 (2018), p. 392.

[BW99] Max Born and Emil Wolf. *Principles of optics: electromagnetic theory of propagation, interference and diffraction of light*. 7th. Cambridge University Press, 1999.

[Bow+94] Mark J Bowick et al. "The cosmological kibble mechanism in the laboratory: string formation in liquid crystals." In: *Science (New York, NY)* 263 (1994), p. 943.

[BS99] Martin Bucher and David Spergel. "Is the dark matter a solid?" In: *Physical Review D* 60 (1999), p. 043505.

[BF11] Richard L. Burden and J. Douglas Faires. *Numerical analysis*. Brooks/Cole, Cencag Learning, 2011.

[Car01] Moshe Carmeli. *Classical fields: general relativity and gauge theory*. World Scientific Publishing Company, 2001.

[Car04] Sean M Carroll. *Spacetime and geometry. An introduction to general relativity*. 2004.

[Car90] Brandon Carter. "Integrable equation of state for noisy cosmic string". In: *Physical Review D* 41 (1990), p. 3869.

[Che14] Chin-Hao Chen. "Studying the Early Universe via Quark-Gluon Plasma". In: *Nuclear Physics B-Proceedings Supplements* 246 (2014), p. 38.

[CCS10] Huanyang Chen, Che Ting Chan, and Ping Sheng. "Transformation optics and metamaterials". In: *Nature materials* 9 (2010), p. 387.

[Chu+91] Isaac Chuang et al. "Cosmology in the laboratory: Defect dynamics in liquid crystals". In: *Science* 251 (1991), p. 1336.

[CK10] Edmund J. Copeland and Thomas W B Kibble. "Cosmic strings and superstrings". In: *Proceedings of the Royal Society of London A: Mathematical, Physical and Engineering Sciences* (2010).

[CPV11] Edmund J Copeland, Levon Pogosian, and Tanmay Vachaspati. "Seeking string theory in the cosmos". In: *Classical and Quantum Gravity* 28 (2011), p. 204009.

[Cru+07] Marcos Cruz et al. "A cosmic microwave background feature consistent with a cosmic texture". In: *Science* 318 (2007), p. 1612.

[Dat05] Supriyo Datta. *Quantum Transport*. Cambridge University Press, 2005.

[DLKV97] Andrew A De Laix, Lawrence M Krauss, and Tanmay Vachaspati. "Gravitational lensing signature of long cosmic strings". In: *Physical review letters* 79 (1997), p. 1968.

[Dir31] Paul AM Dirac. "Quantised singularities in the electromagnetic field". In: *Proceedings of the Royal Society of London. Series A* 133 (1931), p. 60.

[DM89] Victor V Dodonov and Vladimir I Man'ko. "Gravitational waveguide". In: *Journal of Soviet Laser Research* 10 (1989), p. 240.

[Dun90] Timothy M Dunster. "Bessel functions of purely imaginary order, with an application to second-order linear differential equations having a large parameter". In: *SIAM Journal on Mathematical Analysis* 21 (1990), p. 995.

[DT99] Gia Dvali and S-H Henry Tye. "Brane inflation". In: *Physics Letters B* 450 (1999), p. 72.

[DB07] Sergei Dyda and Robert H Brandenberger. "Cosmic strings and weak gravitational lensing". In: *arXiv preprint arXiv:0710.1903* (2007).

[Eve+90] Kevin Eveker et al. "The two-dimensional hydrogen atom with a logarithmic potential energy function". In: *American Journal of Physics* 58 (1990), p. 1183.

[Fee+12] Stephen M Feeney et al. "Robust Constraint on Cosmic Textures from the Cosmic Microwave Background". In: *Physical review letters* 108 (2012), p. 241301.

[Fen12] Fa-Bo Feng. "Radio jets and galaxies as cosmic string probes". In: *Frontiers of Physics* 7 (2012), p. 461.

[FNB16a] Isabel Fernández-Núñez and Oleg Bulashenko. "Anisotropic metamaterial as an analogue of a black hole". In: *Physics Letters A* 380 (2016), p. 1.

[FNB16b] Isabel Fernández-Núñez and Oleg Bulashenko. "Wave diffraction by a cosmic string". In: *Physics Letters A* 380 (2016), p. 2897.

[Fer+15] Lorenzo Ferrari et al. "Hyperbolic metamaterials and their applications". In: *Progress in Quantum Electronics* 40 (2015), p. 1.

[Fig+16] David Figueiredo et al. “Modeling Kleinian cosmology with electronic metamaterials”. In: *Physical Review D* 94 (2016), p. 044039.

[Fig+17] David Figueiredo et al. “Cosmology in the laboratory: an analogy between hyperbolic metamaterials and the Milne universe”. In: *Phys. Rev. D* 96 (10 2017), p. 105012.

[FM08] Cleverson Filgueiras and Fernando Moraes. “On the quantum dynamics of a point particle in conical space”. In: *Annals of Physics* 323 (2008), p. 3150.

[Fra58] Frederick C Frank. “I. Liquid crystals. On the theory of liquid crystals”. In: *Discussions of the Faraday Society* 25 (1958), p. 19.

[FG11] J. Franklin and T. Garon. “Approximate Born–Infeld effects on the relativistic hydrogen spectrum”. In: *Physics Letters A* 375 (2011), p. 1391.

[Fri22] Georges Friedel. “The mesomorphic states of matter”. In: *Annales de Physique* 18 (1922), p. 273.

[Fuk+05] Takeshi Fukuyama et al. “SO(10) Group Theory for the Unified Model Building”. In: *J. Math. Phys.* 46 (2005), p. 033505.

[Ful89] Stephen A Fulling. *Aspects of quantum field theory in curved spacetime*. Cambridge university press, 1989.

[Fum+15] Sébastien Fumeron et al. “Optics near a hyperbolic defect”. In: *Physical Review A* 92 (2015), p. 063806.

[Gan01] Alejandro Gangui. “Topological defects in cosmology”. In: *arXiv preprint astro-ph/0110285* (2001).

[Gar85] David Garfinkle. “General relativistic strings”. In: *Physical Review D* 32 (1985), p. 1323.

[Gar11] Todd S. Garon. “The Two-dimensional Hydrogen Atom”. PhD thesis. Reed College, 2011.

[GMM13] Todd S. Garon, Nelia Mann, and Ellen M. McManis. “Re-examining the value of old quantization and the Bohr atom approach”. In: *American Journal of Physics* 81 (2013), p. 92.

[GPP95] Pierre-Gilles De Gennes, Jacques Prost, and Robert Pelcovits. “The physics of liquid crystals”. In: *Physics Today* 48 (1995), p. 67.

[GZZ09] Dentcho A Genov, Shuang Zhang, and Xiang Zhang. “Mimicking celestial mechanics in metamaterials”. In: *Nature Physics* 5 (2009), p. 687.

[GG72] Howard Georgi and Sheldon L Glashow. “Unified weak and electromagnetic interactions without neutral currents”. In: *Physical Review Letters* 28 (1972), p. 1494.

[GP78] F Gesztesy and L Pittner. "Electrons in logarithmic potentials. I. Solution of the Schrodinger equation". In: *Journal of Physics A: Mathematical and General* 11 (1978), p. 679.

[GBY17] Min-Jun Gim, Daniel A Beller, and Dong Ki Yoon. "Morphogenesis of liquid crystal topological defects during the nematic-smectic A phase transition". In: *Nature communications* 8 (2017), p. 15453.

[GDJM06] Pedro F Gonzalez-Diaz and José A Jiménez Madrid. "Wiggly cosmic strings accrete dark energy". In: *International Journal of Modern Physics D* 15 (2006), p. 603.

[Gor23a] Walter Gordon. "Zur Lichtfortpflanzung nach der Relativitätstheorie". In: *Ann. Phys. Leipzig* 72 (1923), p. 421.

[Gor23b] Walter Gordon. "Zur Lichtfortpflanzung nach der Relativitätstheorie". In: *Annalen der Physik* 377 (1923), p. 421.

[GI85] John Richard Gott III. "Gravitational lensing effects of vacuum strings-Exact solutions". In: *The Astrophysical Journal* 288 (1985), p. 422.

[HL90] Diego Harari and Carlos Lousto. "Repulsive gravitational effects of global monopoles". In: *Physical Review D* 42 (1990), p. 2626.

[HH05] John F Hawley and Katherine A Holcomb. *Foundations of modern cosmology*. Oxford University Press, 2005.

[Her+17] Lukas Hergt et al. "Searching for cosmic strings in CMB anisotropy maps using wavelets and curvelets". In: *Journal of Cosmology and Astroparticle Physics* 2017 (2017), p. 004.

[HK95] Mark Hindmarsh and Thomas W B Kibble. "Cosmic strings". In: *Reports on Progress in Physics* 58 (1995), p. 477.

[HW90] Mark Hindmarsh and Andrew Wray. "Gravitational effects of line sources and the zero-width limit". In: *Physics Letters B* 251 (1990), p. 498.

[His85] William A Hiscock. "Exact gravitational field of a string". In: *Physical Review D* 31 (1985), p. 3288.

[Hoo74] Gerard Hooft. "Magnetic monopoles in unified gauge theories". In: *Nuclear Physics: B* 79 (1974), p. 276.

[Hub29] Edwin Hubble. "A relation between distance and radial velocity among extra-galactic nebulae". In: *Proceedings of the National Academy of Sciences* 15 (1929), p. 168.

[IS18] Anna Ijjas and Paul J Steinhardt. "Bouncing Cosmology made simple". In: *Classical and Quantum Gravity* 35 (2018), p. 135004.

[Jac99] John David Jackson. *Classical electrodynamics*. John Wiley & Sons, Inc., New York, NY, 1999.

[JAN06] Zubin Jacob, Leonid V Alekseyev, and Evgenii Narimanov. "Optical hyperlens: far-field imaging beyond the diffraction limit". In: *Optics express* 14 (2006), p. 8247.

[JAN07] Zubin Jacob, Leonid V Alekseyev, and Evgenii Narimanov. "Semiclassical theory of the hyperlens". In: *JOSA A* 24 (2007), A52.

[JRS03] Rachel Jeannerot, Jonathan Rocher, and Mairi Sakellariadou. "How generic is cosmic string formation in supersymmetric grand unified theories". In: *Physical Review D* 68 (2003), p. 103514.

[JR94] Alain Joets and Roland Ribotta. "A geometrical model for the propagation of rays in an anisotropic inhomogeneous medium". In: *Optics communications* 107 (1994), p. 200.

[KS84] Nick Kaiser and Albert Stebbins. "Microwave anisotropy due to cosmic strings". In: *Nature* 310 (1984), p. 391.

[KV92] Mikhail O Katanaev and Igor V Volovich. "Theory of defects in solids and three-dimensional gravity". In: *Annals of Physics* 216 (1992), p. 1.

[Ken06] Ralph Kenna. "Homotopy in statistical physics". In: *Condensed Matter Physics* 9 (2006), p. 283.

[Kib76] Thomas W B Kibble. "Topology of cosmic domains and strings". In: *Journal of Physics A: Mathematical and General* 9 (1976), p. 1387.

[Kib97] Thomas W B Kibble. "Phase transitions and topological defects in the early universe". In: *Australian journal of physics* 50 (1997), p. 697.

[KS11] Alexander V Kildishev and Vladimir M Shalaev. "Transformation optics and metamaterials". In: *Physics-Uspekhi* 54 (2011), p. 53.

[Kit49] Charles Kittel. "Physical theory of ferromagnetic domains". In: *Reviews of modern Physics* 21 (1949), p. 541.

[Klé89] Maurice Kléman. "Defects in liquid crystals". In: *Reports on Progress in Physics* 52 (1989), p. 555.

[KL07] Maurice Kleman and Oleg D Laverntovich. *Soft matter physics: an introduction*. Springer Science & Business Media, 2007.

[KT90] Edward W Kolb and Michael S Turner. *The Early Universe*. 1990.

[KGP15] Karolina Korzeb, Marcin Gajc, and Dorota Anna Pawlak. "Compendium of natural hyperbolic materials". In: *Optics express* 23 (2015), p. 25406.

[LCM87] Pablo Laguna-Castillo and Richard A Matzner. "Coupled field solutions for U (1)-gauge cosmic strings". In: *Physical Review D* 36 (1987), p. 3663.

[LL71] Lev Davidovich Landau and Evgenii Mikhailovich Lifshitz. *The classical theory of fields*. Pergamon, 1971.

[LL75] Lev Davidovich Landau and Evgenii Mikhailovich Lifshitz. "The classical theory of fields". In: *Course of theoretical physics* (1975), p. 281.

[Lem27] Georges Lemaître. "Un Univers homogène de masse constante et de rayon croissant rendant compte de la vitesse radiale des nébuleuses extra-galactiques". In: *Annales de la Société scientifique de Bruxelles*. 1927, p. 49.

[LP10] Ulf Leonhardt and Thomas Philbin. *Geometry and light: the science of invisibility*. Dover Publications, 2010.

[LP09] Ulf Leonhardt and Thomas G Philbin. "Transformation optics and the geometry of light". In: *Progress in Optics* 53 (2009), p. 69.

[LBM11] Bertúlio de Lima Bernardo and Fernando Moraes. "Data transmission by hypergeometric modes through a hyperbolic-index medium". In: *Optics Express* 19 (2011), p. 11264.

[Lin85] Bernard Linet. "The static metrics with cylindrical symmetry describing a model of cosmic strings". In: *General Relativity and Gravitation* 17 (1985), p. 1109.

[LC17] Martín López-Corredoira. "Tests and problems of the standard model in Cosmology". In: *Foundations of Physics* 47 (2017), p. 711.

[ML10] Tom G Mackay and Akhlesh Lakhtakia. "Towards a metamaterial simulation of a spinning cosmic string". In: *Physics Letters A* 374 (2010), p. 2305.

[ML15] Tom G Mackay and Akhlesh Lakhtakia. "Metamaterial models of curved spacetime". In: *Metamaterials, Metadevices, and Metasystems 2015*. International Society for Optics and Photonics. 2015, 95442K.

[MUGGMV96] Juan F Van der Maelen Uría, Santiago García-Granda, and Amador Menéndez-Velázquez. "Solving one-dimensional Schrödinger-like equations using a numerical matrix method". In: *American Journal of Physics* 64 (1996), p. 327.

[MK72] Patricia E. Cladis et Maurice Kléman. "Non-singular disclinations of strength $S = +1$ in nematics". In: *J. Phys. France* 33 (1972), p. 591.

[MM11] Babak Memarzadeh and Hossein Mosallaei. "Array of planar plasmonic scatterers functioning as light concentrator". In: *Optics Letters* 36 (2011), p. 2569.

[Mor00] Fernando Moraes. "Condensed matter physics as a laboratory for gravitation and cosmology". In: *Brazilian Journal of Physics* 30 (2000), p. 304.

[NB10] Gururaj V Naik and Alexandra Boltasseva. "Semiconductors for plasmonics and metamaterials". In: *physica status solidi (RRL)–Rapid Research Letters* 4 (2010), p. 295.

[NK15] Evgenii E Narimanov and Alexander V Kildishev. "Metamaterials: naturally hyperbolic". In: *Nature Photonics* 9 (2015), p. 214.

[NO73] Holger Bech Nielsen and Poul Olesen. "Vortex-line models for dual strings". In: *Nuclear Physics B* 61 (1973), p. 45.

[Nog+08] Mikhail A Noginov et al. "Stimulated emission of surface plasmon polaritons". In: *Physical review letters* 101 (2008), p. 226806.

[Nöt91] Dirk Nötzold. "Gravitational effects of global textures". In: *Physical Review D* 43 (1991), R961.

[Olv+10] Frank WJ Olver et al. *NIST handbook of mathematical functions*. Cambridge University Press, 2010.

[PPFM98] Antonio de Padua, Fernando Parisio-Filho, and Fernando Moraes. "Geodesics around line defects in elastic solids". In: *Phys. Lett.* 238 (1998), p. 153.

[Pen00] John B Pendry. "Negative Refraction Makes a Perfect Lens". In: *Phys. Rev. Lett.* 85 (2000), p. 3966.

[PSS06] John B Pendry, David Schurig, and David R Smith. "Controlling electromagnetic fields". In: *science* 312 (2006), p. 1780.

[PM11a] Erms Pereira and Fernando Moraes. "Diffraction of light by topological defects in liquid crystals". In: *Liquid Crystals* 38 (2011), p. 295.

[PM11b] Erms Pereira and Fernando Moraes. "Flowing liquid crystal simulating the Schwarzschild metric". In: *Central European Journal of Physics* 9 (2011), p. 1100.

[Pet94] Patrick Peter. "Comments on some metric properties of cosmic strings having a non-degenerate stress–energy tensor". In: *Classical and Quantum Gravity* 11 (1994), p. 131.

[Pod+13] Alexander Poddubny et al. "Hyperbolic metamaterials". In: *Nature photonics* 7 (2013), p. 958.

[Pol96] Alexander M Polyakov. "Particle spectrum in quantum field theory". In: *30 Years Of The Landau Institute—Selected Papers*. World Scientific, 1996, p. 540.

[Pre86] John Preskill. *Vortices and monopoles*. Tech. rep. 1986.

[Rab11] Stuart Raby. "Searching for the Standard Model in the String Landscape: SUSY GUTs". In: *Rep. Prog. Phys.* 74 (2011), p. 036901.

[Rao02] Sumathi Rao. *Field theories in condensed matter physics*. CRC Press, 2002.

[SC11] Alessandro Salandrino and Demetrios N Christodoulides. "Reverse optical forces in negative index dielectric waveguide arrays". In: *Optics letters* 36 (2011), p. 3103.

[ST02] Saswat Sarangi and S-H Henry Tye. "Cosmic string production towards the end of brane inflation". In: *Physics Letters B* 536 (2002), p. 185.

[SDMCM09] Caio Satiro, A.M. De M. Carvalho, and Fernando Moraes. "An asymmetric family of cosmic strings". In: *Modern Physics Letters A* 24 (2009), p. 1437.

[SM05] Caio Sátiro and Fernando Moraes. "A liquid crystal analogue of the cosmic string". In: *Modern Physics Letters A* 20 (2005), p. 2561.

[SM06] Caio Sátiro and Fernando Moraes. "Lensing effects in a nematic liquid crystal with topological defects". In: *The European Physical Journal E* 20 (2006), p. 173.

[Saz+03] Mikhail V Sazhin et al. "CSL-1: chance projection effect or serendipitous discovery of a gravitational lens induced by a cosmic string?" In: *Monthly Notices of the Royal Astronomical Society* 343 (2003), p. 353.

[Saz+06] Mikhail V Sazhin et al. "The true nature of CSL-1". In: *arXiv preprint astro-ph/0601494* (2006).

[Saz+07] Mikhail V Sazhin et al. "Gravitational lensing by cosmic strings: what we learn from the CSL-1 case". In: *Monthly Notices of the Royal Astronomical Society* 376 (2007), p. 1731.

[Sch09] Jan Pieter van der Schaar. "Cosmic Strings". In: (2009).

[Sch82] Albert S Schwarz. "Field theories with no local conservation of the electric charge". In: *Nuclear Physics B* 208 (1982), p. 141.

[She+13] Chong Sheng et al. "Trapping light by mimicking gravitational lensing". In: *Nature Photonics* 7 (2013), p. 902.

[SL91] Xin Shi and Xinzhou Li. "The gravitational field of a global monopole". In: *Classical and Quantum Gravity* (1991), p. 761.

[Sky61] Tony H R Skyrme. "Particle states of a quantized meson field". In: *Proc. R. Soc. Lond. A* 262 (1961), p. 237.

[SPW04] David R Smith, John B Pendry, and Mike CK Wiltshire. "Metamaterials and negative refractive index". In: *Science* 305 (2004), p. 788.

[Smo11] Igor I Smolyaninov. "Critical opalescence in hyperbolic metamaterials". In: *Journal of Optics* 13 (2011), p. 125101.

[Smo18] Igor I Smolyaninov. *Hyperbolic Metamaterials*. 2053. Morgan Claypool Publishers, 2018. ISBN: 978-1-6817-4565-7.

[SN10] Igor I Smolyaninov and Evgenii E Narimanov. "Metric signature transitions in optical metamaterials". In: *Physical Review Letters* 105 (2010), p. 067402.

[Sni61] Elias Snitzer. “Cylindrical dielectric waveguide modes”. In: *JOSA* 51 (1961), p. 491.

[Spe+03] David N Spergel et al. “First-year Wilkinson Microwave Anisotropy Probe (WMAP)* observations: determination of cosmological parameters”. In: *The Astrophysical Journal Supplement Series* 148 (2003), p. 175.

[Ste06] João E Steiner. “The origin of the universe”. In: *Estudos avançados* 20 (2006), p. 231.

[Ste+09] Hans Stephani et al. *Exact solutions of Einstein's field equations*. Cambridge University Press, 2009.

[SES17] Matthew J Stott, Thomas Elghozi, and Mairi Sakellariadou. “Gravitational wave bursts from cosmic string cusps and pseudocusps”. In: *Physical Review D* 96 (2017), p. 023533.

[Tsv42] Viktor N Tsvetkov. “Acta Physicochim”. In: *URSS* 16 (1942), p. 132.

[Tur91] Neil Turok. “Global texture as the origin of cosmic structure”. In: *Physica Scripta* 1991 (1991), p. 135.

[VV85] Tanmay Vachaspati and Alexander Vilenkin. “Gravitational radiation from cosmic strings”. In: *Physical Review D* 31 (1985), p. 3052.

[VV91] Tanmay Vachaspati and Alexander Vilenkin. “Large-scale structure from wiggly cosmic strings”. In: *Physical Review Letters* 67 (1991), p. 1057.

[Ves02] Viktor G Veselago. “Formulating Fermat's principle for light traveling in negative refraction materials”. In: *Physics-Uspekhi* 45 (2002), p. 1097.

[Vil81] Alexander Vilenkin. “Gravitational field of vacuum domain walls and strings”. In: *Physical Review D* 23 (1981), p. 852.

[Vil84] Alexander Vilenkin. “Cosmic strings as gravitational lenses”. In: *The Astrophysical Journal* 282 (1984), p. L51.

[Vil85] Alexander Vilenkin. “Cosmic strings and domain walls”. In: *Physics reports* 121 (1985), p. 263.

[Vil90] Alexander Vilenkin. “Effect of small-scale structure on the dynamics of cosmic strings”. In: *Physical Review D* 41 (1990), p. 3038.

[VS94] Alexander Vilenkin and Edward P S Shellard. *Cosmic strings and other topological defects*. Cambridge University Press, 1994.

[WNW05] David W Ward, Keith A Nelson, and Kevin J Webb. “On the physical origins of the negative index of refraction”. In: *New Journal of Physics* 7 (2005), p. 213.

[Wei08] Steven Weinberg. *Cosmology*. Oxford University Press, 2008.

[Wei89] Victor Weisskopf. "The origin of the universe". In: *Bulletin of the American Academy of Arts and Sciences* 42 (1989), p. 22.

[Wes+10] Paul R West et al. "Searching for better plasmonic materials". In: *Laser & Photonics Reviews* 4 (2010), p. 795.

[WF00] John Archibald Wheeler and Kenneth Ford. *Geons, black holes and quantum foam: a life in physics*. 2000.

[Zel80] Ya B Zeldovich. "Cosmological fluctuations produced near a singularity". In: *Monthly Notices of the Royal Astronomical Society* 192 (1980), p. 663.

[Zur85] Wojciech H Zurek. "Cosmological experiments in superfluid helium?" In: *Nature* 317 (1985), p. 505.

Résumé Détaillé sur la Thèse

***

Dans cette thèse, notre étude porte sur les défauts topologiques en cosmologie et en physique de la matière condensée. Nous proposons d'étudier l'analogie entre les défauts qui apparaissent dans ces domaines. Par exemple, nous discutons l'analogie entre les cordes cosmiques et les disinclinaisons présentes dans les cristaux liquides. Cependant, nous concentrons nos efforts sur l'étude de la gravité et des aspects géométriques des défauts linéaires; cordes cosmiques «ondulées» et les disinclinaisons hyperboliques. Le champ gravitationnel des cordes ondulées est analogue à celui des cordes régulières mais avec un potentiel newtonien non nul. Pour cette raison, outre le fait que l'espace-temps a une géométrie conique, les cordes exercent également une traction gravitationnelle sur les objets situés dans leur voisinage. Ceci a pour conséquence: l'apparition de nouveaux effets en plus de la lentille gravitationnelle. Bien que la disinclinaison hyperbolique soit très similaire à la disinclinaison ordinaire, le milieu résultant est un métamatériau anisotrope dans lequel le rapport entre les permittivités ordinaire et extraordinaire est négatif.

1 Introduction

Selon le modèle du Big Bang, qui décrit l'histoire de l'Univers depuis l'instant initial jusqu'à nos jours, l'Univers a débuté il y a environ 14 milliards d'années et depuis lors, il s'est élargi et refroidi. Au début de l'Univers, il y avait une séquence de transitions de phase qui brisaient la symétrie,

$$G \to H \to \cdots SU(3) \times SU(2) \times U(1) \to SU(3) \times U(1)_{em}.$$

Dans le contexte cosmologique, le schéma présenté ci-dessus implique des transitions de phase successives au tout début de l'univers, dans lesquelles des défauts peuvent se former [KT90; VS94].

Les transitions de phase spontanées dans les cristaux liquides sont strictement liées à la production de défauts en cosmologie, le mécanisme de Kibble utilisé pour décrire la formation et l'évolution de défauts dans le contexte cosmologique s'est révélé pertinent pour la formation de défauts dans les cristaux liquides nématiques [Chu+91; Bow+94]. En effet, les différentes phases des cristaux liquides peuvent être obtenues par brisure spontanée de symétrie, ce qui conduit à l'apparition de défauts topologiques exactement comme cela se produit en cosmologie; l'échantillon dans la phase la plus symétrique (à hautes

températures) se refroidit en une phase moins symétrique (à basses températures), et pendant ce processus, des «défauts» peuvent apparaître, voir Fig. 1.

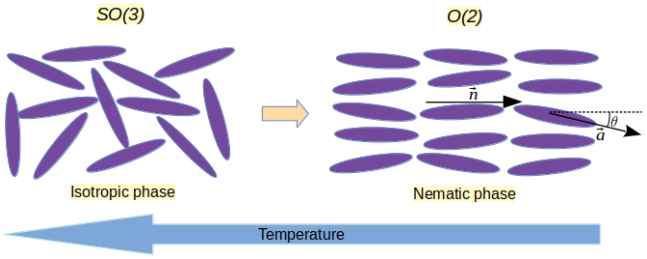

FIGURE 1: La transition de phase isotrope-nématique est représentée (avec le directeur $\vec{n}$ et les axes moléculaires $\vec{a}$). Le vecteur $\vec{n}$ nommé *directeur* est un vecteur unitaire avec symétrie miroir $\vec{n} = -\vec{n}$, qui décrit la direction moyenne d'alignement des molécules.

Nous avons ici une analogie parfaite avec ce qui se passe en laboratoire lors du refroidissement d'un échantillon de cristaux liquides nématique avec transitions de phase au tout début de l'Univers.

Parmi les défauts qui peuvent avoir été formés dans l'Univers, nous avons les cordes cosmiques. Ce sont des objets linéaires très intrigants ayant des longueur beaucoup plus grandes que leur largeur (la même taille d'un proton, ou plus petit) et possédant une énergie énorme. Par exemple, une corde ordinaire dont la longueur est égale à celle du diamètre du Soleil aurait approximativement la même masse solaire [HK95]. En considérant la limite d'épaisseur zéro, une corde cosmique linéaire statique située le long de l'axe z possède les composantes de tenseur énergie-impulsion données par [Vil81; Vil85; VS94]:

$$T^{\mu}_{\nu} = \mu_0 \delta(x)\delta(y)\ \mathrm{diag}\,(1,0,0,1), \tag{1}$$

où μ_0 est la densité d'énergie par unité de longueur de la corde. Pour une corde non perturbée (sans «wiggle»), la densité d'énergie μ_0 correspond exactement à la tension T_0, de sorte que l'équation d'état de la corde est écrite sous la forme $\mu_0 = T_0$ [Car90]. En résolvant les équations d'Einstein linéarisées, on obtient $(c = 1)$ [VS94; Vil81]:

$$ds^2 = dt^2 - dr^2 - \alpha^2 r^2 d\theta^2 - dz^2, \tag{2}$$

où $\alpha^2 = 1 - 8G\mu_0$ avec $G\mu_0 < 10^{-7}$ [Ade+14]. Cette métrique décrit l'espace-temps où la géométrie est plane partout (localement plane), sauf sur le noyau de la corde $(r = 0)$. C'est-à-dire que la corde introduit un petit angle de déficit dans l'espace-temps, qui est donné par $\Delta = 8\pi G\mu_0$. Par conséquent, les cordes linéaires sont des défauts pour lesquels la géométrie est globalement celle d'un cône [Vil81; VS94; HK95].

La conséquence la plus directe de la géométrie globalement conique est l'effet de lentille gravitationnelle planaire. La présence d'une corde cosmique dans l'univers peut affecter les trajectoires lumineuses, en formant une double image d'objets derrière la corde.

Les cordes cosmiques sont des analogues des disinclinaisons présentes dans les cristaux liquides nématiques. L'analogie est également valable du point de vue de la gravitation [Mor00], car les effets sur la propagation de la lumière du aux deux objets sont équivalents. [SM05]. Dans les milieux anisotropes uniaxiaux sous forme de cristaux liquides nématiques, la propagation de la lumière est décrite en termes de deux indices, $n_\perp$, l'indice de réfraction ordinaire où le milieu se comporte comme un milieu isotrope et $n_{||}$, l'indice de réfraction extraordinaire dépend de la direction de propagation. En ce qui concerne la propagation de la lumière, il faut distinguer entre un *rayon ordinaire* et un *rayon extraordinaire*. Dans ce cas, la propagation de l'énergie est donc régie par

$$N_r^2 = n_\perp^2 \cos^2\beta + n_{||}^2 \sin^2\beta \tag{3}$$

où β est l'angle entre le directeur et le vecteur de Poynting.

Les rayons lumineux obéissant le principe de Fermat peuvent être identifiés comme géodésiques dans certaines géométries riemanniennes [BW99]:

$$\underbrace{\int_A^B N_r dl}_{\text{Principe de Fermat}} \quad = \quad \underbrace{\int_A^B ds}_{\text{Géométries riemanniennes}} \tag{4}$$

Ainsi, le trajet optique dans un milieu avec des propriétés de réfraction sont des géodésiques dans la géométrie effective:

$$ds_{4D}^2 = dt^2 - \underbrace{\sum_{i,j} g_{ij} dx^i dx^j}_{ds^2 = N_r^2 dl^2}. \tag{5}$$

Les trajectoires données selon le principe de Fermat dans une métrique spatiale tridimensionnelle sont les mêmes que pour les géodésiques nulles dans une métrique à quatre dimensions [PM11].

2 Propagation de la Lumière et des Champs Massifs le Long d'une Corde Ondulée

Des modèles plus réalistes pour les cordes cosmiques montrent que les longues cordes ne sont peut-être pas parfaitement linéaires, mais impliquent des perturbations et des déformations [AS90; BB90]. Ces cordes cosmiques sont connues sous le nom de cordes ondulées [VV91; VS94]. L'effet de ces perturbations le long de la corde augmente la densité de masse linéaire $\tilde{\mu}$ et diminue la tension de la corde $\tilde{T}$, en respectant l'équation d'état $\tilde{\mu}\tilde{T} = \mu_0^2$ [Car90; Vil90; Gan01]. De la même manière que la corde linéaire, une corde ondulée le long de l'axe z a les composantes du tenseur énergie-moment donné par [VV91; VS94]

$$T_\nu^\mu = \delta(x)\delta(y)\,\mathrm{diag}\,(\tilde{\mu}, 0, 0, \tilde{T}). \tag{6}$$

En utilisant la méthode d'approximation de champ faible pour résoudre les équations d'Einstein, l'élément de ligne représentant l'espace-temps d'une corde ondulée peut être trouvé comme ($c = 1$) [VV91; VS94]:

$$ds^2 = (1 + 8\varepsilon \ln(r/r_0))\, dt^2 - dr^2 - \alpha^2 r^2 d\theta^2 - (1 - 8\varepsilon \ln(r/r_0))\, dz^2, \tag{7}$$

où $\alpha^2 = 1 - 4G(\tilde{\mu} + \tilde{T})$, avec $4G(\tilde{\mu} + \tilde{T}) \ll 1$, ce qui signifie que l'angle de déficit $\tilde{\Delta} = 4G\pi(\tilde{\mu} + \tilde{T})$ associé à la corde est très petit. Cette métrique est très similaire à celle d'une corde non perturbée, du moins en ce sens qu'elle représente un espace globalement conique, mais son angle de déficit est devient plus grand. L'excès de densité d'énergie représenté par le paramètre ε ($2\varepsilon = G(\tilde{\mu} - \tilde{T})$) entraîne la corde ondulée à exercer une attraction gravitationnelle sur les objets voisins [HK95; VS94].

Si nous considérons que la lumière se propage le long de la corde, sa propagation sera donc affecté par de nouveaux effets. L'équation d'onde régissant la propagation d'un champ scalaire (la lumière en tant qu'onde scalaire) dans une géométrie de fond incurvée doit prendre en compte sa courbure [Ful89; PM11]:

$$\nabla_\mu \nabla^\mu \Phi = \frac{1}{\sqrt{-g}} \partial_\mu (\sqrt{-g} g^{\mu\nu} \partial_\nu) \Phi = 0. \tag{8}$$

Selon la métrique de la corde ondulée et en utilisant le ansatz $\Phi(r, \theta, z, t) = e^{il\theta} e^{i(\omega t - kz)} R(r)$, où $k \in \mathbb{R}$ et $l = 0, \pm 1, \pm 2...$, on obtient l'équation de valeur propre:

$$-\frac{1}{\rho} \frac{d}{d\rho} \left(\rho \frac{dR}{d\rho} \right) + \underbrace{\left(\frac{l^2}{\alpha^2 \rho^2} + \ln \frac{\rho}{\rho_0} \right)}_{V_{eff}} R = \bar{\zeta} R \tag{9}$$

avec

$$\bar{\zeta} = \frac{1}{8\varepsilon} \frac{\omega^2 - k^2}{\omega^2 + k^2}. \tag{10}$$

L'équation ci-dessus est formellement équivalente à l'équation de Schrödinger qui décrit l'atome d'hydrogène en 2D. Par contre, le terme potentiel de l'équation ci-dessus, $V_{\text{eff}} = \frac{l^2}{\alpha^2 \rho^2} + \ln \frac{\rho}{\rho_0}$, n'est pas pris en compte que pour les états liés. En conséquences, les trajectoires sont des hélices radialement confinées, comme indiqué dans la Fig. 3. La figure 3 montre explicitement l'attraction gravitationnelle par la corde.

Nous avons calculé numériquement la partie radiale des ondes se propageant le long de la corde ondulée avec leurs valeurs propres correspondantes, voir la Fig. 4. Les différents états sont étiquetés par les nombres quantiques n (nombre quantique radial) et l. Le nombre de modes d'ondes pouvant se propager est grand mais fini. En plus d'être quantifiés par n et l, leurs fréquence dépend également de la densité d'énergie et de la tension de la corde.

Il est intéressant d'examiner ce qui se passe avec des particules massives dans les mêmes circonstances précédentes. Afin d'étudier cette possibilité, nous

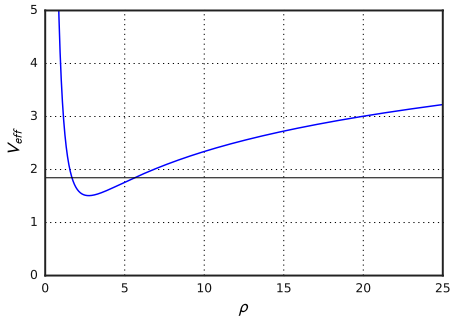

FIGURE 2: Potentiel effectif, V_{eff} (dans les unités où $\rho_0 = 1$), pour $l = 2$. La ligne continue horizontale représente l'état fondamental $\bar{\zeta}$ à la valeur de l.

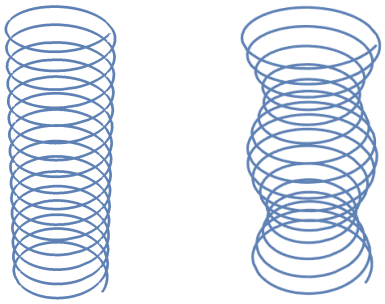

(a) (b)

FIGURE 3: Les trajets de rayons: (a) lorsque «l'énergie totale» $\bar{\zeta}$ est au minimum du potentiel effectif et (b) à un certain point au-dessus de celui-ci.

écrivons l'équation de Klein-Gordon ($\hbar = 1$) dans la géométrie de la corde ondulée [Ful89]:

$$\left[\frac{1}{\sqrt{-g}}\partial_\mu(\sqrt{-g}g^{\mu\nu}\partial_\nu) - m^2\right]\Phi(r,\theta,z,t) = 0. \tag{11}$$

Nous arrivons à une équation de valeur propre identique à celle de la propagation de champ sans masse, mais maintenant avec valeur propre

$$\bar{\mathcal{E}}_{nl} = \frac{1}{8\varepsilon}\frac{\omega^2 - k^2 - m^2}{\omega^2 + k^2}. \tag{12}$$

Les fonctions d'onde $R_{nl}(\rho)$ et les valeurs propres $\bar{\mathcal{E}}_{nl}$ sont numériquement identiques à la solution de propagation de champ sans masse. La discussion sur la trajectoire du champ sans masse est toujours valable pour les champs massifs. Cependant, pour la propagation de champs massifs, une fréquence de coupure ω_c est requise dans la relation de dispersion.

Il existe une forte similitude entre la propagation des champs scalaires le

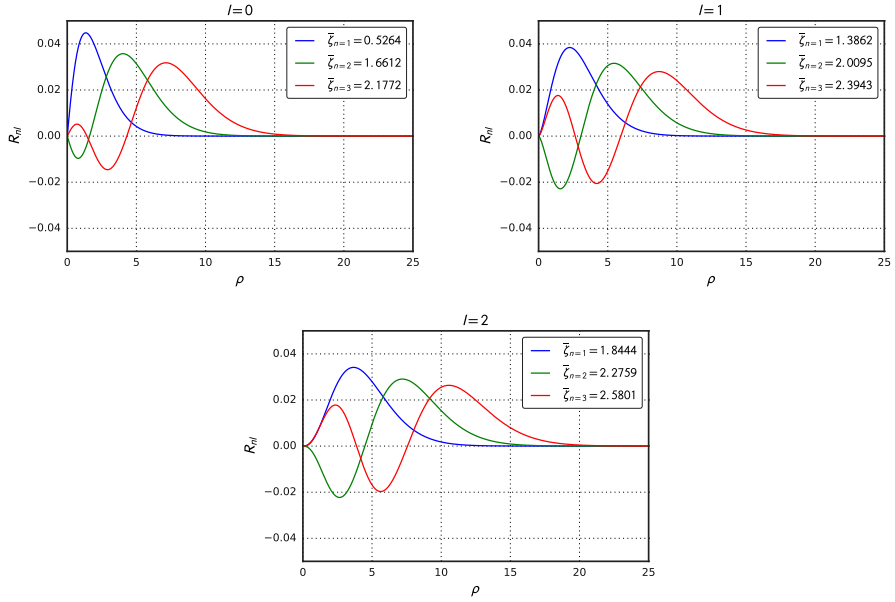

FIGURE 4: Modes d'onde pour les premières valeurs propres $n = 1,2,3$ de l'équation (9) pour chaque $l = 0,1,2$.

long d'une corde cosmique ondulée et la propagation d'ondes électromagnétiques dans des guides d'ondes optiques. Nous explorons cette analogie en proposant un moyen de concevoir une fibre optique imitant la corde ondulée dans le contexte décrit ci-dessus.

Nous concevons un guide d'onde d'indice de réfraction $n = n(r)$ où les champs sont azimutalement symétriques. Ainsi, pour les ondes se propageant le long de la fibre optique $\Phi(r,z) = e^{-ikz}R(r)$, on obtient l'équation d'onde radiale:

$$-\frac{1}{r}\frac{d}{dr}\left(r\frac{dR}{dr}\right) - n^2(r)\omega^2 R + k^2 R = 0. \tag{13}$$

Nous choisissons l'indice de réfraction donné par

$$n(r) = \left(1 - \Omega \ln \frac{r}{r_0}\right)^{1/2}, \tag{14}$$

avec le paramètre sans dimension $\Omega \ll 1$ et r_0 est un rayon central opaque. Par conséquent, un guide d'onde optique à l'indice de réfraction $n(r) = \left(1 - \Omega \ln \frac{r}{r_0}\right)^{1/2}$ imitera les effets d'une corde ondulée pour les champs se propageant avec $l = 0$.

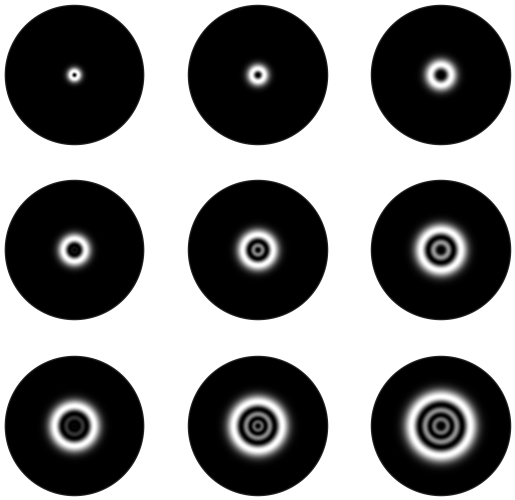

FIGURE 5: Profils d'intensité pour les premières solutions R^2_{nl} de l'équation (9), avec $n = 1, 2, 3$ et $l = 0, 1, 2$. Les profils sont disposés comme dans une matrice où n et l donnent le numéro de ligne et de colonne, respectivement. La première colonne correspond aux modes de la fibre optique.

3 Propagation de la Lumière dans une Disinclinaison Hyperbolique

Les métamatériaux sont des matériaux optiques offrant la possibilité d'avoir des indices de réfraction négatifs [SPW04]. Cette caractéristique fournit de nombreuses utilisations dans les applications technologiques et conduit également à d'autres d'analogies avec les systèmes cosmologiques. Récemment, des métamatériaux ont été proposé comme moyen d'imiter les aspects de l'espace-temps incurvé en laboratoire [GZZ09; ML15].

Nous présentons ici une nouvelle classe de défauts; la disinclinaison hyperbolique existant dans un métamatériau constitué de cristaux liquides nématiques. Nous examinons les propriétés optiques de deux configurations différentes de métamatériaux, l'axe optique défini par un directeur circulaire et radial. En premier lieu, nous le considérons le directeur comme étant $\hat{n} = \hat{\phi}$ (directeur circulaire), puis nous considérons comme $\hat{n} = \hat{r}$ (directeur radial), voir Fig. 6. Le trajet optique $ds^2 = N_r^2 dl^2$ peut donc être trouvé sous la forme:

$$ds^2 = N_r^2 dl^2 = -d\rho^2 + \alpha^2 \rho^2 d\phi^2 - d\zeta^2, \tag{15}$$

pour la configuration 6 (a) et

$$ds^2 = N_r^2 dl^2 = \alpha^2 d\rho^2 - \rho^2 d\phi^2 - d\zeta^2, \tag{16}$$

pour la configuration 6 (b), avec $\alpha^2 = \frac{\varepsilon_\perp}{|\varepsilon_{||}|}$.

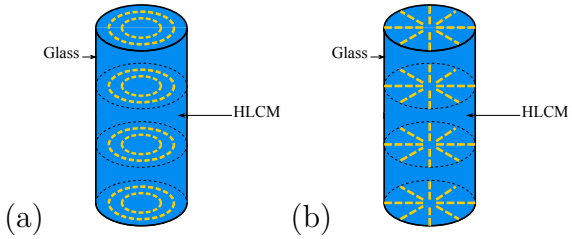

FIGURE 6: Les deux configurations cylindriques (en fonction de la disposition du directeur) recouvertes d'un matériau réfléchissant. (a) Configuration du directeur avec $\hat{n} = \hat{\phi}$ (directeur circulaire). (b) Configuration du directeur avec $\hat{n} = \hat{r}$ (directeur radial).

L'équation de conservation de l'énergie pour la propagation de la lumière dans le dispositif est donnée par:

$$\frac{\rho'^2}{2} - \frac{\alpha^2 C^2}{2\rho^2} = \frac{-(A^2+B)}{2} = E, \tag{17}$$

où le paramètre de énergie $E \leq 0$, puisque $A > 0$ et $B > 0$. En manipulant ces équations, on trouve $\rho = \rho(\phi)$:

$$\rho(\phi) = \frac{\rho_M}{\cosh \alpha\phi}, \tag{18}$$

avec $\rho_M = \frac{\alpha|C|}{\sqrt{2|E|}}$ qui est le rayon maximum des trajectoires. Cette solution est connue sous le nom de spirale de Poinsot confiné, voir Fig. 7. Plus la valeur de

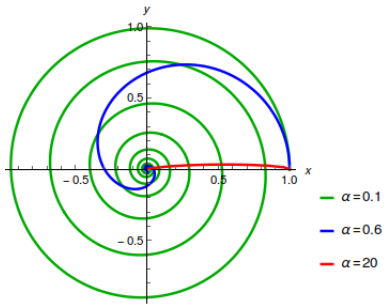

FIGURE 7: Projection des trajectoires sur le plan $x-y$ avec ρ en unités de ρ_M, pour quelques valeurs de α.

α est faible, plus le comportement en spirale est fort. Pour les grandes valeurs de α, par exemple $\alpha = 20$, les rayons se déplacent presque linéairement vers le centre de dispositif. Le même effet peut être visualisé dans les trajectoires tridimensionnelles, voir Fig. 8.

Pour le dispositif avec disposition du directeur radial, la conservation de l'énergie donne:

$$\frac{\rho'^2}{2} - \frac{C^2}{2\alpha^2\rho^2} = \frac{B+A^2}{2\alpha^2} = E. \tag{19}$$

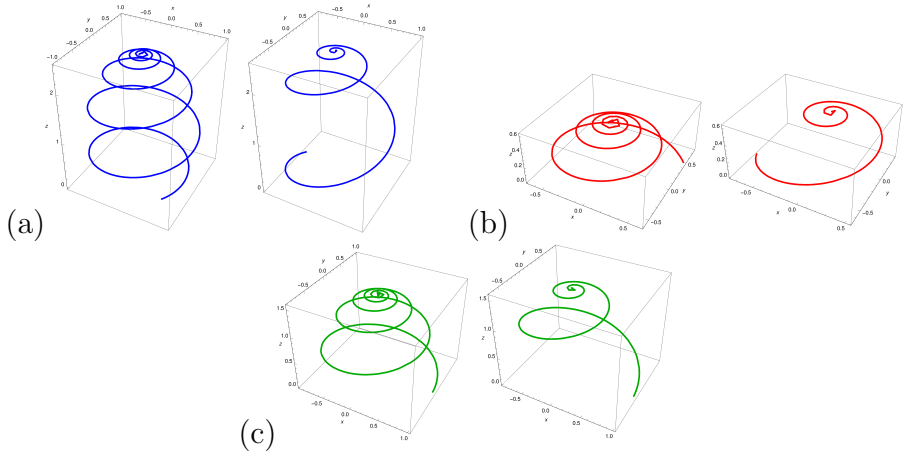

FIGURE 8: Trajectoires en trois dimensions pour $\rho_M = 1$, $\rho_0 = 0.8$, $K = 0.64$ et $\alpha = 0.1, 0.2$; l'image à gauche (droite) font référence à $\alpha = 0.1$ ($\alpha = 0.2$). (a) Trajectoire pour les rayons croissant à partir de ρ_0. (b) Trajectoire pour les rayons décroissant à partir de ρ_0. (c) Trajectoire pour les rayons à partir $\rho_0 = \rho_M$.

Les trajectoires ne sont pas confinées et la lumière n'est pas concentrée. Ces arguments découlent de l'équation $\rho(\phi) \sim \frac{1}{\sinh \alpha\phi}$, autre cas de la spirale de Poinsot, mais pas du type confiné.

Nous concluons que la configuration du directeur circulaire devrait être privilégiée pour concevoir un dispositif permettant de concentrer la lumière.

Nous examinons maintenant la structure des modes optiques qui se propagent dans le dispositif muni du directeur circulaire, voir Fig. 6 (a). En utilisant, l'approximation d'onde scalaire, par la forme généralisée de l'équation de d'Alembert:

$$\nabla_i \nabla^i \Phi - \frac{1}{c^2}\frac{\partial^2 \Phi}{\partial t^2} = \frac{1}{\sqrt{|g|}} \partial_i \left(\sqrt{|g|} g^{ij} \partial_j \right) \Phi - \frac{1}{c^2}\frac{\partial^2 \Phi}{\partial t^2} = 0. \tag{20}$$

En cas de dépendance temporelle de la forme $\Phi(\rho, \phi, \zeta, t) = F_{\ell,k_\zeta}(\rho) e^{\pm i\ell\phi} e^{\pm i k_\zeta \zeta} e^{-i\omega t}$, où ω est la fréquence angulaire, nous obtenons l'équation

$$\rho^2 \frac{d^2 F_{\ell,k_\zeta}}{d\rho^2} + \rho \frac{dF_{\ell,k_\zeta}}{d\rho} - \left[\left(\frac{\omega^2}{c^2} + k_\zeta^2 \right) \rho^2 - \frac{\ell^2}{\alpha^2} \right] F_{\ell,k_\zeta} = 0. \tag{21}$$

On retrouve l'équation différentielle de Bessel modifiée d'ordre imaginaire $i\ell/\alpha$, avec les solutions [Dun90; Olv+10]

$$F_{\ell,k_\zeta}(\rho) = e_\ell \tilde{I}_{\ell/\alpha}(\bar{\omega}\rho) + f_\ell \tilde{K}_{\ell/\alpha}(\bar{\omega}\rho), \tag{22}$$

où $\bar{\omega} = \sqrt{k_\zeta^2 + \omega^2/c^2}$ et e_ℓ, f_ℓ sont constantes d'intégration [Olv+10]. La première solution peut être rejetée car elle diverge à de grandes distances de l'axe, ce qui signifie que $e_\ell = 0$. Comme nous avons obtenu de l'optique géométrique, les champs se concentrent le long de l'axe du dispositif, comme le montre la figure

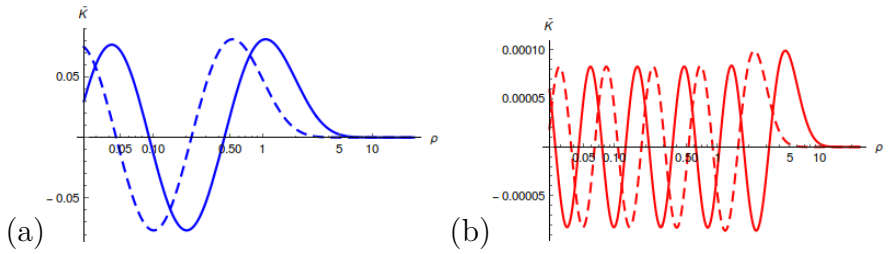

FIGURE 9: Les amplitudes d'onde radiale $\tilde{K}$ pour les valeurs fixes $\ell = 1$, $\alpha = 0.17, 0.5$ et $\bar{\omega} = 1, 2$. (a) pour $\alpha = 0.5$ et (b) pour $\alpha = 0.17$. Les lignes continues et pointillées font référence à $\bar{\omega} = 1$ et $\bar{\omega} = 2$, respectivement. Plus la valeur de α est faible, plus les champs oscillent près de l'origine. Sur de grandes distances, le comportement est exponentiel et ne dépend pas de ℓ/α.

9. Pour un plan $z = const.$, la distribution d'intensité des champs en propagation peut être représentée sous la forme $|\tilde{K}_{\ell/\alpha}(\bar{\omega}\rho)|^2$, voir Fig. 10.

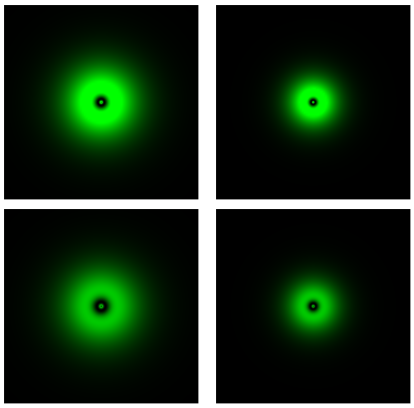

FIGURE 10: Ceux à gauche (droite) correspondent à $\bar{\omega} = 0.67$ ($\bar{\omega} = 1$). Ceux du haut (bas) correspondent à $\alpha = 0.90$ ($\alpha = 0.83$). Tous les cas sont pour $\ell = 1$.

4 Conclusions

Nous constatons que les champs massiques et non-massiques sont confinés à la corde cosmique «ondulée» quand nous examinons la propagation non perpendiculaire à son axe. Cette affirmation est basée sur l'analyse des trajectoires et l'application du formalisme ondulatoire. Enfin, nous proposons la conception d'un guide d'onde optique ayant l'indice de réfraction spécifique permettant de simuler l'effet des cordes ondulées en laboratoire. En fait, notre analyse concernant la disinclinaison hyperbolique étant très proche de la précédente pour la corde ondulée, nous permet d'appliquer le formalisme ondulatoire avec des traitements d'optique géométrique pour comprendre la propagation de la lumière. Nous trouvons que pour un agencement spécifique du directeur (directeur circulaire) du cristal liquide hyperbolique, la lumière est confinée et dirigée vers l'axe du métamatériau. Plus précisément, on obtient un dispositif optique qui concentre les rayons de lumière, quelles que soient les conditions d'injection.

Références

***

[Ade+14] Peter A R Ade et al. “Planck 2013 results. XXV. Searches for cosmic strings and other topological defects”. In: *Astronomy & Astrophysics* 571 (2014), A25.

[AS90] Bruce Allen and Edward P S Shellard. “Cosmic-string evolution: a numerical simulation”. In: *Physical review letters* 64 (1990), p. 119.

[BB90] David P Bennett and Francois R Bouchet. “High-resolution simulations of cosmic-string evolution. I. Network evolution”. In: *Physical Review D* 41 (1990), p. 2408.

[BW99] Max Born and Emil Wolf. *Principles of optics: electromagnetic theory of propagation, interference and diffraction of light*. 7th. Cambridge University Press, 1999.

[Bow+94] Mark J Bowick et al. “The cosmological kibble mechanism in the laboratory: string formation in liquid crystals.” In: *Science (New York, NY)* 263 (1994), p. 943.

[Car90] Brandon Carter. “Integrable equation of state for noisy cosmic string”. In: *Physical Review D* 41 (1990), p. 3869.

[Chu+91] Isaac Chuang et al. “Cosmology in the laboratory: Defect dynamics in liquid crystals”. In: *Science* 251 (1991), p. 1336.

[Dun90] Timothy M Dunster. “Bessel functions of purely imaginary order, with an application to second-order linear differential equations having a large parameter”. In: *SIAM Journal on Mathematical Analysis* 21 (1990), p. 995.

[Ful89] Stephen A Fulling. *Aspects of quantum field theory in curved spacetime*. Cambridge university press, 1989.

[Gan01] Alejandro Gangui. “Topological defects in cosmology”. In: *arXiv preprint astro-ph/0110285* (2001).

[GZZ09] Dentcho A Genov, Shuang Zhang, and Xiang Zhang. “Mimicking celestial mechanics in metamaterials”. In: *Nature Physics* 5 (2009), p. 687.

[HK95] Mark Hindmarsh and Thomas W B Kibble. “Cosmic strings”. In: *Reports on Progress in Physics* 58 (1995), p. 477.

[KT90] Edward W Kolb and Michael S Turner. *The Early Universe*. 1990.

[ML15] Tom G Mackay and Akhlesh Lakhtakia. "Metamaterial models of curved spacetime". In: *Metamaterials, Metadevices, and Metasystems 2015*. International Society for Optics and Photonics. 2015, 95442K.

[Mor00] Fernando Moraes. "Condensed matter physics as a laboratory for gravitation and cosmology". In: *Brazilian Journal of Physics* 30 (2000), p. 304.

[Olv+10] Frank WJ Olver et al. *NIST handbook of mathematical functions*. Cambridge University Press, 2010.

[PM11] Erms Pereira and Fernando Moraes. "Diffraction of light by topological defects in liquid crystals". In: *Liquid Crystals* 38 (2011), p. 295.

[SM05] Caio Sátiro and Fernando Moraes. "A liquid crystal analogue of the cosmic string". In: *Modern Physics Letters A* 20 (2005), p. 2561.

[SPW04] David R Smith, John B Pendry, and Mike CK Wiltshire. "Metamaterials and negative refractive index". In: *Science* 305 (2004), p. 788.

[VV91] Tanmay Vachaspati and Alexander Vilenkin. "Large-scale structure from wiggly cosmic strings". In: *Physical Review Letters* 67 (1991), p. 1057.

[Vil81] Alexander Vilenkin. "Gravitational field of vacuum domain walls and strings". In: *Physical Review D* 23 (1981), p. 852.

[Vil85] Alexander Vilenkin. "Cosmic strings and domain walls". In: *Physics reports* 121 (1985), p. 263.

[Vil90] Alexander Vilenkin. "Effect of small-scale structure on the dynamics of cosmic strings". In: *Physical Review D* 41 (1990), p. 3038.

[VS94] Alexander Vilenkin and Edward P S Shellard. *Cosmic strings and other topological defects*. Cambridge University Press, 1994.